THE UNIVERSITY *of* EDINBURGH

Adaptive Array Antenna Design for Wireless Communication Systems

Nurul Hazlina Noordin

A thesis submitted for the Degree of Doctor Philosophy

The University of Edinburgh

2013

Declaration of Originality

I hereby declare that the research reported in this thesis and the thesis itself was composed and originated entirely by myself in the School of Engineering at The University of Edinburgh.

Nurul Hazlina Binti Noordin
September 2013
Edinburgh, U.K.

To my husband,

Mohamad Isnizam Mat Alit

Acknowledgements

I would like to thank my supervisors, Professor Tughrul Arslan and Dr. Brian W. Flynn, for their excellent guidance, advice and expertise throughout my research work. This appreciation also goes to Dr. Ahmet T. Erdogan for his feedbacks and comments in numerous discussions during my studies in Edinburgh.

To the members of the System Level Integration Group (SLiG) and Advanced Smart Antenna Technologies (ASAT) research group, I owe sincere and earnest thankfulness for the unforgettable and unique experience of my life.

I would like to acknowledge my sponsors, Universiti Malaysia Pahang (UMP) and the Ministry of Higher Education Malaysia (MoHE), for funding my studies. Also, thanks to those in the School of Engineering, the University of Edinburgh, for providing excellent research and administrative support.

Also, I would like to thank Professor R. Badlishah Ahmad, Dr. Fareq Malek and Mrs Hasliza Abdul Rahim, from Universiti Malaysia Perlis (UniMAP) for their expertise in RF measurement.

I am hugely grateful to my family, Mak, Abah, Mak Nizam, Pizah, and my lovely kids; Batrisya, Ilyas and Madihah, for their endless love, motivations and encouragements, especially throughout this period of my life.

And most of all, Praise to Allah, who made all things possible. *Alhamdulillah*.

Abstract

Adaptive array antennas use has been limited to non-commercial applications due to their high cost and hardware complexity. The implementation cost of adaptive array antennas can be kept to a minimum by using cost effective antennas, reducing the number of elements in the array and implementing efficient beamforming techniques. This thesis presents techniques for the design of adaptive array antennas which will enable their cost effective implementation in wireless communication systems. The techniques are investigated from three perspectives, namely, reconfigurable antenna design, wide scan array design and single-port beamforming technique.

A novel single-feed polarisation reconfigurable antenna design is proposed in the first stage of this study. Different polarisation states, namely, linear polarisation (LP), left-hand circular polarisation (LHCP) and right-hand circular polarisation (RHCP), are achieved by perturbing the shape of the main radiating structure of the antenna. The proposed antenna exhibits good axial ratio (< 3 dB at 2.4 GHz) and has high radiation efficiency in both polarisation modes (91.5 % - LHCP and 86.9 % - RHCP). With a compact single feeding structure, the antenna is suitable for implementation in wireless communication devices.

The second stage of the study presents the design procedure of wide scan adaptive array antennas with reduced number of elements. Adaptive array antennas with limited number of elements have limited scanning range, reduced angular scanning resolution and high sidelobe levels. To date, design synthesis of adaptive array antennas has been targeted on arrays with a large number of elements. This thesis presents a comprehensive analysis of adaptive array antennas with less than 10 elements. Different array configurations are analysed and various array design parameters such as number of elements, separation between elements and orientation of the elements are analysed in terms of their 3 dB scan range. The proposed array, the 3-faceted array, achieves a scanning range up to ±70°, which is higher than ±56° obtained from the Uniform Linear Array. The faceted arrays are then evaluated in the context of adaptive beamforming properties. It was shown that the 3-faceted array is suitable for adaptive array applications in wireless communication systems as it achieves the highest directivity compared to other faceted structures. The 3-faceted array is then synthesised for low sidelobe level. Phase correction together with amplitude tapering technique is applied to the 3-faceted array. The use of conventional and tuneable windowing techniques on the 3-faceted array is also analysed.

The final stage of the study investigates beamforming techniques for the adaptive array antenna. In the first part, beamforming algorithms using different performance criteria, which include maximum signal-to noise-ratio (SINR), minimum (mean-square Error) MSE and power minimisation, are evaluated. In the second part, single-port beamforming techniques are explored. In previous single-port beamforming methods, the spatial information of the signals is not fully recovered and this limits the use of conventional adaptive beamforming algorithms. In this thesis, a novel signal estimation technique using pseudo-inverse function for single-port beamforming is proposed.

The proposed polarisation reconfigurable antenna, the 3-faceted array antenna and the single-port beamforming technique achieve the required performance, which suggests the potential of adaptive array antennas to be deployed commercially, especially in wireless communication industry.

Table of Contents

List of Figures

List of Tables

Acronyms and Abbreviations

1D	1 Dimensional
2D	2 Dimensional
3D	3 Dimensional
ADC	Analog to Digital Converter
CMA	Constant Modulus Algorithm
DoA	Direction of Arrival
FIR	Finite Impulse Response
FM	Frequency-Modulated
FPGA	Field Programmable Gate Array
GA	Genetic Algorithm
HPBW	Half Power Beam Width
LHCP	Left-hand circularly polarised
LMS	Least Mean Squares
LNA	Low Noise Amplifier
LO	Local Oscillator
LPF	Low Pass Filter
MEMS	Microelectromechanical systems
mMSE	Minimum Mean-Square Error
MSE	Mean-Square Error
mSINR	Maximum Signal to Interference-plus-Noise Ratio
PM	Phase-Modulated
PSO	Particle Swarm Optimisation
RF	Radio Frequency
RHCP	Right-hand circularly polarised
RLS	Recursive Least Squares
SINR	Signal to Interference-plus-Noise Ratio
SLL	Sidelobe Level
SMI	Sample-Matrix-Inversion
SMILE	Spatial Multiplexing of Local Elements
SNOI	Signal not of interests
SNR	signal-to noise-ratio
SOI	Signal of interests
TDMA	Time Division Multiple Addressing
TPSW	Time Sequence Phase Weighting
UCA	Uniform Circular Array
UCCA	Uniform Cocentric Circular Array
UHA	Uniform Hexagonal Array
ULA	Uniform Linear Array
URA	Uniform Rectangular Array

Chapter 1
Introduction

1.1 Research Motivation

The widespread of wireless communication technology applications in our life has increased the requirement for efficient and reliable signal transmission. One way of achieving these requirements is by using smart antenna system.

Conventional antenna systems use standard omni-directional antenna that transmits signal in all directions including in the directions where the signal is not required. However, in real situations, the required signal is not necessarily coming from all directions. This results in inefficient signal transmission and power wastage. Hence, the idea of a smart antenna is introduced. A smart antenna produces highly directive radiation pattern that can be electronically controlled. This means the radiation of a smart antenna can be steered over the best signal path, and consequently reduce the power consumption of the wireless devices.

Smart antennas are divided into two categories, which are switched-beam antennas and adaptive array antennas [1-3]. A switched-beam antenna, as shown in Figure 1.1 (a), has a set of fixed radiation pattern and the appropriate pattern is selected based on the requirement of the wireless system. Although this technique exploits the spatial dimension of an antenna,

the main beam sometimes could not point to the signal of interest (SOI), as shown in Figure 1.1 (b).

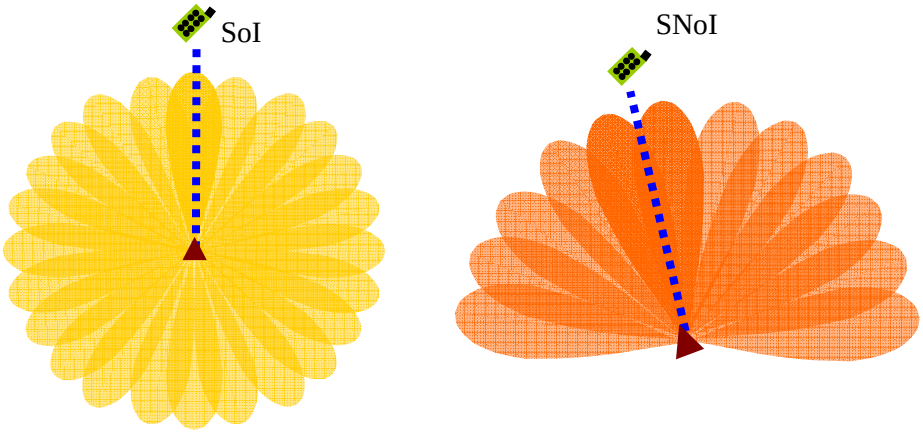

Figure 1.1: Switched-beam antenna, (a) pre-determined switching scheme, and (b) low resolution of the main beam.

On the other hand, the radiation pattern of an adaptive array antenna is controlled by adjusting the complex excitation of its elements and this allows the main beam to be arbitrarily placed, as illustrated in Figure 1.2 (a) [2, 3]. These excitations can also be manipulated so that the radiation points at the SOI while suppressing the radiation in the direction of signals not of interest (SNOI), as shown in Figure 1.2 (b). This feature is known as 'adaptive beamforming' and it allows the antenna to maximise its spatial usability [4-6].

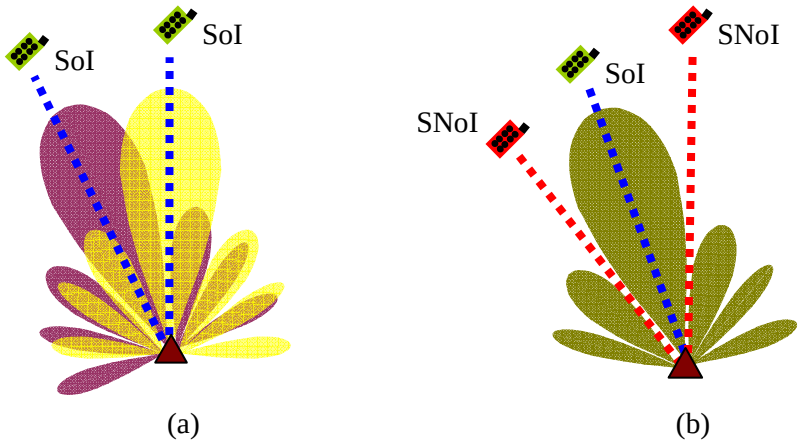

Figure 1.2: Adaptive array antenna, (a) arbitrary steering, and (b) adaptive beamforming.

However, despite their advantages, adaptive array antennas have not been commercially used due to implementation issues such as high cost and hardware complexity [4, 7-14]. Adaptive array antenna use has been limited to non-commercial applications such as ultrasound medical systems and military radar systems. To regain its commercial value and widespread usage in commercial wireless communication devices, the implementation cost of the adaptive array arrays must be kept to a minimum. This can be achieved by employing cost effective antennas, reducing the number of elements in the array and implementing an efficient beamforming technique.

1.2 Research Investigations

The main components of an adaptive array antenna are the antenna, the array and the signal processing unit. In order to reduce the cost of an adaptive array antenna for wireless communication applications, several challenges related to the components have to be addressed.

1.2.1 Adaptive Array Antenna Design Challenges

1.2.1.1 Antenna Design

One technique that can be used to design a cost-effective adaptive array is by employing reconfigurable antenna as the array elements. This is because, with the same radiating structure, the antenna has the ability to reconfigure its radiation properties such as the frequency, radiation pattern and polarisation [15-19]. The challenges associated with reconfigurable antenna designs include the reconfiguration mechanism and maintaining certain antenna characteristics while achieving the radiation diversities [18, 19]. Besides the configurable properties, the dimensions of the antenna also need to be considered, as only limited space is available in most communication devices.

This research investigates the design of a polarisation reconfigurable antenna for use in wireless communication systems. Polarisation reconfiguration is targeted because it enables frequency reuse and reduces the multi-path effects in the wireless communication channel [15, 20-22]. This is important in order to achieve high quality signal transmission. The aim is to develop a polarisation reconfigurable antenna that is compact, operates at 2.4 GHz and has directional radiation pattern.

1.2.1.2 Array Design

The geometry of an array, which is described by the arrangement of the elements in the array, influences the resulting radiation pattern of the adaptive array antenna. The array

elements are fed in accordance with the desired amplitude and phase using suitable feeding network.

Generally, to avoid high coupling between elements in an antenna array, the ideal separation between two adjacent elements is 0.5 λ. Elements that are separated less than 0.5 λ have high coupling level and this consequently will distort the radiation pattern of the array [23, 24]. On the other hand, when the separations of the elements are more than 0.5 λ, the tendency for grating lobes to occur is high [25]. Grating lobe degrades the peak directivity of the array as the radiation power is transferred from the main beam to the lobes [26-28].

The cost of an adaptive array antenna is proportional to the number of the array elements. Hence, one technique of minimising the cost is by employing adaptive arrays with a small number of elements. However, adaptive array antennas with limited number of elements present their own challenges, which include limited scanning range, reduced angular scanning resolution and high sidelobe levels [29-31].

Array geometries consisting of fewer than 10 elements are investigated in this research. The aim is to develop an array with wide angle scanning abilities. Wide scan coverage is important, especially in wireless communication system, as the transmission link is not always within the boresight of an antenna. In the first stage, an adaptive array antenna with a wide scanning range is designed and developed. Various array configurations, such as uniform linear arrays and uniform circular arrays, are considered. In the second stage, these arrays are evaluated in the context of adaptive beamforming. The arrays are evaluated in environments that contain interference sources and beamforming algorithms are used to calculate the excitation weights of the array elements. Comparisons of the beamforming properties, such as the accuracy of the main beam and null placement, are then made. Finally, a technique to synthesise the wide scan array for low sidelobe level is explored.

1.2.1.3 Signal Processing Unit

The signal processing algorithm implemented in an adaptive array antenna contributes to its ‘intelligence’. The signals induced on each element are analysed and processed so as to adjust the array radiation characteristic in order to adapt to the environment.

The attractive features of this intelligence are its ability to locate the desired signal, normally termed as directional-of-arrival (DoA), and adaptive beamforming. The DoA is calculated based on the time delays due to the impinging signals onto the adaptive array antenna. Once

the DoA of a desired signal is estimated, beamforming algorithms are then used to optimise the complex excitations of the array elements.

Another technique for reducing the cost of an adaptive array antenna is by implementing a single-port signal processing architecture. In the single-port beamforming architecture, signals received at each antenna element are coherently combined using a power combiner before going through a single RF channel [32, 33]. A typical RF channel consists of a bandpass filter, a low noise amplifier, a mixer, a lowpass amplifier and an ADC. This means that the quantity of hardware required in a single-port beamformer is less than that of the multi-port beamformer. In addition, the single-port architecture consumes less power compared to the multi-port architecture as fewer hardware components are required. However, in return, due to the signal combination in the single-port architecture, the spatial and signal information from the array element is lost [34]. This information is essential when conventional beamforming algorithms are used in the adaptive array antenna.

This thesis investigates the single-port beamforming technique for use in wireless communication systems. In the first part of the investigation, beamforming algorithms using different performance criteria such as maximum signal to noise ratio (SINR), minimum mean square error (MSE) and power minimisation are explored. Then, the single-port beamforming algorithm is applied to the proposed wide scan array and the performance of the algorithm is evaluated.

The final development of the smart antenna system involves the design of power divider circuits and the estimation of Directional of Arrival (DoA) of a signal. However, these components are well-established as individual topics and are not covered in this thesis. This research focuses on the main structure of the adaptive array antenna in order to produce a low cost adaptive array antenna design. Design requirements of the adaptive array antenna for wireless communication system investigated in this thesis are tabulated in Table 1.1 and the research investigations of this thesis are summarised in Figure 1.3.

Table 1.1: Design Requirements for the Low Cost Adaptive Array Antenna for Wireless Communication Systems.

Components	Design Requirements	
Antenna Design	Operational Frequency	2.4 GHz
	Reconfiguration	Polarisation (LHCP /RHCP)
	Beamwidth	> 70° (Unidirectional)
Array Design	Operational Frequency	2.4 GHz
	Array Size	< 10 elements
	Scanning Range	> 60°
Beamforming Algorithm	Operational Frequency	2.4 GHz
	Array Size	< 10 elements
	Beamforming structure	Single-port

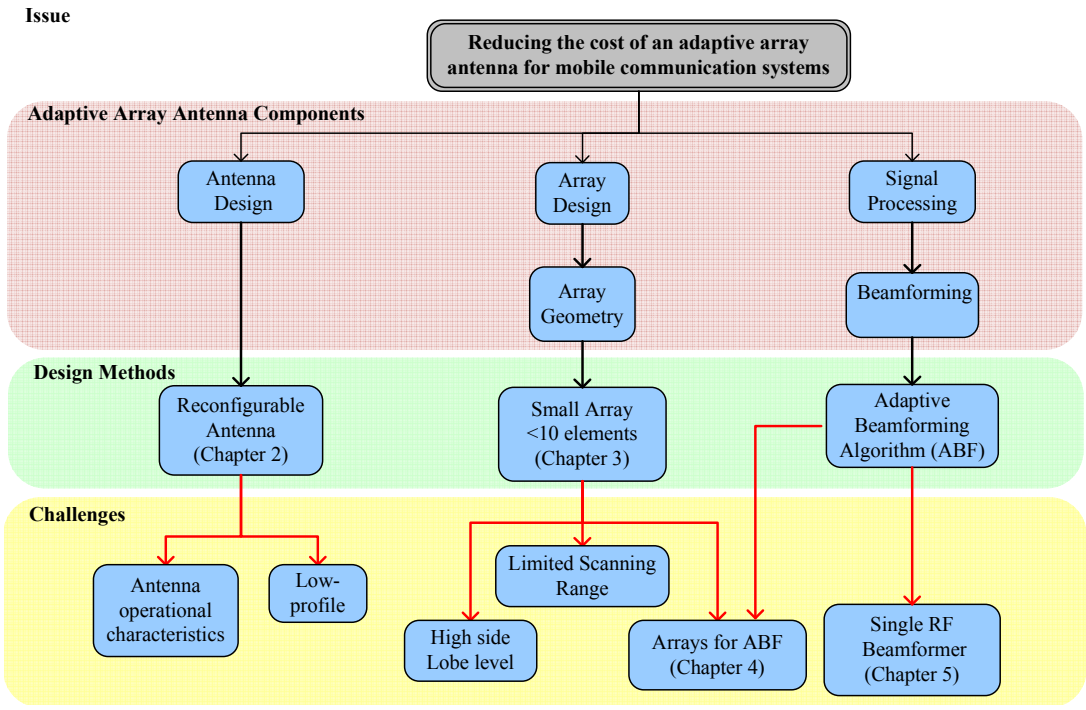

Figure 1.3: The structure of this research.

1.2.2 Research Objectives

The main objectives of this research are:

1. to design a polarisation reconfigurable antenna for wireless communication systems,
2. to design a wide scan range adaptive array antenna with a limited number of elements for wireless communication systems, and
3. to develop a signal estimation technique in a single-port beamforming architecture for wireless communication systems.

1.3 Publications Arising from This Research

Publications arising from this research are as follows:-

Peer-Reviewed Journal

2013

N. H. Noordin, Tughrul Arslan, Brian W. Flynn, Ahmet T. Erdogan, Ahmed O. El-Rayis, *Single-port Beamforming System for 3-faceted Phased Array Antenna*, IEEE Antenna and Wireless Propagation Letter, pp. 813-816, 2013.

2012

N. H. Noordin, T. Arslan, B. W. Flynn, and A. T. Erdogan, *Low-cost Antenna Array with Wide Scan Angle Property*, IET Microwaves, Antennas & Propagation, vol. 6, pp. 1717-1727, 2012.

Selected Refereed Conference

2013

N. H. Noordin, Tughrul Arslan, Brian W. Flynn, Ahmet T. Erdogan, *Faceted Arrays for Adaptive Beamforming Application* – accepted in Personal, Indoor and Mobile Radio Communications (PIMRC 2013).

N. H. Noordin, Tughrul Arslan, Brian W. Flynn, *Low Sidelobe Level Synthesis Technique for Faceted Arrays*, 7th European Conference on Antennas and Propagation (EuCAP 2013), Gothenburg, Sweden, April 8-12, 2013, pp. 592 - 596.

2012

N. H. Noordin, Nakul Haridas, Ahmed O. El-Rayis, Ahmet T. Erdogan, Tughrul Arslan, *Antenna Array with Wide Angle Scanning Properties*, 6th European Conference on Antennas and Propagation Prague (EuCAP 2012), Czech Republic, March 26-29, 2012, pp. 1636 - 1640.

N. H. Noordin, W. Zhou, Nakul Haridas, Ahmed O. El-Rayis, Ahmet T. Erdogan, Tughrul Arslan, *Single-Feed Polarization Reconfigurable Patch Antenna*, Antennas and Propagation Society International Symposium (APSURSI 2012), Chicago, Illinois, USA July 8-14, 2012, pp. 1 - 2.

N. H. Noordin, Ahmet T. Erdogan, Brian Flynn, Tughrul Arslan, *Compact Directional Patch Antenna with Slotted Ring for LTE Frequency Band*, Loughborough Antennas & Propagation Conference 2012 (LAPC 2012), Loughborough, UK, November 12-13, 2012.

N. H. Noordin, Ahmet T. Erdogan, Brian Flynn, Tughrul Arslan, *Compact Directional Patch Antenna with Slotted Ring for LTE Frequency Band*, Loughborough Antennas & Propagation Conference 2012 (LAPC 2012), Loughborough, UK, November 12-13, 2012.

N. H. Noordin, Yan Chiew Wong, Ahmet T. Erdogan, Brian Flynn, Tughrul Arslan, *Meandered Inverted-F Antenna for MIMO Mobile Devices*, Loughborough Antennas & Propagation Conference 2012 (LAPC 2012), Loughborough, UK, November 12-13, 2012.

Rahmat Sanudin, **N. H. Noordin**, Tughrul Arslan, *DOA Estimation Using Modified Covariance Matrix*, Loughborough Antennas & Propagation Conference 2012, Loughborough, UK, November 12-13, 2012.

2011

N. H. Noordin, Ahmed O. El-Rayis, Nakul Haridas, Ahmet T. Erdogan, Tughrul Arslan, *Triangular Lattices for Mutual Coupling Reduction in Patch Antenna Arrays*, Loughborough Antennas & Propagation Conference 2011 (LAPC 2011), Loughborough, UK, November 14-15, 2011, pp. 1-4.

N. H. Noordin, Virgilio Zuniga, Ahmed O. El-Rayis, Nakul Haridas, Ahmet T. Erdogan, Tughrul Arslan, *Uniform Circular Arrays for Phased Array Antenna*, Loughborough Antennas & Propagation Conference 2011 (LAPC 2011), Loughborough, UK, November 14-15, 2011, pp. 1-4.

Wei Zhou, **N. H. Noordin**, Nakul Haridas, Ahmed O. El-Rayis, Ahmet T. Erdogan, Tughrul Arslan, *A WiFi/4G Compact Feeding Network for an 8-Element Circular Antenna Array*, Loughborough Antennas & Propagation Conference 2011 (LAPC 2011), pp. 1-4, Loughborough, UK, November 14-15, 2011.

Rahmat Sanudin, **N. H. Noordin**, Ahmed O. El-Rayis, Nakul Haridas, Ahmet T. Erdogan and Tughrul Arslan, *Analysis of DOA Estimation for Directional and Isotropic Antenna Arrays*, Loughborough Antennas & Propagation Conference 2011 (LAPC 2011), pp. 1-4, Loughborough, UK, November 14-15, 2011.

Rahmat Sanudin, **N. H. Noordin**, Ahmed O. El-Rayis, Nakul Haridas, Ahmet T. Erdogan and Tughrul Arslan, *Capon-Like DOA Estimation Algorithm for Directional Antenna Arrays*, Loughborough Antennas & Propagation Conference 2011 (LAPC 2011), pp. 1-4, Loughborough, UK, November 14-15, 2011.

Haoyu Zhang, **N. H. Noordin**, Ahmet T. Erdogan, Tughrul Arslan, *Smart Antenna Array for Brain Cancer Detection*, Loughborough Antennas & Propagation Conference 2011 (LAPC 2011), pp. 1-4, Loughborough, UK, November 14-15, 2011.

Yan Chiew Wong, **N. H. Noordin**, Ahmed O. El-Rayis, Nakul Haridas, Ahmet T. Erdogan, Tughrul Arslan, *An Evaluation of 2-phase Charge Pump Topologies with Charge Transfer Switches for Green Mobile Technology*, 20th IEEE International Symposium on Industrial Electronics (ISIE 2011), pp. 136-140, Poland, Jun 27-30, 2011.

1.4 Thesis structure

In Chapter 2, a polarisation reconfigurable microstrip antenna is proposed. Microstrip antenna design techniques to achieve circular polarisation are discussed. The proposed antenna achieves different polarisation states, namely, linear polarisation (LP), left-hand circular polarization (LHCP) and right-hand circular polarisation (RHCP), by perturbing the

shape of its main radiating structure. Key dimensions of the antenna are varied in order to understand their effect on the radiation properties of the antenna.

Chapter 3 explores the design of an array with wide scan coverage for use in wireless communication systems. Various configurations such as a uniform linear array, a uniform circular array and faceted arrays, are considered. The influence of different design parameters, such as number of elements, separation between elements and orientation of the elements, to the scanning range of the array is analysed. This chapter also presents the procedures of synthesising the 3-faceted array for low sidelobe level. Phase corrections together with amplitude tapering technique are used, which allows the faceted structure to be synthesised for low sidelobe level (SLL) in a similar way to the linear array. Amplitude tapering techniques discussed in this chapter include conventional windows, such as Binomial and Hamming Windows, and tuneable windows, such as Taylor and Kaiser Windows.

In Chapter 4, the performances of the faceted arrays, described in Chapter 3, are evaluated. The faceted arrays are compared in the context of adaptive beamforming properties. The beamforming is achieved with two different optimisation criteria, namely, minimum MSE and maximum SINR. This chapter also discusses beamforming algorithms for wireless communication systems. Beamforming algorithms using different optimisation criteria, namely, minimum Mean Square Error (MSE), blind beamforming, maximum signal-to-interference ratio (SINR) and power minimisation are explored. The adaptive algorithms and biologically inspired algorithms are used in order to achieve the criteria.

Chapter 5 discusses the beamforming implementation strategy is which are the single-port and multi-port beamforming architectures. A single-port beamforming technique using pseudo-inverse function is proposed and implemented in the beamforming algorithm that uses minimum MSE as the optimisation criteria. Radiation patterns generated by this technique are then compared with the multi-port beamforming system.

Chapter 6 summarises and concludes this thesis. In addition, the contribution of this thesis is re-highlighted and further research based on the techniques developed in this thesis is suggested.

1.5 Summary

Adaptive array antennas have the potential to be used in wireless communication devices. The technology could optimise the wireless channel usage while minimising the power consumption of the devices. However, due to high implementation cost and hardware complexity, adaptive array antennas are not used commercially. This thesis proposes an adaptive array antenna design for wireless communication devices, where particular attention is given to:

i. low-profile reconfigurable antenna design,

ii. wide scanning range array design, and

iii. single-port beamforming technique.

Chapter 2
Polarisation Reconfigurable Antenna Design

2.1 Introduction

This chapter discusses the design of a polarisation reconfigurable antenna for use in wireless communication systems. The radiation pattern of an adaptive array antenna is dependent on the individual radiation pattern of the array element and the geometry of the array. An array of directional antennas will generate a radiation pattern with narrow main beam. This kind of array is better suited to systems with limited power and those that involve data communication with known locations. Apart from that, low profile antennas, such as microstrip antennas, are more suitable than other types of antenna due to the limited space available on wireless communication devices. Therefore, besides having the ability to radiate different polarised waves, the antenna should be compact and have a directional radiation pattern. This chapter is divided into seven sections. The theory behind the antenna design is presented in Section 2.2 and Section 2.3 discusses the designs of existing polarised reconfigurable antenna. The proposed antenna structure is modelled in CST Design Suite 2011 and the analysis of varying key dimensions on the antenna performance is discussed in Section 2.4 and Section 2.5, respectively. The performance on the antenna is discussed in Section 2.6 and finally, Section 2.7 summaries the chapter.

2.2 Antenna Theory

An antenna is a device that radiates electromagnetic energy from electric current. A desired electromagnetic radiation distribution of an antenna, normally termed as radiation pattern, is achieved by controlling the current flow on the antenna. The antenna is an essential block in a radio link, as it is the critical transition unit between the wireless devices and the communication medium. Figure 2.1 illustrate the antenna as a transition device. There are various types of antennas, as shown in Figure 2.2, which include wire antennas, aperture antennas and microstrip antennas.

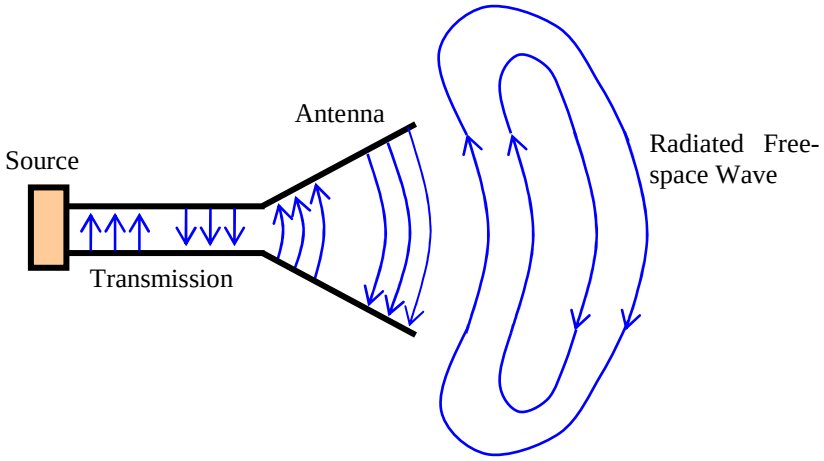

Figure 2.1: Antenna as a transition device [35].

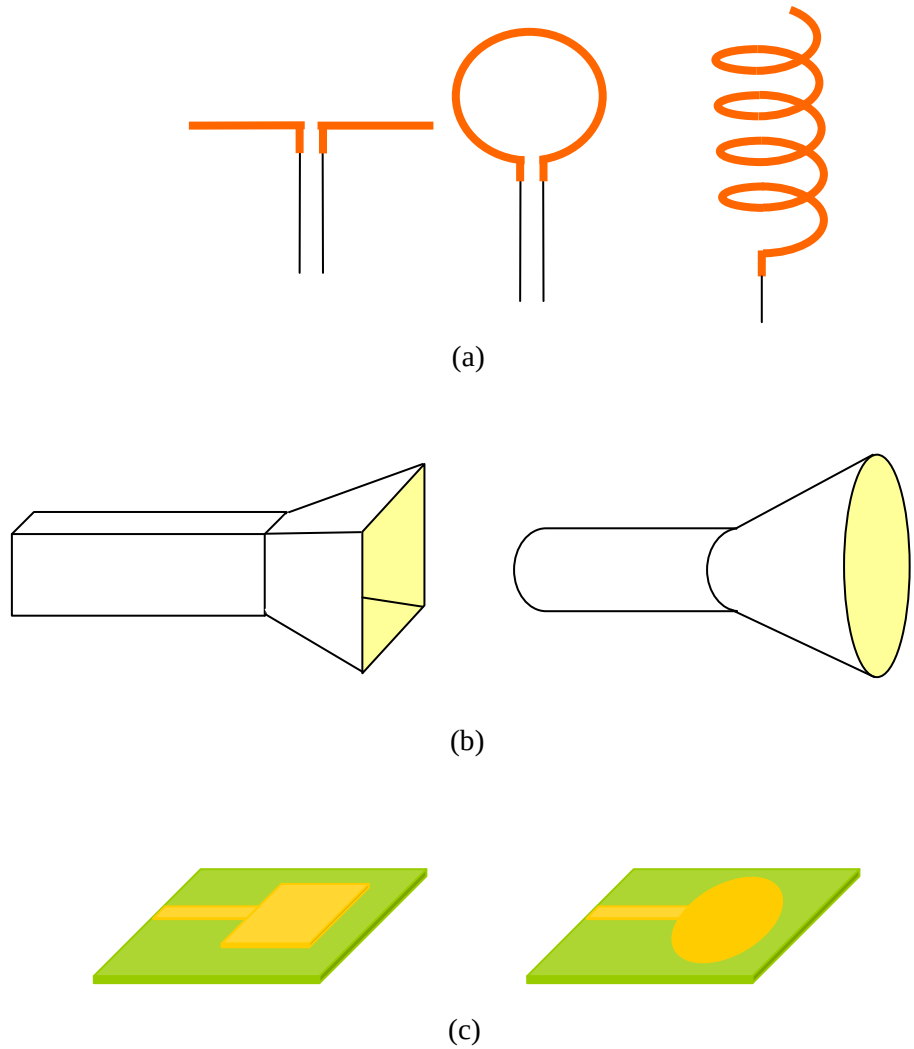

Figure 2.2: Types of antenna, (a) wire antenna, (b) horn antenna, and (c) microstrip antenna [35].

2.2.1.1 Antenna Properties

The circuit representation of a transmitting antenna is illustrated in Figure 2.3 [35]. The antenna impedance, Z_A, is given by Equation (2.1).

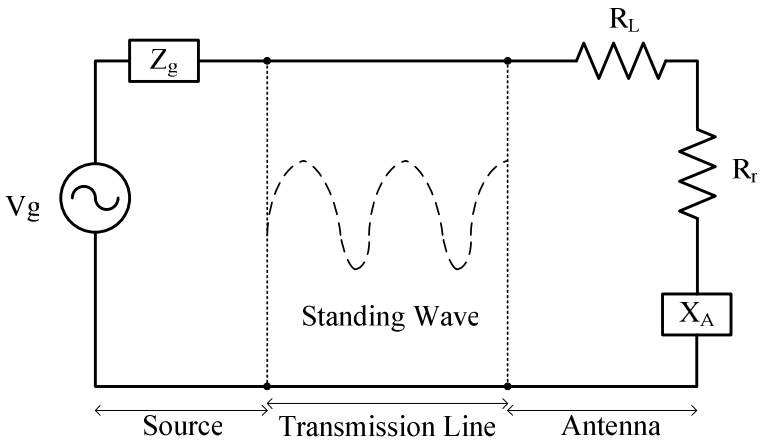

Figure 2.3: Transmission-line for Thevenin equivalent of antenna in transmitting mode [35].

$$Z_A = (R_L + R_r) + jX_A \tag{2.1}$$

where R_L is the loss resistance, R_r is the radiation resistance and jX_A is antenna reactance.

By matching the impedance of the antenna to the characteristic impedance of the transmission line, the standing waves can be reduced, and the energy storage capacity of the line minimised [35]. Hence, maximum power is transferred from the source to the antenna. This condition is given by Equation (2.2) [35].

$$\begin{aligned} R_g &= R_r + R_L \\ X_g &= -X_A \end{aligned} \tag{2.2}$$

where R_s is the source resistance, R_a is the antenna resistance, X_s is the source impedance and X_a is the antenna impedance.

In practice, the power reflected from the antenna, as illustrated above, is described using S-parameter. The S-parameters describe the input-output relationship between ports in an electrical system. S_{11} represents how much power is reflected from the antenna, and is sometimes called as the reflection coefficient.

The radiated power density, P_r (Watts/m^2), is the average power radiated by an antenna in a particular direction and is obtained by the time-averaging Poynting vector. The power density can be described by Equation (2.3).

$$P_r(r,\theta,\phi) = \frac{1}{2}\left[E \times H^*\right] = \frac{1}{2\eta}\left|\overline{E}(r,\theta,\phi)\right|^2 \tag{2.3}$$

where E is the electric field intensity, H is the magnetic field intensity and η is the intrinsic impedance.

Radiation power of the antenna per unit solid angle can be described by its radiation intensity, U (Watts/unit solid angle), as described by Equation (2.4).

$$U = r^2 P_r \tag{2.4}$$

The total power radiated by the antenna, P_{tot}, in the spherical coordinates as illustrated in Figure Figure 2.4, is given by Equation (2.5).

$$P_{tot} = \int_0^{2\pi}\int_0^{\pi} U(\theta,\phi)\sin(\theta)\delta\theta\delta\phi \tag{2.5}$$

The directivity of the antenna can be calculated using Equation (2.6) [35]. Directivity of an antenna is influenced by its aperture size. The microstrip antenna has higher directivity when lower permittivity substrate is used as lower permittivity would result in larger radiating patch.

$$D = \frac{4\pi U_{\max}(\theta,\phi)}{P_{tot}} \tag{2.6}$$

where P_{tot} is the total radiated power and $U_{\max}(\theta,\phi)$ is the maximum radiation intensity.

The gain of antenna can be described using Equation (2.7) [35].

$$Gain = \frac{4\pi U(\theta,\phi)}{P_{in}} \tag{2.7}$$

where P_{in} is the input power and $U(\theta,\phi)$ is the radiation intensity.

The antenna radiation efficiency is given by Equation (2.8) [35].

$$e_{cd} = \frac{P_{rad}}{P_{in}} \tag{2.8}$$

where P_{rad} is the total radiated power and P_{in} is the total input power to the antenna.

2.2.1.2 Microstrip Antenna

The microstrip antenna offers a number of advantages including low profile, and low cost, which makes it attractive for use in wireless communication devices [35]. Basic structure of a microstrip antenna is illustrated in Figure 2.4. The antenna consists of a conductor strip on a grounded dielectric substrate. The metal conductor can be in various shapes such as circular and square.

The substrates that are normally used in a microstrip antennas are ceramic (ε_r = 10), air (ε_r = 1), FR4 (ε_r = 4.3) or glass (ε_r = 5.5). The thickness of the substrate influences the impedance bandwidth and the radiation efficiency. The thickness of the substrates is proportional to the impedance bandwidth, while its permittivity is inversely proportional to the impedance bandwidth.

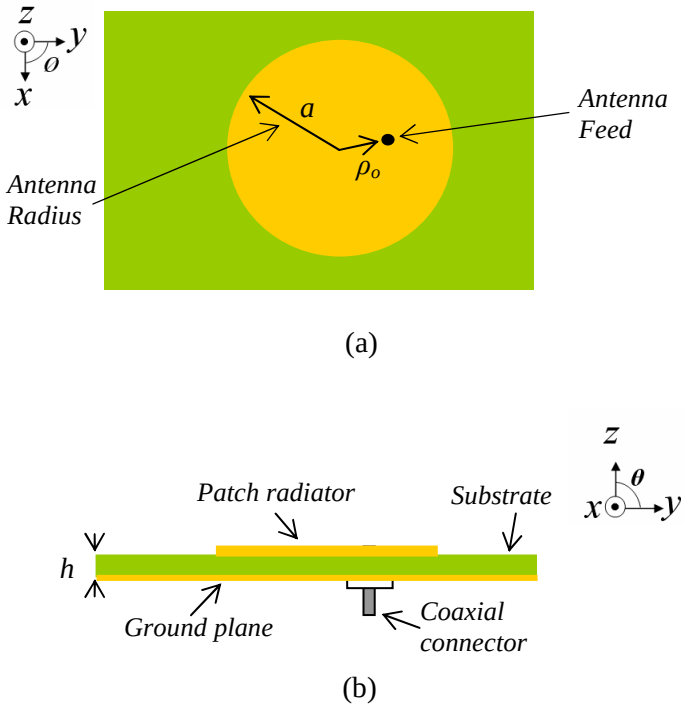

Figure 2.4: Microstrip antenna structure (a) top view, and (b) side view [35].

The resonant frequency of a circular shaped microstrip antenna for TM^{z}_{mn0}, described using cavity model, is given by Equation (2.9) [35].

$$(f_r)_{mn0} = \frac{1}{2\pi\sqrt{\mu\varepsilon}}\left(\frac{x'_{mn}}{a_e}\right) = \frac{1.8412}{2\pi a_e\sqrt{\mu\varepsilon}} \tag{2.9}$$

where a_e is the effective area of the microstrip patch that takes into account the fringing effects and x'_{mn} represents the zero derivative of Bessel function $J_m(x)$ ($x'_{11} = 1.8412$).

2.2.1.3 Radiation Pattern

The radiation properties of an antenna as a function of angle can be graphically represented by its radiation pattern [36]. Generally, the radiation pattern of an antenna is classified in three categories, which are isotropic, directional and omni-directional. Isotropic radiation is generated when the antenna has equal radiation in all direction. Antenna with uniform radiation is not physically realisable, but often used as reference to describe the directive properties of actual antennas [35]. An antenna that generates a stronger radiation in one direction is known to have a directional radiation pattern and it consists of several lobes, as

depicted in Figure 2.5. The lobe with the strongest radiation intensity is known as the major lobe while the others are called sidelobes. The width of the main lobe is estimated by the angular separation between its half-power points (3 dB), as shown in Figure 2.5, and normally termed as half power beamwidth (HPBW). Finally, an antenna is said to radiate an omni-directional pattern when it has a non-directional pattern in a given plane and a directional pattern in any orthogonal plane [35].

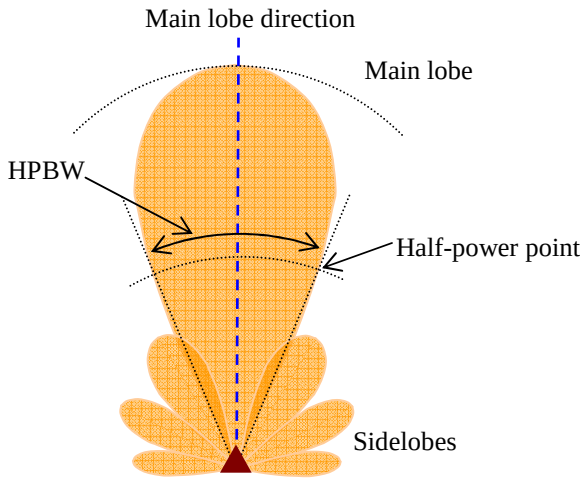

Figure 2.5: Directive radiation pattern.

2.2.1.4 Antenna Polarisation

The polarisation of an antenna describes the electric field orientation of the propagated wave, as shown in Figure 2.6. In general, it can be categorised into linear polarisation and circular polarisation. The electric field of a linearly polarised antenna is directed along a line, while a circularly polarised antenna radiates a wave in a corkscrew pattern making one complete revolution in each wavelength. This rotation is either in a clockwise, right-hand circularly polarised (RHCP), or anti-clock wise, left-hand circularly polarised (LHCP).

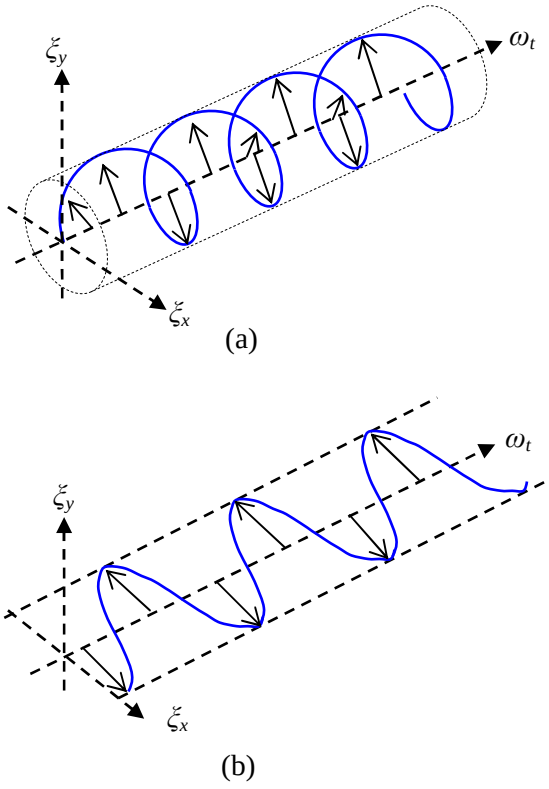

Figure 2.6: Rotation of the waves, (a) circular polarisation, and (b) linear polarisation.

Antenna with polarisation reconfiguration is capable of increasing the number of channels in a communication link, due to its ability to switch from one polarisation state to another. In order to achieve this, the polarisation changes of the antenna should have minimal effects on the operating frequency of the antenna [18]. Techniques that can be used to achieve circular polarisation with microstrip antennas include dual-feed with delay line and single-feed with nearly degenerate eigenmodes. Microstrip antennas with dual-feed technique generate circularly polarised radiation when two identical orthogonal modes are excited to a symmetrical shape patch [35]. The orthogonal modes need to be 90° out-of-phase with respect to time, and this can be achieved either by using 90° hybrid phase shifters, as shown in Figure 2.7 (a), or by having dual feed with delay line, as illustrated in Figure 2.7 (b). However, as seen in the figure, the technique requires an external polariser to be attached to the antenna. This method complicates the fabrication of the antenna and is undesirable especially in wireless communication devices.

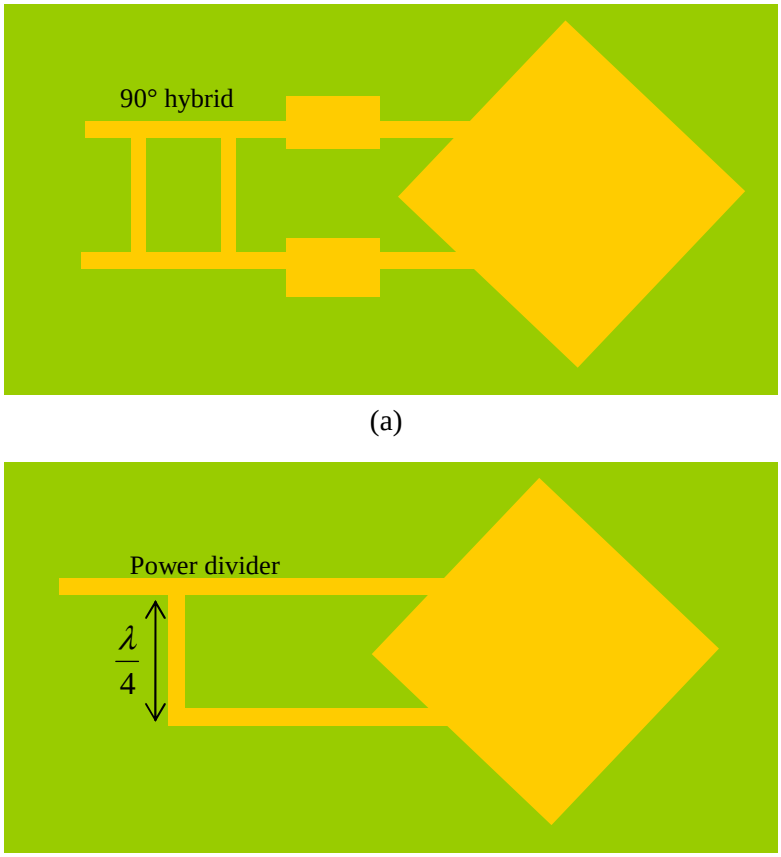

Figure 2.7 Microstrip antenna driven at adjacent sides through a, (a) 90° hybrid, and (b) power divider [35].

A circularly polarised antenna can also be achieved by using single-feed structures, where the circularly polarised wave can be generated by exciting a quasi-symmetrical shape that supports the two degenerated modes [37]. This can be achieved by proper optimisation of the patch dimensions and probe position. An example of the microstrip design is illustrated in Figure 2.8 (a) [38]. The antenna yields LHCP at boresight when the feed is placed at the left diagonal corner while RHCP is obtained when the feed is placed at the opposite corner. Another method to create circular polarisation radiation is by having an elliptical patch, as illustrated in Figure 2.8 (b) [39].

Alternatively, a truncated square antenna, as shown in Figure 2.8 (c), can be used to generate circular polarised radiation. The antenna consists of a square-shaped radiating structure with two of its opposite corners truncated. The removed corners result in higher resonant frequency along the truncations compared to that along the other edges of the structure [40].

Using similar approach, circular polarisation is also achieved when the circular-shaped microstrip is loaded with a pair of notches as shown in Figure 2.8 (d) [41]. The notches create two degenerated orthogonal modes on the structure and produce circularly polarised waves.

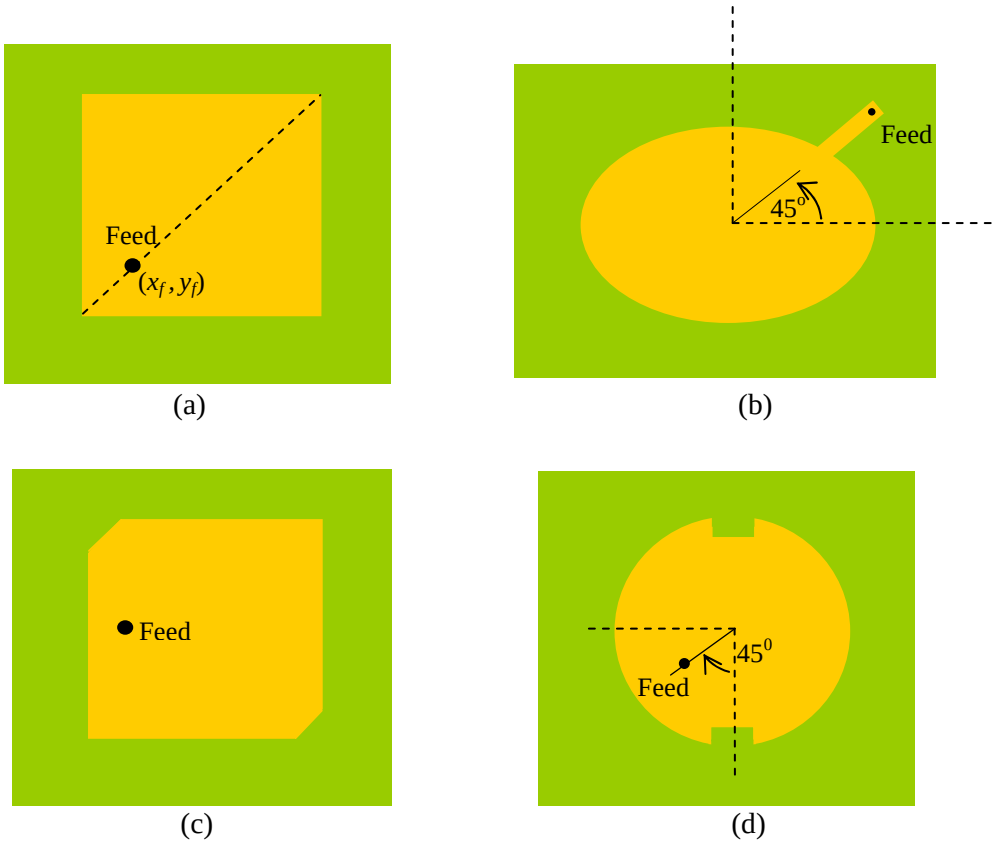

Figure 2.8: single-feed microstrip antenna design techniques for circular polarisation, (a) diagonal feed [38], (b) elliptical microstrip antenna shaped [39], (c) truncated square[40], and (d) circular patch with notches [41].

2.3 Polarisation Reconfigurable Antenna

As previously mentioned, using reconfigurable antennas as the element of an adaptive array antenna is another way of reducing the cost of an adaptive array antenna [16, 17]. In general, reconfigurable antennas are antenna structures that can alter their operating frequencies, polarisation and radiation pattern [14-19]. Adaptive arrays with reconfigurable antennas have the ability to reconfigure the antenna properties for adaptation, additional functionality and versatility [15]. Antennas with polarisation diversity can be used to increase the capacity of a wireless communication channel and can reduce multi-path effects [15, 20-22]. This is important especially when reliable and high quality signal transmission is required, such as

in wireless communication systems. For these reasons, antenna design with polarisation reconfiguration is targeted in this thesis.

2.3.1 Single-feed Polarisation Reconfigurable Antenna

Several single-feed patch antennas with reconfigurable polarisation have been previously proposed [42-45]. One such antenna is the corner-truncated inset-feed antenna, where its polarisation state can be switched by controlling the connection between the radiating patch and the triangular conductors on the edges of the antenna as shown in the structure of the antenna in Figure 2.9 [42]. The truncated structure causes the antenna to have two orthogonal resonant modes for circular polarisation. To operate in RHCP mode, the right top corner and the left bottom corner are connected to the main radiating structure. Similarly, LHCP mode is obtained by connecting the main radiating structure to the left top corner and the right bottom corner. In both polarisation modes, the antenna operates at 1.56 GHz with an impedance bandwidth of 1.8% and axial bandwidth of 1.5%.

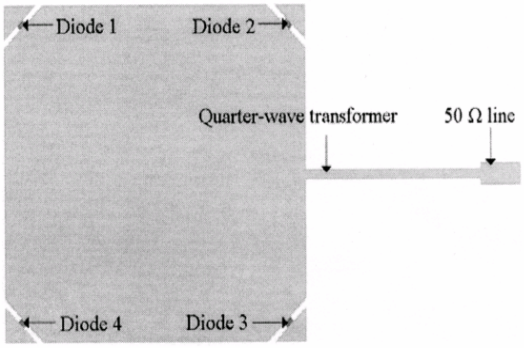

Figure 2.9: Polarisation reconfigurable antenna – inset feed square microstrip [42].

Different polarisation states of an inset-feed antenna are achieved by controlling the connection between the arc and the radiating element as shown in Figure 2.10 [43]. The antenna radiates a linearly-polarised wave when the sides of the arc are connected to the antenna, while a circularly polarised wave is obtained when either side of the arc is connected. The antenna operates at 2.45 GHz and has impedance bandwidth and axial ratio bandwidth of 1.2% and 0.7%, respectively.

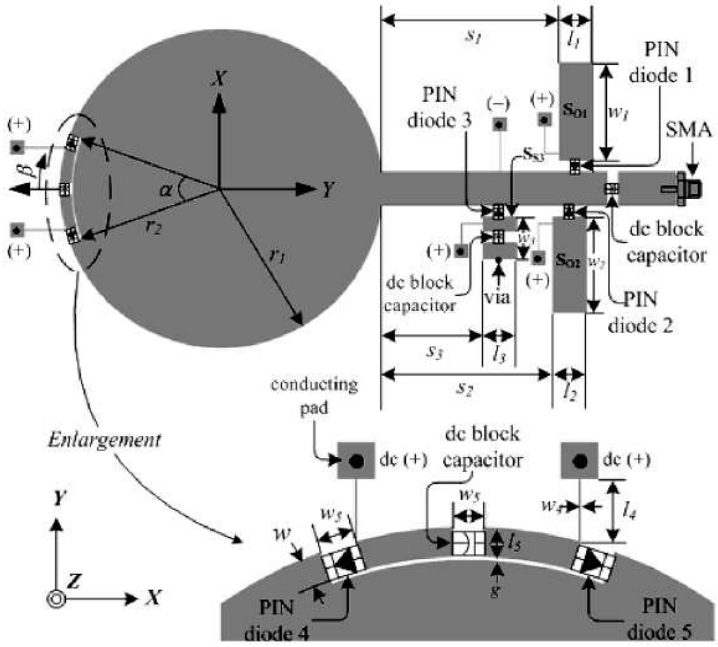

Figure 2.10: Polarisation reconfigurable antenna – inset feed circular microstrip [43].

The aperture-coupling fed antenna, shown in Figure 2.11, obtains its polarisation diversity by connecting the radiating structure to an additional rectangular perturbation patch [44]. In the initial state, the antenna radiates linearly-polarised waves and with the connection, circular polarisation state is achieved. The antenna operates at 2.45 GHz and has an axial bandwidth ratio of 2.2%. RF choke is used to block higher-frequency alternating current in an electrical circuit, while allowing lower frequency current to pass.

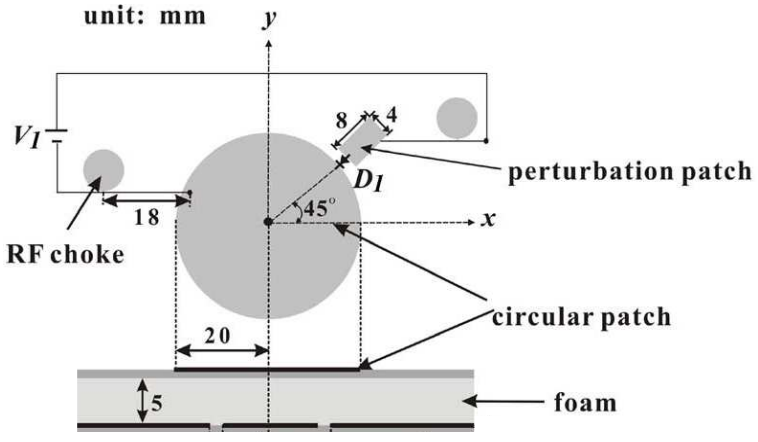

Figure 2.11: Polarisation reconfigurable antenna – additional structure [44].

The shape of an antenna can also be altered by embedding slits into the radiating structure [45]. Different polarisation states are then achieved by controlling the shape of the slits at the edge of the antenna, as shown in Figure 2.12.

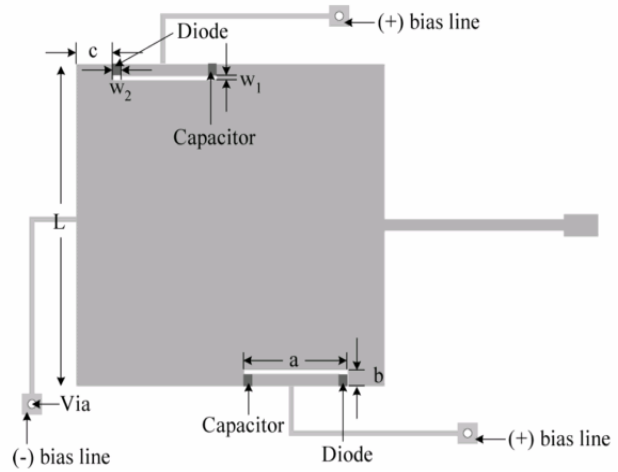

Figure 2.12: Polarisation reconfigurable antenna – slit [45].

By modifying the shape of the radiating structure, the antennas mentioned above radiate circularly-polarised waves. However, the overall dimensions of these antennas are increased because the antennas are geometrically asymmetric due to the inserted feeding structure [42, 43, 45] and have bulky perturbation structures [44]. Apart from that, the feed structure could also contribute to the overall radiation pattern of the antenna. Hence, a compact single-feed circular patch antenna with polarisation reconfiguration is proposed and discussed in this chapter.

2.4 Single-Feed Polarisation Reconfigurable Antenna Design

The proposed antenna consists of a circular radiating structure with four identical notches filled with rectangular parasitic elements. The polarisation state of the antenna, namely, linear polarisation (LP), RHCP and LHCP is achieved by controlling the connections between the notches and the parasitic elements. The antenna is modelled and simulated in CST Design Suite 2011. CST determines the required antenna parameters, such as input impedance, mutual coupling, near field and far field, by dividing the antenna structure into smaller segments and calculating the current density of each segment. The antenna is illustrated in in Figure 2.13.

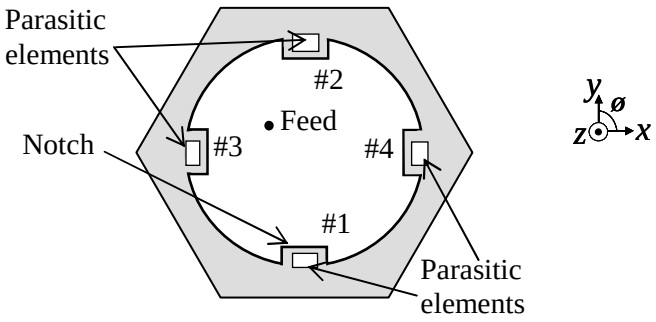

Figure 2.13: The structure of the proposed antenna.

Detailed dimensions of the antenna are shown in Table 2.1. The polarisation characteristics of the antenna are divided into three cases depending on the bias of the connections between the radiating structure and the parasitic elements.

Table 2.1: Dimensions of the Proposed Antenna.

Parameter	Dimension (mm)
Patch radius (a_p)	34
Notch width (n_w)	4
Gap width (w_g)	0.5
Parasitic element	1.3 x 2.7
Ground plane size	64
Substrate	FR4 (ε_r = 4.3)

The operational mode of the antenna is illustrated in Figure 2.14. The antenna is linearly polarised when the structure is physically and electrically symmetrical, in which case all the notches are either disconnected (ANT 1 - Figure 2.14 (a)) or connected (ANT 2 - Figure 2.14 (b)) with the parasitic elements. In order to obtain two orthogonal near-degenerate resonant modes for LHCP (ANT 3 - Figure 2.14 (c)), the structure is modified by connecting the notch pair (#1 and #2) to the antenna. Similarly, RHCP (ANT 4 - Figure 2.14 (d)) is obtained when the notch pair (#3 and #4) is connected to the antenna.

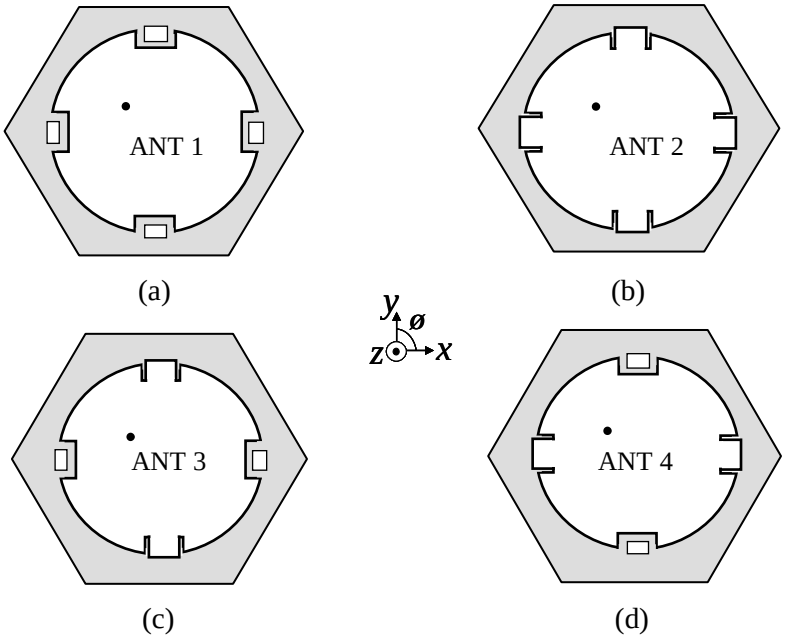

Figure 2.14: The polarisation mode of the proposed antenna, (a) ANT 1 - LP, (b) ANT 2 - LP, (c) ANT3 - LHCP, and (d) ANT4 - RHCP.

The simulated current distribution on the antenna with respect to time at the operating frequency is depicted in Figure 2.15. In LHCP mode, as shown in Figure 2.15 (a), it is observed that the surface current flows in a clockwise direction, contrary to RHCP mode, as shown in Figure 2.15 (b), where the surface current flows in an anti-clockwise direction.

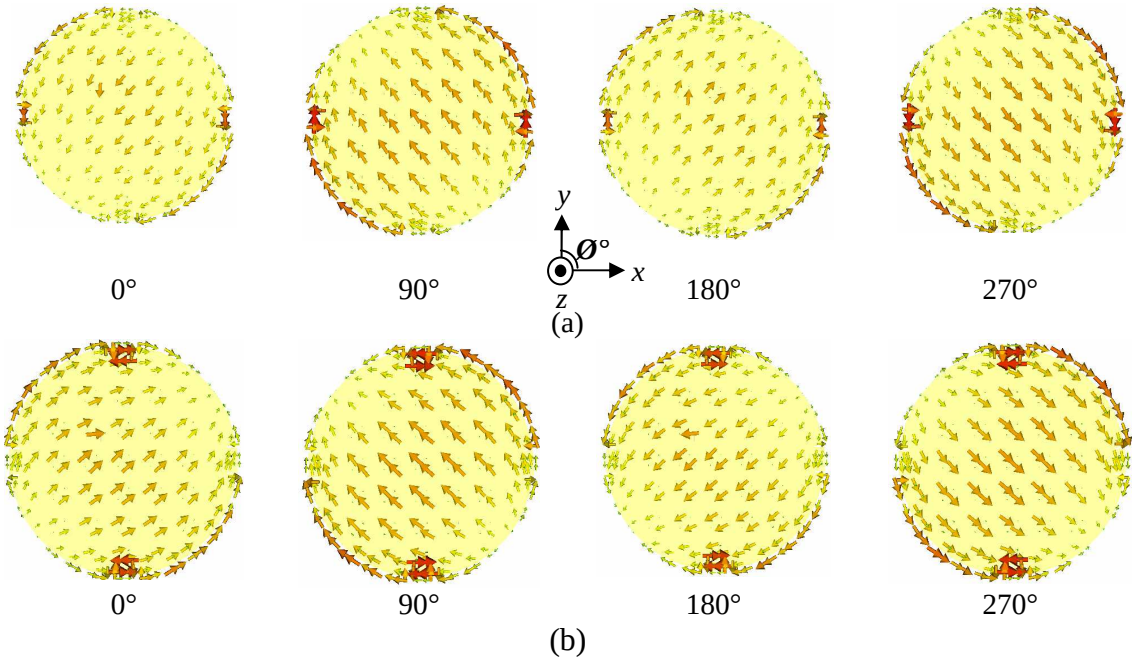

Figure 2.15: Simulated current flow of the proposed antenna. (a) LHCP, and (b) RHCP.

2.5 Parametric Analysis

The aim of this study is not only to understand the frequency shifts of the antenna, but also to obtain a good axial ratio in order to maintain the circular polarisation characteristic of the antenna. The frequency shift and circular polarisation characteristic is monitored for S_{11} values that are less than -10 dB and for axial ratio values that are less than 3 dB. The parameters observed are the patch diameter (a_p), notch width (n_w) and the separation between the notch and the parasitic element (w_g). A parametric study is carried out on ANT 3 (LHCP) structure by varying only one parameter at a time while keeping the other parameters constant at the assumed optimum value.

2.5.1 Patch Diameter

In this study, the simulated results for various antenna diameters are plotted in Figure 2.16. It is noted that the operating frequency increases as the diameter decreases, where the minimum S_{11} is at 2.45 GHz, with patch diameter of 33 mm. Similarly, it is observed from the axial ratio plot that the minimum AR point shifts corresponding to the patch diameter. Hence, it can be concluded that the patch size determines the operating frequency and the circular polarisation characteristics of the antenna.

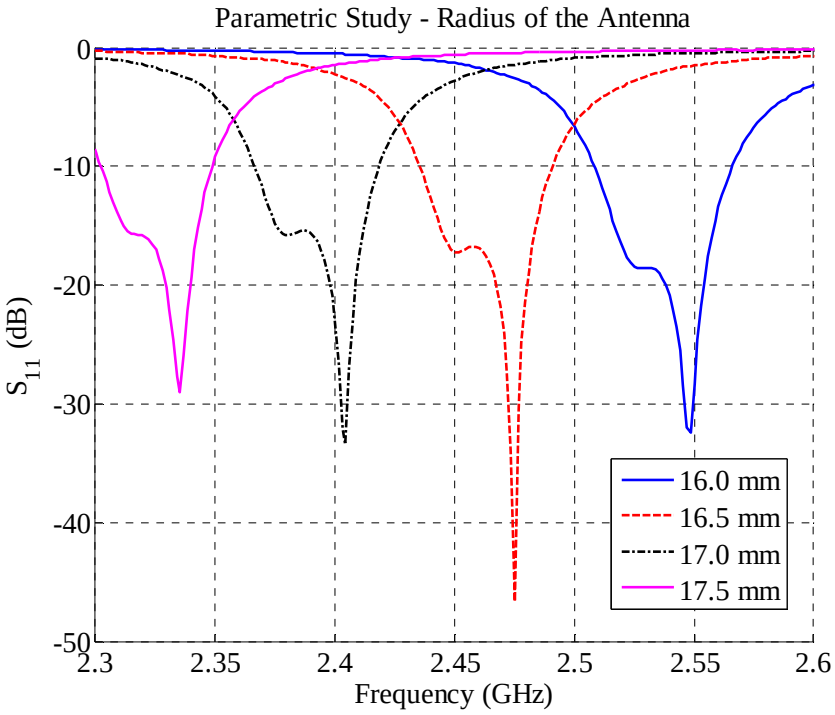

(a)

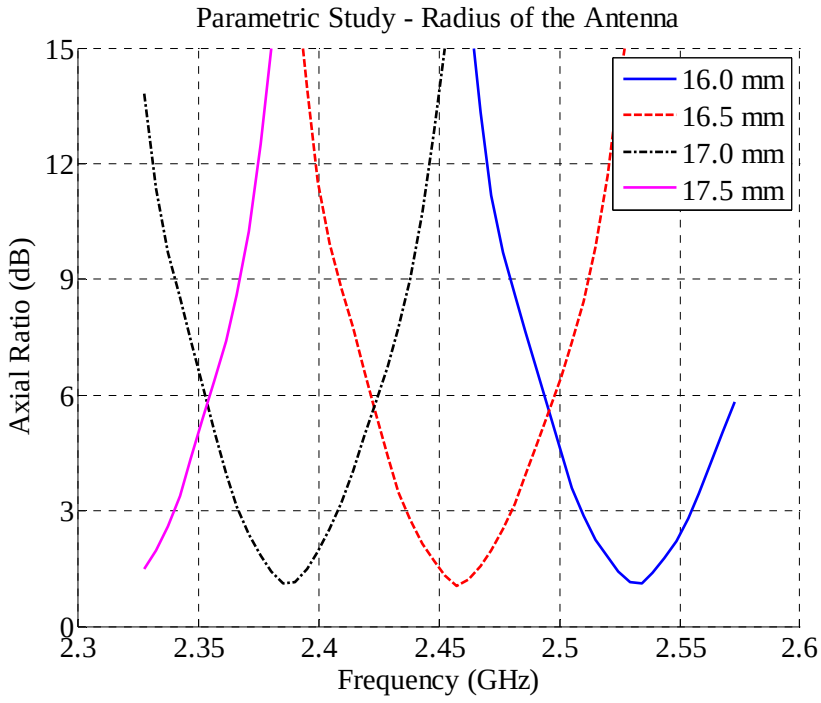

(b)

Figure 2.16: The effects of varying patch diameter (a) reflection coefficient, and (b) axial ratio.

2.5.2 Notch Size

The simulated S_{11} and axial ratio of the antenna when the notch width (n_w) is varied is shown in Figure 2.17. As n_w increases, the minimum S_{11} point is shifted towards a higher resonant frequency while the value of the axial ratio decreases. These results indicate that the minimum size of the notch of 2 mm is required in order to retain the circular polarisation characteristic of the proposed antenna. This notch size also influences the resonant frequency of the antenna.

2.5.3 Gap Size

Another parameter that is observed is the gap between the notch and the parasitic element, w_g, shown in Figure 2.18. As seen in the Figure 2.18 (a), wider gaps result in lower axial ratios. However, this also comes with a trade-off in a shifted minimum resonant frequency point as shown in Figure 2.18 (b).

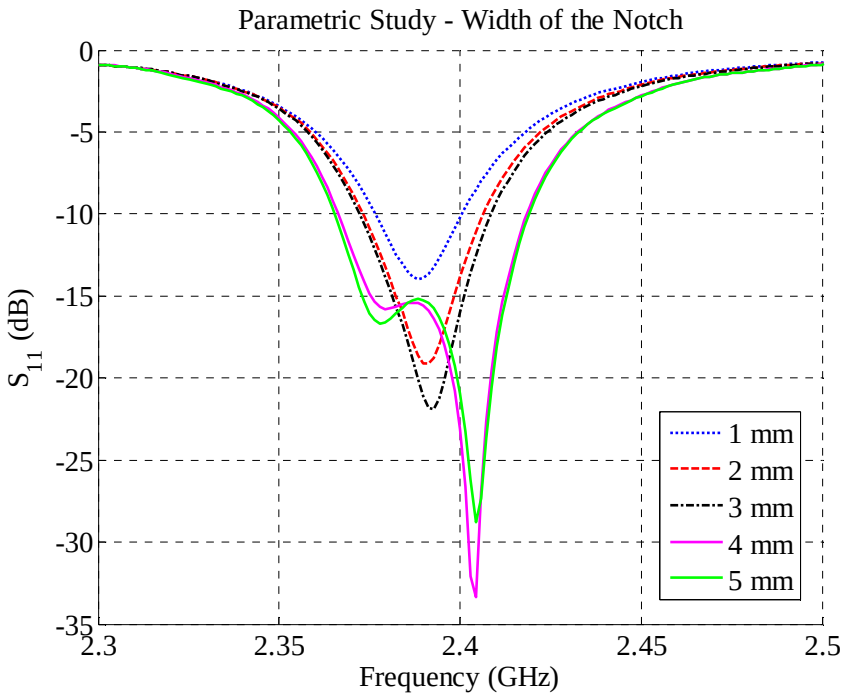

(a)

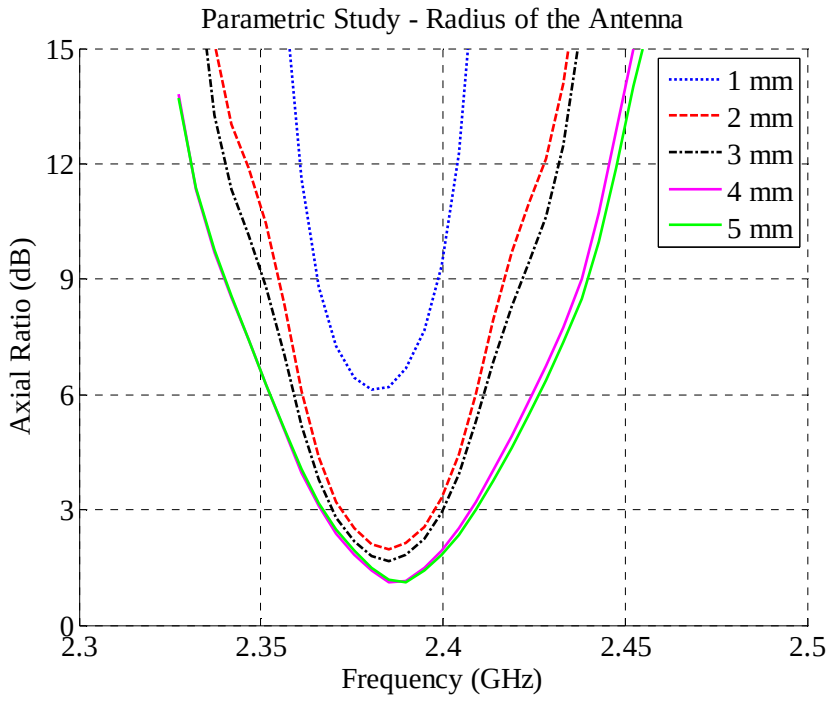

(b)

Figure 2.17: The effects of varying notch size (a) reflection coefficient, and (b) axial ratio.

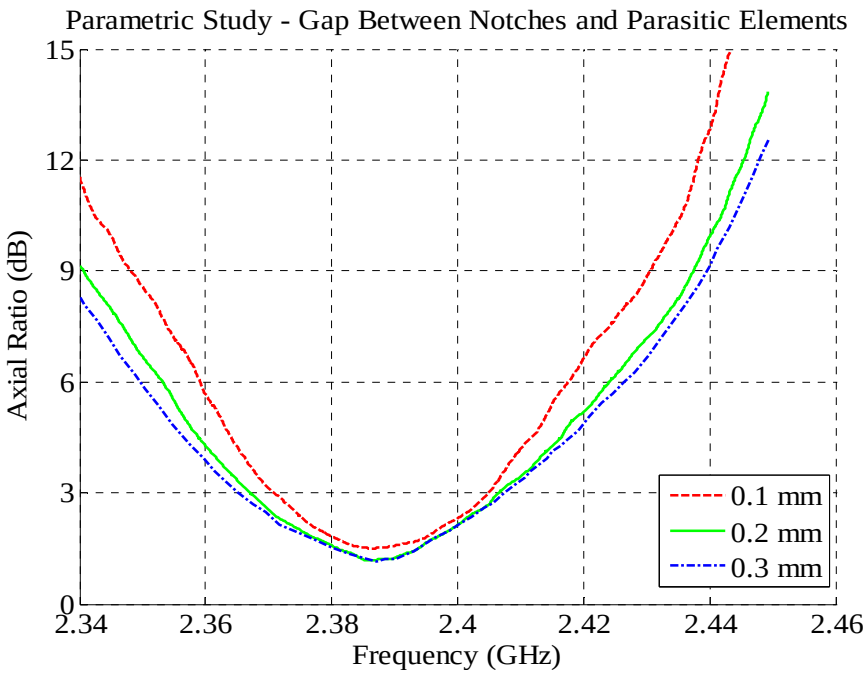

(a)

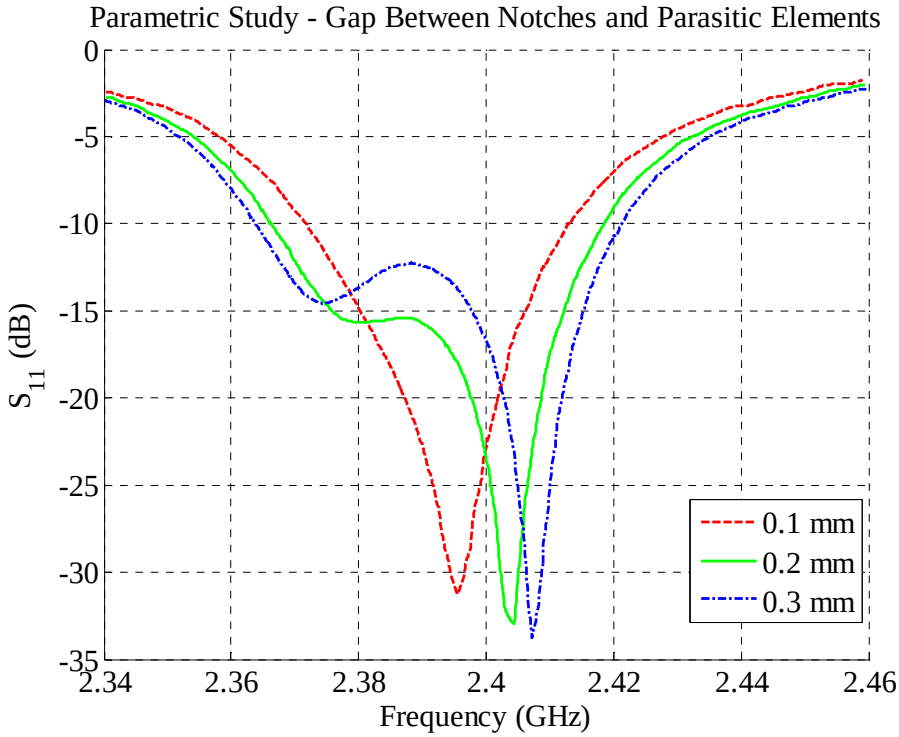

(b)

Figure 2.18: The effects of varying gap (a) reflection coefficient, and (b) axial ratio.

2.5.4 Ground shape

Finally, the shape of the substrate and ground plane of the antenna is analysed. As shown in Figure 2.19, three shapes are considered, namely, square, triangular, and hexagonal shape. The corresponding reflection coefficient and axial ratio for the ground shapes of different sizes are plotted in Figure 2.20. From the results, all the three variations retain the radiation properties of the antenna, as the S_{11} and axial ratio are less than -10 dB and 3 dB respectively.

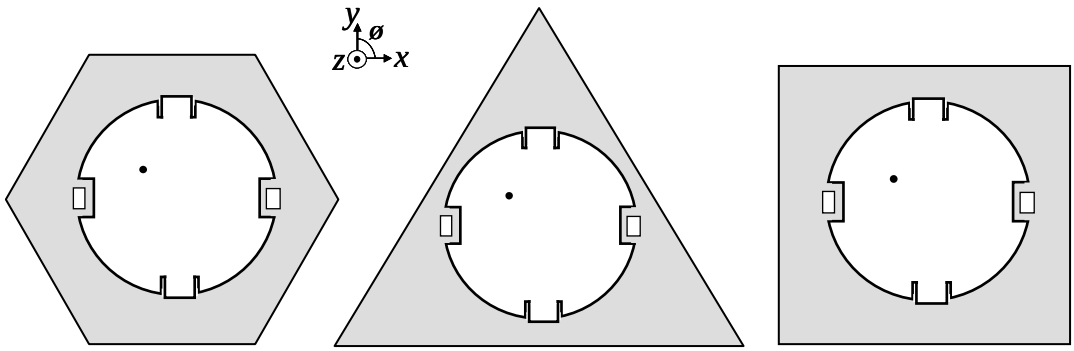

(a) (b) (c)

Figure 2.19: Various ground shape, (a) hexagonal, (b) triangle, and (c) square.

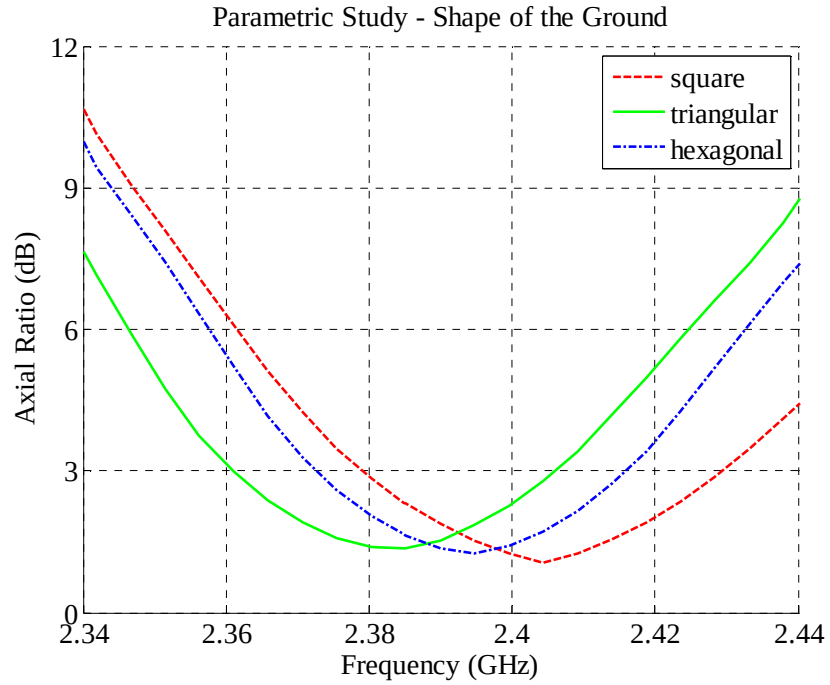

(a)

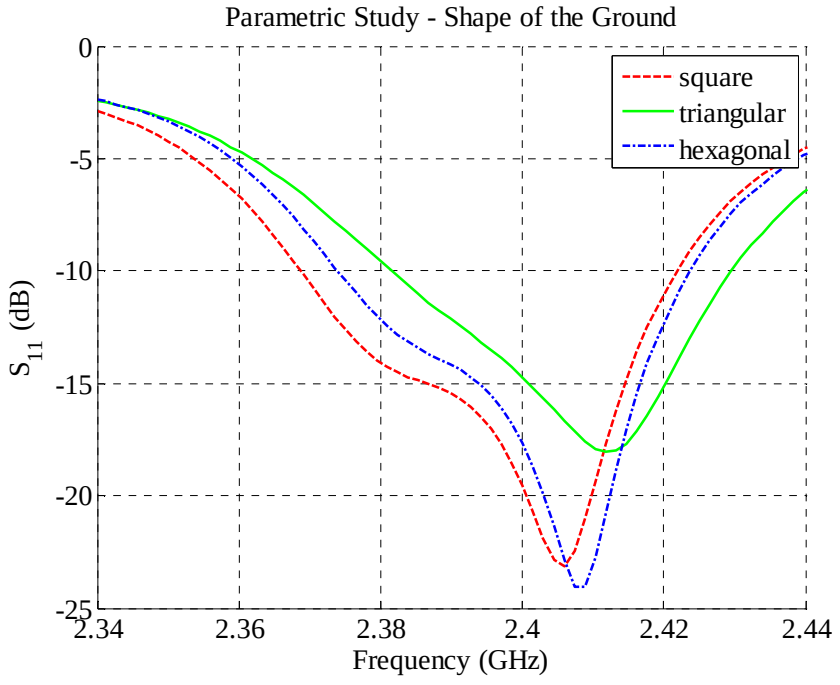

(b)

Figure 2.20: The effects of varying gap (a) reflection coefficient, and (b) axial ratio.

2.6 Performance and Discussion

2.6.1 Resonant Frequency

Figure 2.21 shows the fabricated antenna. Good impedance matching is achieved for all polarisation states, as shown in Figure 2.22. The S-parameter of the antenna is measured using network analyser (HP8510) and the radiation pattern of the antenna is measured in an anechoic chamber. In general, good agreement is achieved between the measured and the simulated results. The discrepancy between the measured and simulated results is caused by the accuracy of the fabrication process. This difference is also attributed to the simplified model used in the simulation which does not include material loss, soldered joints and the SMA connector. Details of the measured and simulated results for the four different antenna prototypes are summarized in Table 2.2.

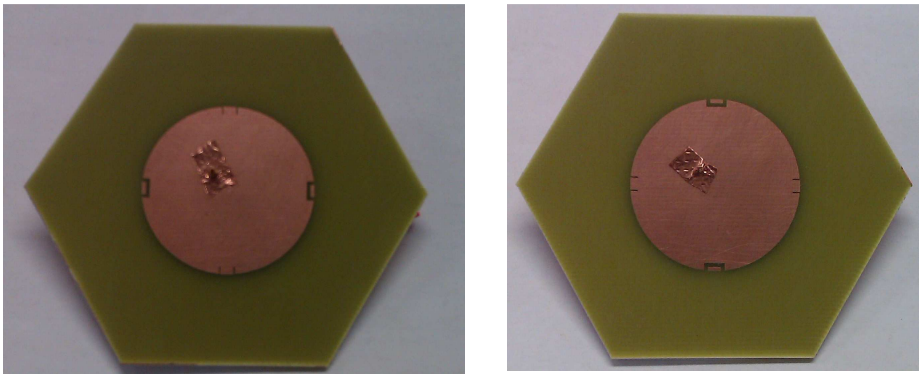

(a) (b)

Figure 2.21: The fabricated antenna, (a) LHCP mode, and (b) RHCP mode.

As seen in Figure 2.22, the operating frequency for the antenna in LHCP (ANT 3) and RHCP (ANT 4) mode are approximately the same. However, it is observed that ANT 1 has the highest operating frequency, followed by ANT 3, ANT 4 and ANT 2. This variation is due to the changes in the physical dimensions of the proposed antenna as the antenna is connected to the parasitic elements. The dimension of ANT 1 is slightly smaller compared to the other antennas, hence the slightly higher operating frequency. Similarly, the operating frequencies of ANT 3 and ANT 4 are approximately the same as the radiating elements are of the same size. The impedance bandwidth of 2.22% for the proposed antenna when ANT 3 and ANT 4 are in CP mode is larger compared to 1.31% when ANT 1 and ANT 2 is in the LP mode.

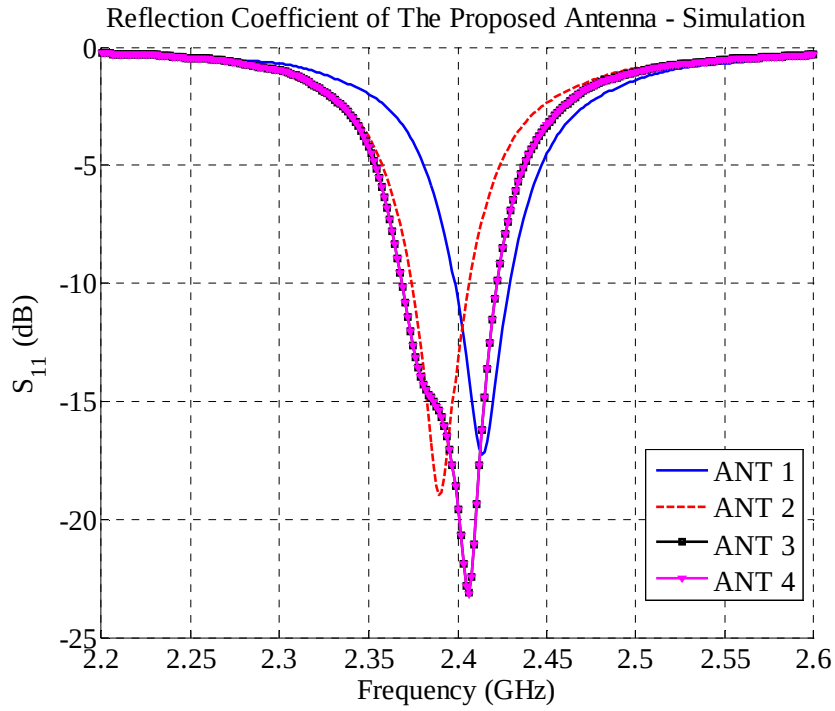

(a)

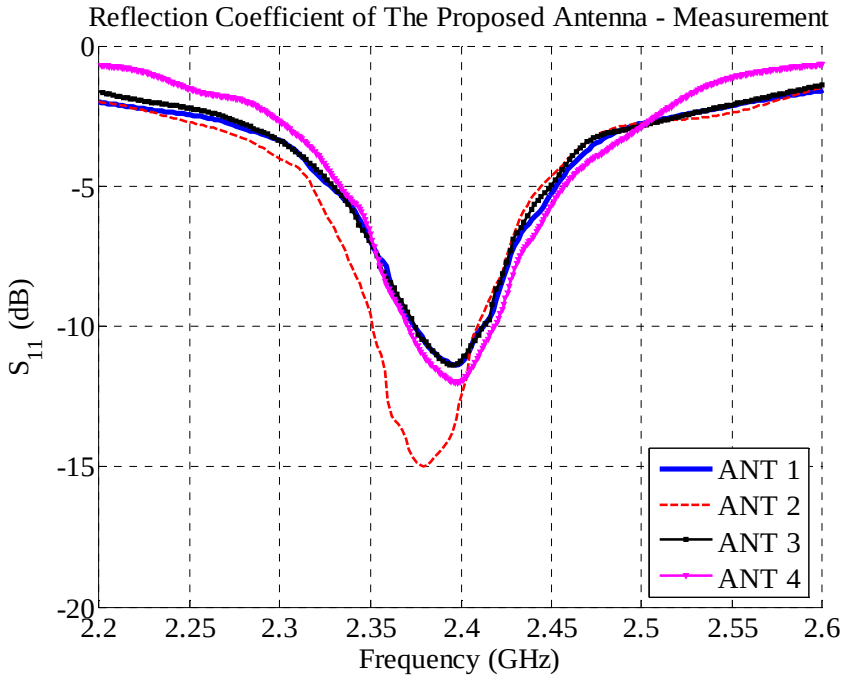

(b)

Figure 2.22: The reflection coefficient of the proposed antenna, (a) simulated results, and (b) measured results.

Table 2.2: Simulated and Measured S_{11} of The Antenna In Different Modes.

Properties	**ANT1**	**ANT2**	**ANT3**	**ANT4**
Polarisation	LP	LP	LHCP	RHCP
BW (-10 dB)	31.4 MHz 1.31%	31.8 MHz 1.3%	52.9 MHz 2.22%	52.9 MHz 2.22%
S_{11} Simulated	-17.473 (2.414 GHz)	-18.373 (2.393 GHz)	-23.13 dB (2.405 GHz)	-23.13 dB (2.402 GHz)
S_{11} Measured	-11.392 (2.398 GHz)	-14.967 (2.379 GHz)	-11.373 dB (2.394 GHz)	-11.999 (2.396 GHz)

2.6.2 Axial Ratio

The simulated axial ratio versus frequency and axial ratio versus elevation angle, θ, of the proposed antenna for CP mode (ANT 3 and ANT 4) are shown in Figure 2.23. Both ANT 3 and ANT 4 exhibit the best axial ratio at boresight at 2.39 GHz with 1.9 % circular polarisation bandwidth (cut off at 3 dB) as shown in Figure 2.23 (a). Also depicted in Figure 2.23 (b), is the axial ratio of the antennas at 2.4 GHz, which covers a broad angular range from -60° to 60° from boresight.

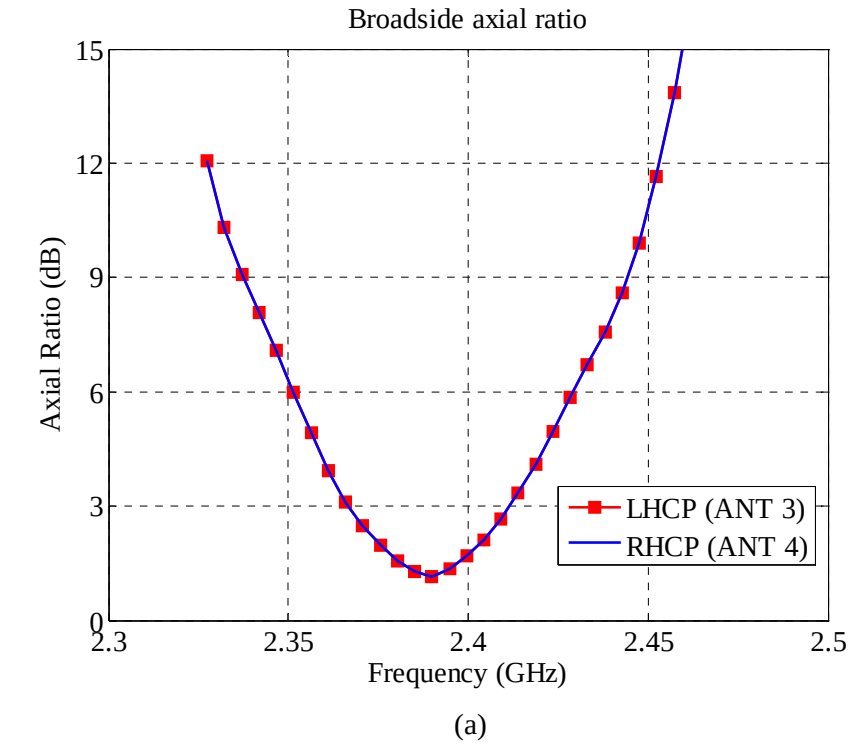

(a)

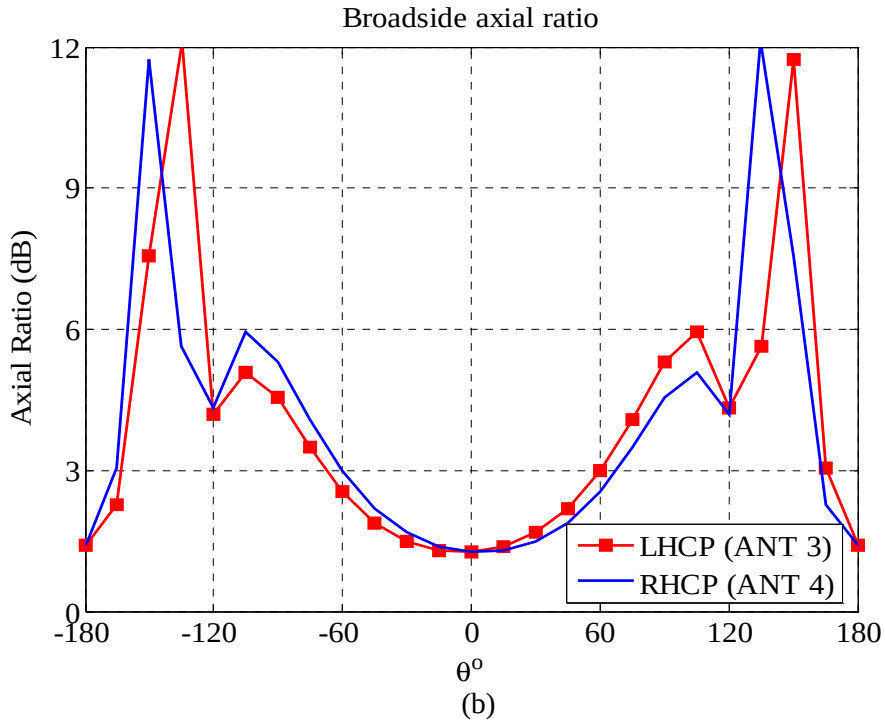

(b)

Figure 2.23: Simulated axial ratio of the proposed antenna, (a) broadside axial ratio, and (b) far-field axial ratio.

The measured axial ratio for the antenna in both LHCP and RHCP modes are shown in Figure 2.24. Good agreement is achieved between the measurement and simulation results.

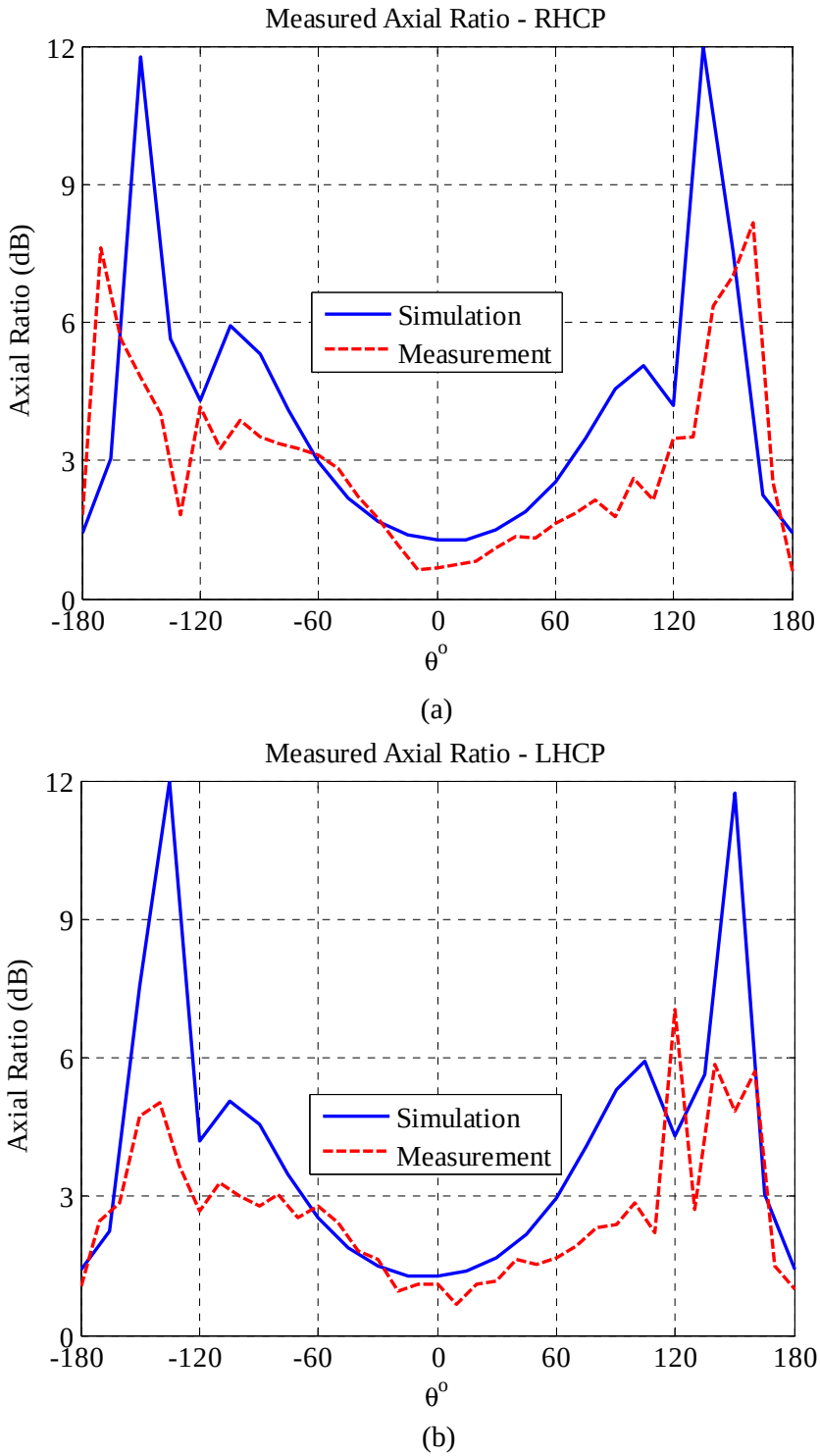

Figure 2.24: The axial ratio of the antenna, (a) RHCP, and (b) LHCP.

2.6.3 Radiation Pattern

Figure 2.25 shows the simulated radiation patterns of the antenna for the entire polarisation mode at 2.4 GHz. Due to the small tweak in the shape of the patch, the radiation pattern for the antenna is approximately the same for every operational mode. The radiation pattern of the antenna is directional with an average beamwidth of 87.9°.

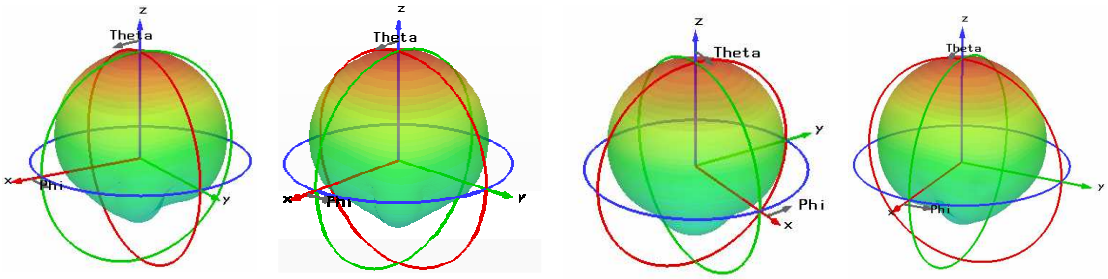

Dir = 6.50 dBi	Dir = 6.77 dBi	Dir = 6.38 dBi	Dir = 6.34 dBi
Rad_{eff} = 93.9%	Rad_{eff} = 94.1%	Rad_{eff} = 91.5%	Rad_{eff} = 86.9%
(a)	(b)	(c)	(d)

Figure 2.25: The radiation pattern of the proposed antenna, (a) ANT 1, (b) ANT 2, (c) ANT 3, and (d) ANT 4.

The measured radiation pattern of the antenna for Ø = 90° in both LHCP and RHCP modes are shown in Figure 2.26. From the results, it is shown that good agreement is achieved between the measurement and simulation results.

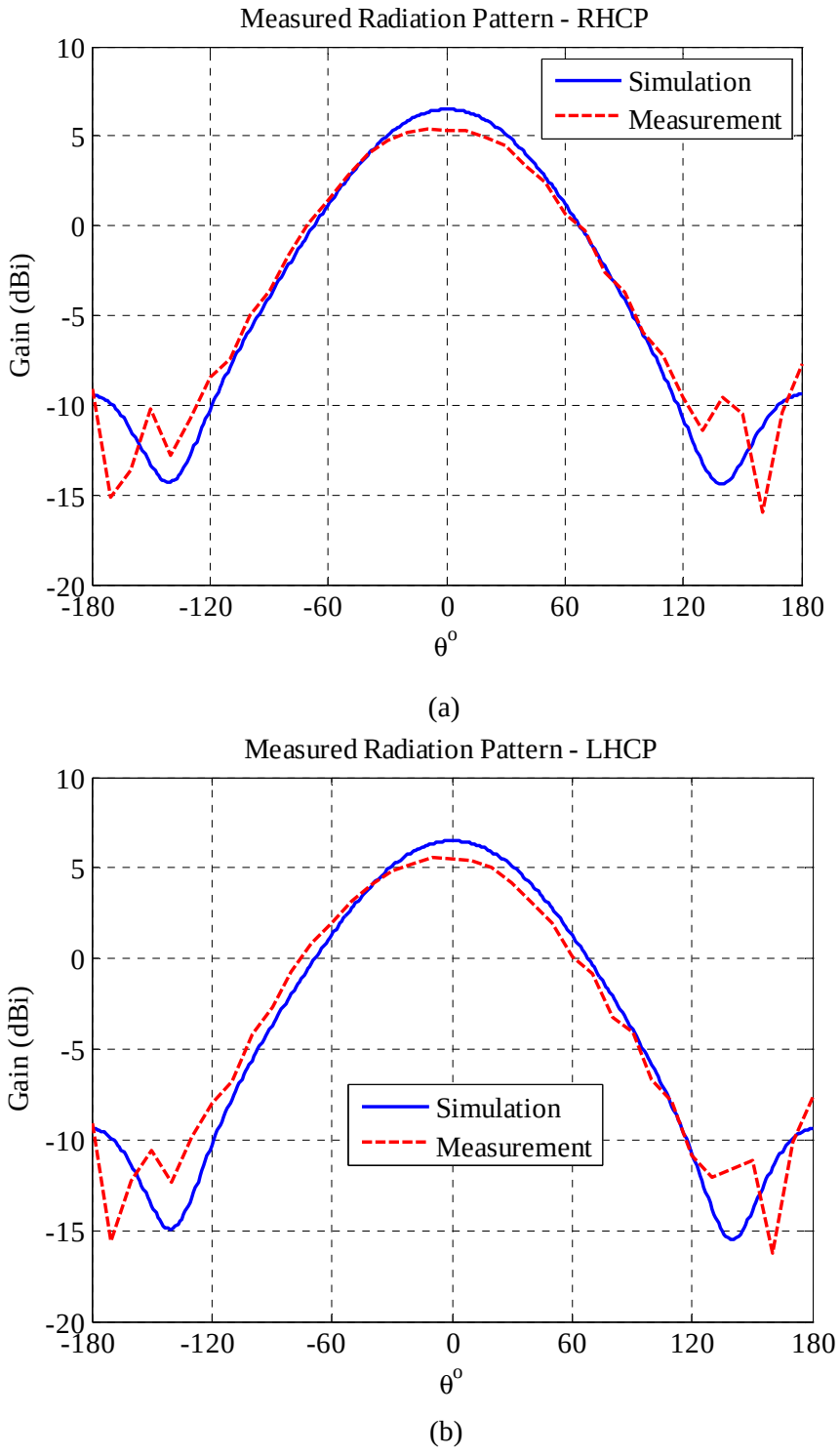

Figure 2.26: The radiation pattern of the antenna, (a) RHCP, and (b) LHCP.

2.7 Summary

In summary, the investigation of this chapter is shown in Figure 2.27.

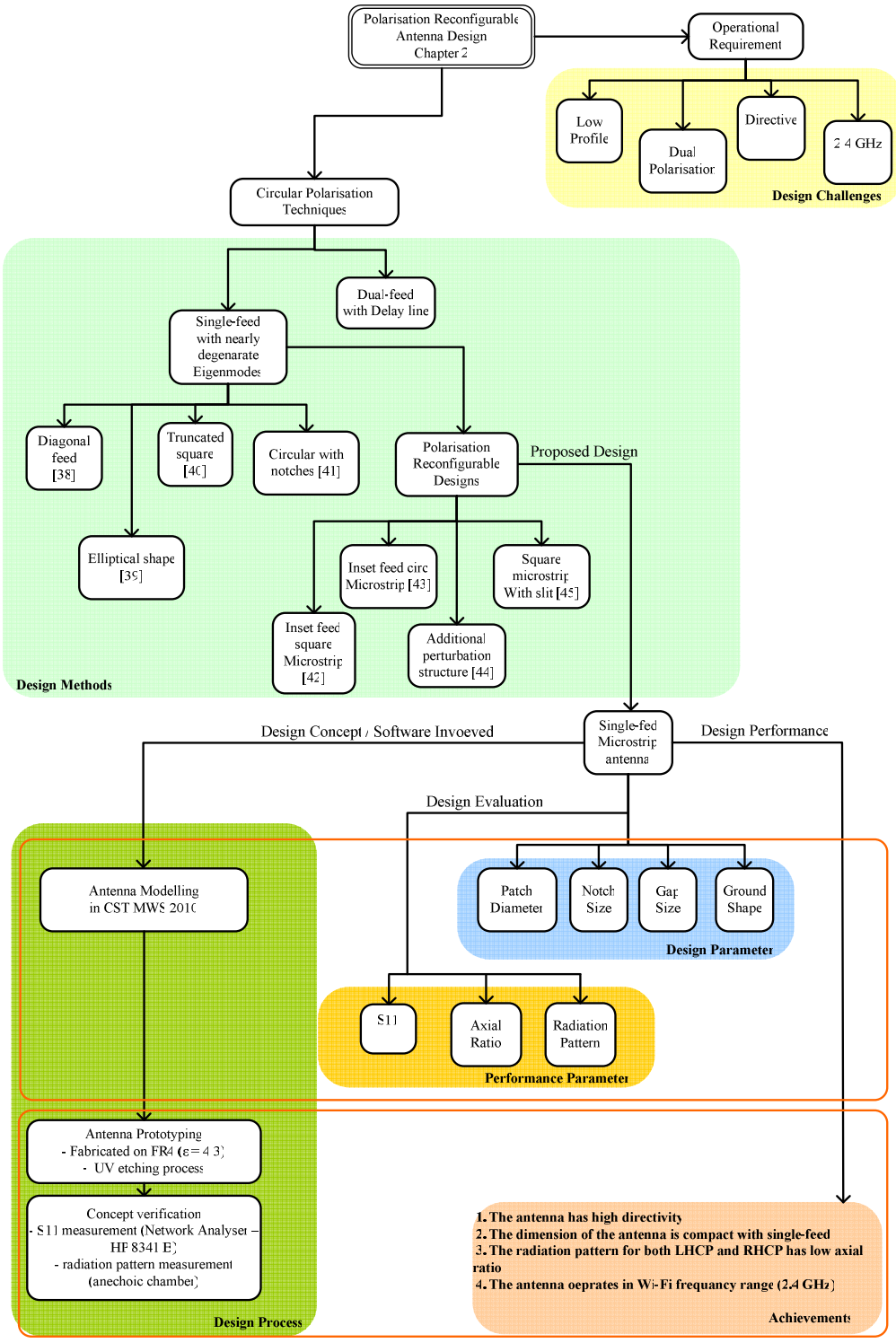

Figure 2.27: The investigation of polarisation reconfigurable antenna design.

In this chapter, a single-feed polarisation reconfigurable antenna design concept is proposed for use in wireless communication systems. Different polarisation state of the antenna is achieved by manipulating the connection between the radiating structure and the parasitic elements using ideal metal bar connection.

The proposed structure exhibits a broad angular axial ratio of 120^{o}. The parametric studies suggest that the patch diameter influences the operational frequency and a careful measure is needed for the notch width and the notch gap as these parameters influence both the axial ratio and the resonant frequency. The radiation efficiencies of the antenna in LHCP and RHCP modes are 91.5 % and 86.9 %, respectively. The antenna was fabricated on 1.6 mm thick FR4 substrate ($\varepsilon_r = 4.3$) and a good agreement is achieved between the simulated and measured performance.

An adaptive array antenna can be cost-effective when reconfigurable antennas are used because different radiation characteristics, such as the operating frequency and the polarisation, can be achieved using the same set of array elements. The proposed single-feed polarisation reconfigurable antenna has high radiation efficiency and good axial ratio performance in both RHCP and LHCP operational modes. The antenna is cost-effective in terms of structure reuse and it is suitable for use in adaptive array antennas for wireless communication system.

In the next chapter, wide scanning array design using fewer than 10 elements is presented and discussed.

Chapter 3
Array Design with Wide Scan Range Properties

3.1 Introduction

Another technique of reducing the cost of an adaptive array antenna is by using arrays with a small number of elements [11]. The next step of this research is to develop a wide scanning adaptive array, in particular one with fewer then 10 elements. The directivity of an adaptive array antenna with a wide scanning angle property is maintained within a certain level, even when the main beam is steered away from the boresight. This is important, especially for communication devices, as the best transmission link is not always within the boresight of an antenna. In this chapter, various array geometries with fewer than 10 elements are synthesised for wide scanning range. The polarisation reconfigurable antenna proposed in Chapter 2 is used as the array elements. The radiation pattern of a single element is simulated in CST Studio Suite 2011, and later imported to Matlab 2008 for synthesis.

This chapter is divided into seven sections. Section 3.2 presents the theory behind array design and the background on wide scanning arrays is discussed in Section 3.3. Section 3.4 describes the method of analysis used in the design process, and Section 3.5 discusses the

array geometries for wide angle scanning. This is followed with the full-wave analysis of the 3-faceted array in Section 3.6. Finally, Section 3.8 summaries the chapter.

3.2 Array Theory

The resulting radiation pattern of an array is influenced by its geometrical construction, the radiation pattern of individual elements, the amplitude and phase excitation of the elements, the number of elements in an array and the separation between these elements.

3.2.1 Array Factor

The characteristic of an array can be mathematically described by its array factor, given by Equation (3.1) [46].

$$AF = \sum_{n=1}^{N} w_n e^{j\psi_n} \tag{3.1}$$

where, N is the number of element in the array, ψ_n is the phase shifts between signals for successive elements and w_n is the complex weight of the n^{th} element.

The main beam of the array is steered to (θ_s, ϕ_s) by applying a phase shift, δ_n, to ψ_n as described by Equation (3.2).

$$AF = \sum_{n=1}^{N} w_n e^{j(\psi_n + \delta_n)} \tag{3.2}$$

An array with elements distributed in three-dimensional space is illustrated in Figure 3.1 and its array factor can be represented by Equations (3.3) – (3.5) [46].

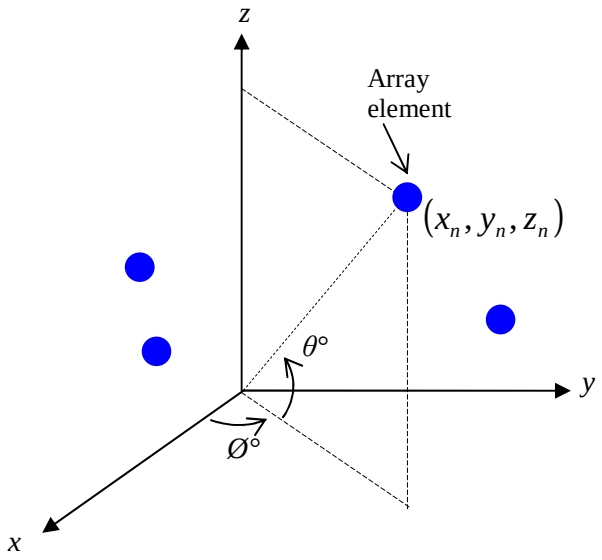

Figure 3.1: Arbitrary antenna array geometry.

$$AF = \sum_{n=1}^{N} w_n e^{jk[x_n(u-u_s)+y_n(v-v_s)+z_n\cos\theta]} \tag{3.3}$$

$$u = \sin\theta\cos\phi\,;\; u_s = \sin\theta_s\cos\phi_s \tag{3.4}$$

$$v = \sin\theta\sin\phi\,;\; v_s = \sin\theta_s\sin\phi_s \tag{3.5}$$

where, N is the number of elements in the array, (x_n, y_n, z_n) is the position of the n^{th} element, w_n is the array weight and (θ_s, ϕ_s) is the steering angle for elevation and azimuth, respectively, as illustrated in the figure.

3.2.2 Radiation Pattern

Typically, an adaptive array uses the same type of antenna as the array elements and the far-field radiation pattern of the array is the total product of a single element radiation pattern, as described by Equation (3.6) [46].

$$AP(\theta,\phi) = \sum_{n=1}^{N} EP_n(\theta,\phi) w_n e^{jk[x_n(u-u_s)+y_n(v-v_s)+z_n\cos\theta]} \tag{3.6}$$

where, $EP_n(\theta,\phi)$ is the radiation field of a single element, N is the number of elements in the array, (x_n, y_n, z_n) is the position of the n^{th} element, w_n is the array weight and (θ_s, ϕ_s) is the steering angle for elevation and azimuth, respectively.

3.2.3 Directivity

The directivity formula for an array is given by Equation (3.7) [46].

$$D = \frac{4\pi\left|EP(\theta,\phi)AF(\theta,\phi)\right|^2}{\int_0^{2\pi}\int_0^{\pi}\left|EP(\theta,\phi)AF(\theta,\phi)\right|^2 \sin\theta\delta\theta\delta\phi} \tag{3.7}$$

where, $EP(\theta,\phi)$ is the element pattern and $AF(\theta,\phi)$ is the array factor.

3.2.4 Rotation of the Array Element

The radiation property of the individual element plays an important role in shaping the overall radiation pattern of the adaptive array antenna. Thus, changes in the rotations of the array elements need to be considered, especially when the elements are arbitrarily arranged in an array. This is achieved by rotating the pattern direction into the coordinate of each antenna [38].

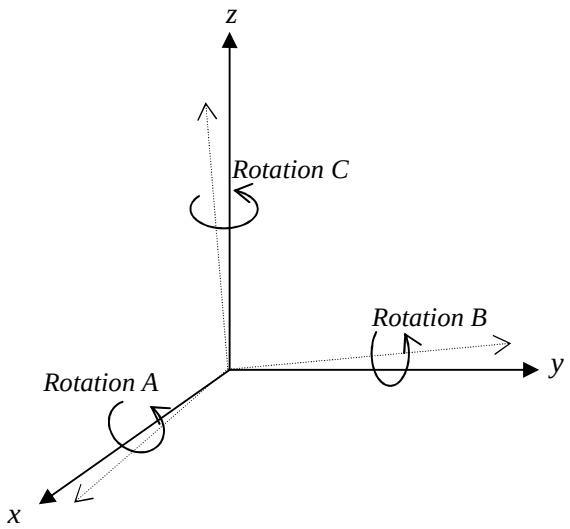

Figure 3.2: Rotation of the coordinate system.

The rotation matrices for rotations around orthogonal axis *-x*, *-y* and *–z* are given by Equations (3.8), (3.9) and (3.10), respectively.

$$rotated\_X-axis=\begin{bmatrix}1 & 0 & 0\\ 0 & \cos A & \sin A\\ 0 & -\sin A & \cos A\end{bmatrix} \tag{3.8}$$

$$rotated\_Y-axis=\begin{bmatrix}\cos B & 0 & -\sin B\\ 0 & 1 & 0\\ \sin B & 0 & \cos B\end{bmatrix} \tag{3.9}$$

$$rotated\_Z-axis=\begin{bmatrix}\cos C & \sin C & 0\\ -\sin C & \cos C & 0\\ 0 & 0 & 1\end{bmatrix} \tag{3.10}$$

3.3 Wide Scanning Arrays

One of the issues regarding the adaptive array antenna, especially arrays with a limited number of elements, is that its directivity decreases as the main beam is steered away from boresight [3, 46]. The directivity reduces as power is transferred from the main beam to the sidelobes [26-28]. However, maintaining the directivity is important especially for high quality signal transmission in wireless communication system. Therefore, several approaches have been proposed to increase the scan range of adaptive array antennas.

One of the techniques used is to introduce a degree of curvature to the structure, as illustrated in Figure 3.3. For example, in [27], the scanning range and directivity properties of three types of array configurations, namely, planar, circular and three-segment arrays, were analysed and compared. Each of these arrays was formed using five vertical sub-arrays and four horizontal sub-arrays of microstrip antennas. Each sub-array are horizontally separated by 0.5 λ and vertically separated by 0.8 λ. In this analysis, the bending angle of the three-segment array is fixed to 45°. It was shown that circular and three-segment configurations allowed beam steering in a wider angular range compared to the planar array, although at the expense of a wider beam and lower directivity. From this study, it is noted that the scanning range of a planar array is increased with the number of elements in the array and with the segmented structure, the scanning range of an array can be increased.

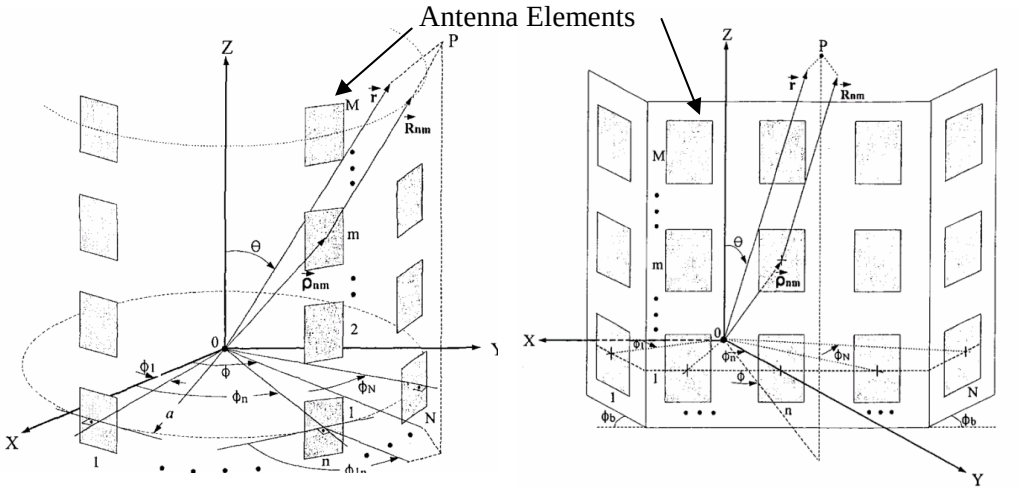

Figure 3.3: Arrays with degree of curvature, (a) cylindrical array, and (b) three-segmented array [27].

Using a similar approach, the pyramidal-frusta structure, shown in Figure 3.4, has been used in order to achieve a hemi-spherical coverage [11]. The elements are divided into several facets which are activated according to the desired scanned angle. Maximum hemi-spherical coverage is achieved by optimising the face elevation of the multi-faceted structure. It was shown that when the pyramidal structure has more facets, less elevation is required by each facet in order to achieve the maximum scan angle. From this study, it was shown that fewer elements are required with multi-faceted array compared to the planar array in order for the array to achieve the same scanned array. It was also suggested that the choice of array structure with wide scan angle property can be considered based different criteria including the required scan angle, antenna dimension, geometric directivity and number of elements.

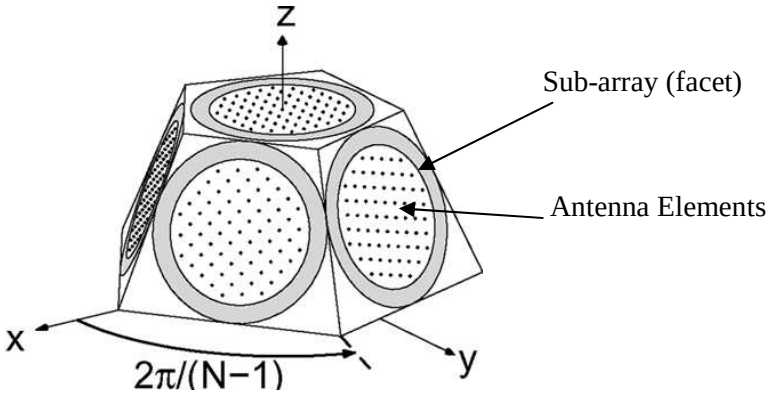

Figure 3.4: Pyramidal-frusta array [11].

Another example is an array of 45 elements arranged in a 3-segmented structure, shown in Figure 3.5 [47]. The array is targeted for automotive radar traffic monitoring to detect approaching collisions. In this system, a total of 45 array elements are used. Each facet formed a linear array with 15 patch antenna elements operating at 77 GHz and the segments are placed 120° from each other. As the main beam is steered away from boresight, only the nearest segment to the required scan angle is activated. With this structure, the scanning range of the array is able to reach more than ±90° from boresight.

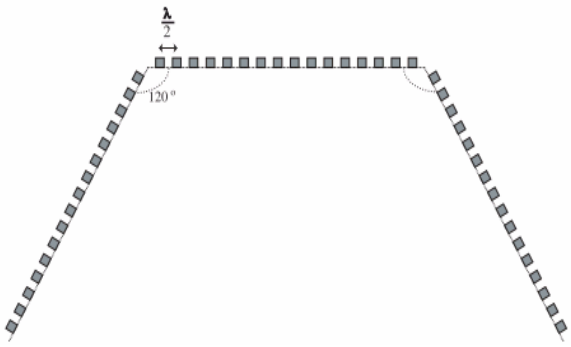

Figure 3.5: 3-segmented automotive radar [47].

In another approach, pattern reconfigurable antennas were used in order to achieve a scan range of ± 60° from boresight [30]. The weighted thinned array consists of eight microstrip Yagi antennas operating at 5.8 GHz, shown in Figure 3.6. The Yagi antenna reconfigured its radiation pattern in three different positions which are broadside (B-mode), positive *y-plane* (R-mode) and negative *y-plane* (L-mode). The wide scanning range of the array is achieved by reconfiguring the radiation pattern of the Yagi antenna according to the required scan angle. For scan angle ranges from 7° to 60°, the array elements operates in R-mode and for the scan angle between -7° to 7°, the array elements should be in B-mode. On the other hand, for scan angle ranges from -60° to -7°, the array elements are reconfigured to operate in L-mode. It was also shown that the use of pattern reconfigurable Yagi antenna in the array also results in radiation pattern with low sidelobe levels.

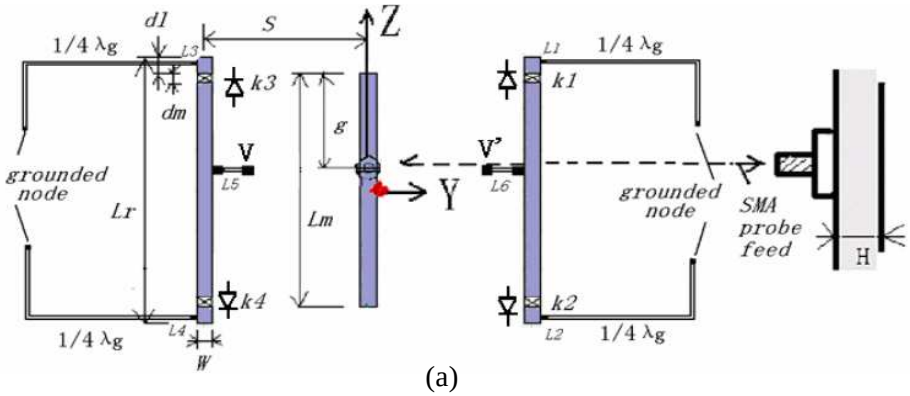

(a)

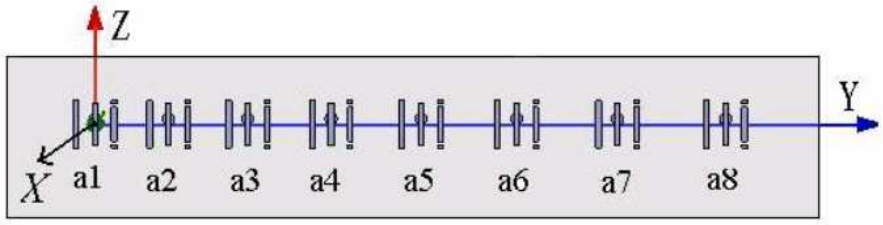

(b)

Figure 3.6: Wide scanning array with pattern reconfigurable elements, (a) antenna elements, and (b) array configuration [30].

Another approach that can be used to achieve wide scanning angle is by tilting the sub-panel of an array mechanically [48]. The elements on the array are divided into smaller panels and each panel operates separately. The tilted elements form a stair-wise structure of the array as illustrated in Figure 3.7. Each panel operates as a separate antenna. In order to steer the main beam of the array, the main beam of each panel is directed towards the desired angle by slanting the panel mechanically. Using this method, the scanning range of the array could reach ±50 ° from boresight.

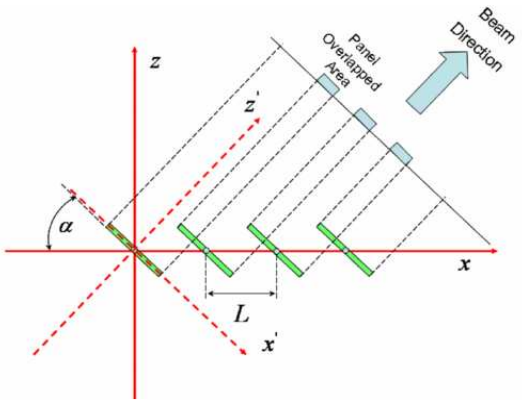

Figure 3.7: Panel tilting arrays [48].

All the array design techniques presented above will increase the scanning range of the antenna. However, these arrays require either a large number of elements [11, 27] or specific types of antennas [30] or complex mechanical control mechanisms [48]. Designing an adaptive array antenna with wide scan range properties is a challenge for systems that have a limited number of elements. Arrays with smaller number of elements have high sidelobe levels, which limit the scanning range of the array [30]. Furthermore, the angular resolution of an array decreases when the number of antenna elements is reduced [29].

3.4 Method of Analysis

In this section, an adaptive array antenna is analysed and is later synthesised and verified in a full-wave solver. Full-wave solvers, such as CST Design Suite 2011, function by dividing the antenna structure into smaller segments and calculating the current density of each segment. From the calculated current densities, the parameters of interest, such as input impedance, mutual coupling, near field and far field, can be derived. However, this is a time consuming process and requires high computational effort.

The geometrical approach on the other hand is less complex as it only yields pattern information with no redundant calculation. In this approach, the radiation pattern of the antenna is geometrically combined in the far field and the radiation performance such as the directivity of the array can be calculated with less computational effort. Furthermore, rapid evaluation of the array pattern is essential since synthesising the array for wide angle scanning requires changing many design parameters. However, despite the simplicity offered by the geometrical approach, the importance of antenna parameters such as mutual coupling, input impedance and near-field radiation is acknowledged. The optimised array obtained from the geometrical approach is then modelled in a full-wave environment and is discussed in Section 3.6.

In this analysis, the scanning range is identified from boresight to the scan angle where the directivity of the antenna array is reduced by 3 dB (50 %) from the maximum directivity. The main beam of the array is steered to a scan angle by adjusting the phase excitation of the array elements while keeping the amplitude excitation constant. The excitation values are obtained by calculating the difference between the desired scan angle and the boresight of the array. The directivity of the array at a given angle is then calculated. The influence of various design parameters, such as the number of elements in the array, separation distance between adjacent elements, the orientation of the elements and the geometry of the array, on the scanning range of the array is evaluated and analysed.

3.4.1.1 Array Modelling in Matlab

The arrays are modelled in Matlab by incorporating the radiation pattern of the polarisation reconfigurable antenna, obtained from simulation in CST Design Suite 2011, into the array factor as given by Equation (3.3). The radiation pattern of an array is then calculated in Matlab using Equation (3.6). For verification, the radiation patterns calculated using Matlab and CST Design Suite are compared in Figure 3.8. In general, both radiation patterns have similar profile. However, the differences in the directivity of the main beam and sidelobe levels are noted, and this is expected as the radiation pattern generated in Matlab does not include mutual coupling effects.

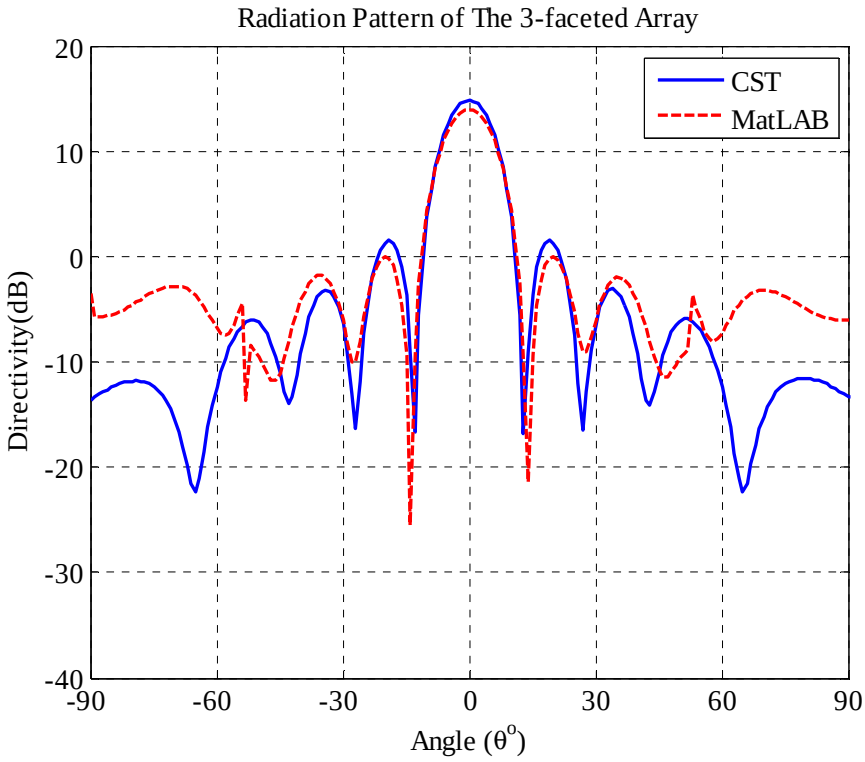

Figure 3.8: Radiation pattern of the 3-faceted array calculated by Matlab and CST Design Suite.

3.5 Array Geometry with Wide Angle Scanning

Generally, the radiation pattern of an adaptive antenna array is heavily influenced by its geometrical structure [3]. For example, with a one-dimensional array (1D-array), such as the uniform linear array (ULA), the scanning range is limited either to the elevation angle for a fixed azimuth angle or the azimuth angle for a fixed elevation angle. On the other hand, two-dimensional arrays (2D-array) and three-dimensional arrays (3D-array), have the ability to scan throughout the hemispherical region, in azimuth and elevation angle [11, 49-51]. However, due to its simpler implementation compared to the 2D and 3D-arrays, the 1D-array has become the most commonly used structure in adaptive array antennas.

The 2D-array is sub-divided into three other categories: circular, rectangular, and square. Among the three categories, the uniform circular arrays (UCA) do not have edge elements. Without edge constraints, the array structure can be easily rotated. Besides, circular arrays also have the capability to compensate for the effects of mutual coupling by breaking down the array excitation into a series of symmetrical spatial components [6, 51]. The circular array can also be designed with an element at the centre, normally termed a uniform

concentric circular array (UCCA) [52] . Even though, the UCA has two-dimensional scanning coverage, the computation and analysis of the array are more complex compared to the ULA [53].

3.5.1 2-element Array

3.5.1.1 Array orientation

Figure 3.9 illustrates four different configurations based on a two-element antenna arrays and they have been analysed using CST Design Suite 2011. In this simulation, the operating frequency for the antenna is 2.4 GHz. In each configuration, the element separation between the antennas, d_p, is fixed at 0.6 λ. Antennas for Configuration-1 and Configuration-2 are arranged along the x-axis and y-axis, respectively. Meanwhile, in Configuration-3 and Configuration-4, the antennas are arranged diagonally. The radiation patterns of the array configurations is shown in Figure 3.10, while the corresponding mutual coupling (S_{21}) and radiation pattern characteristics at 2.4 GHz are tabulated in Table 3.1.

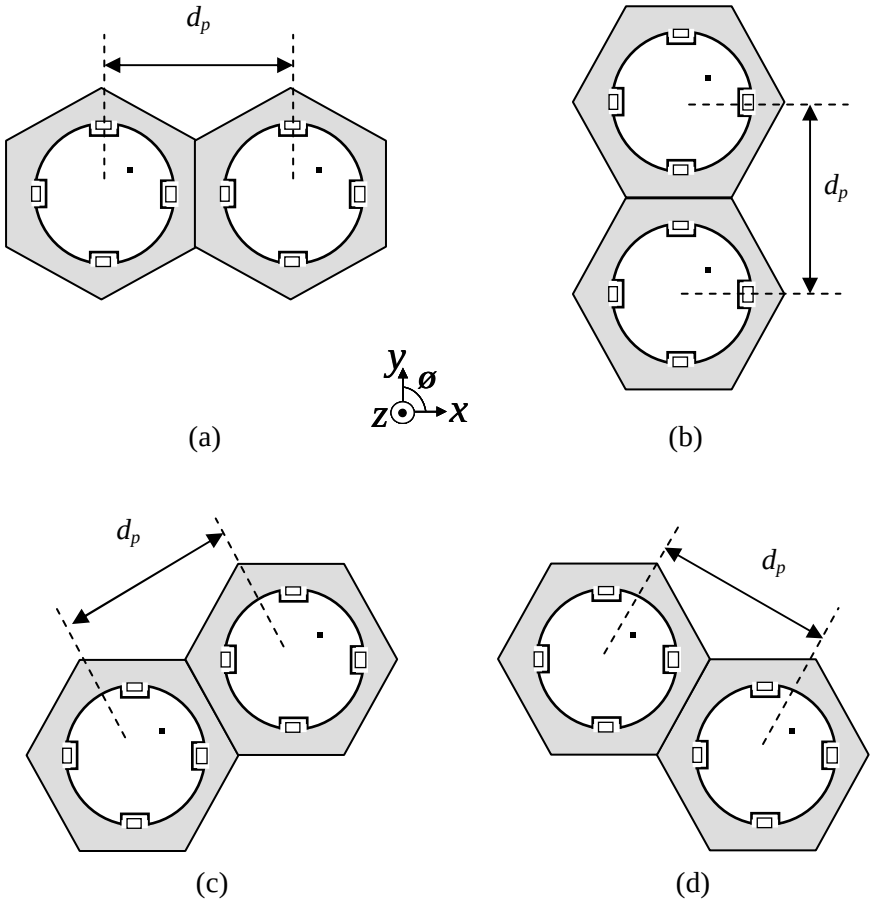

Figure 3.9: The geometry of a two-element array, (a) configuration-1, (b) configuration-2, (c) configuration-3, and (d) configuration-4.

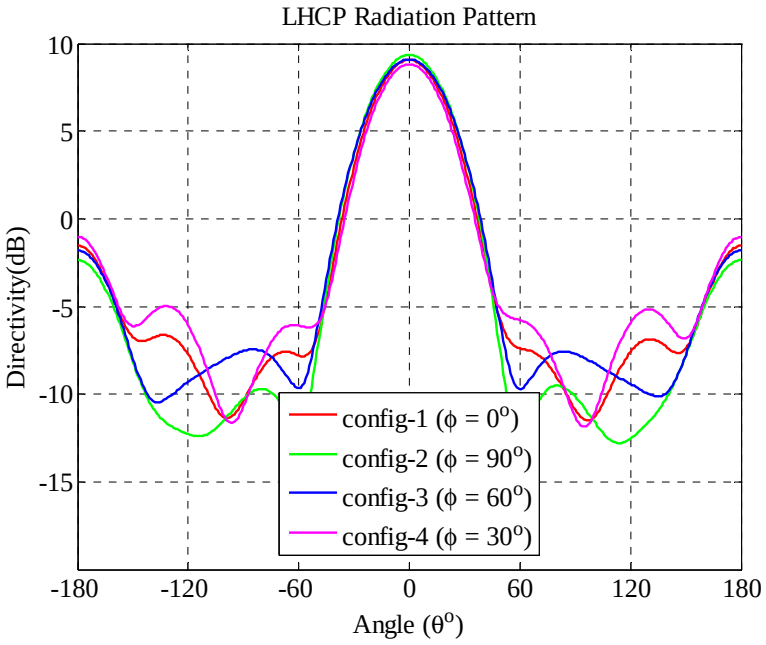

(a)

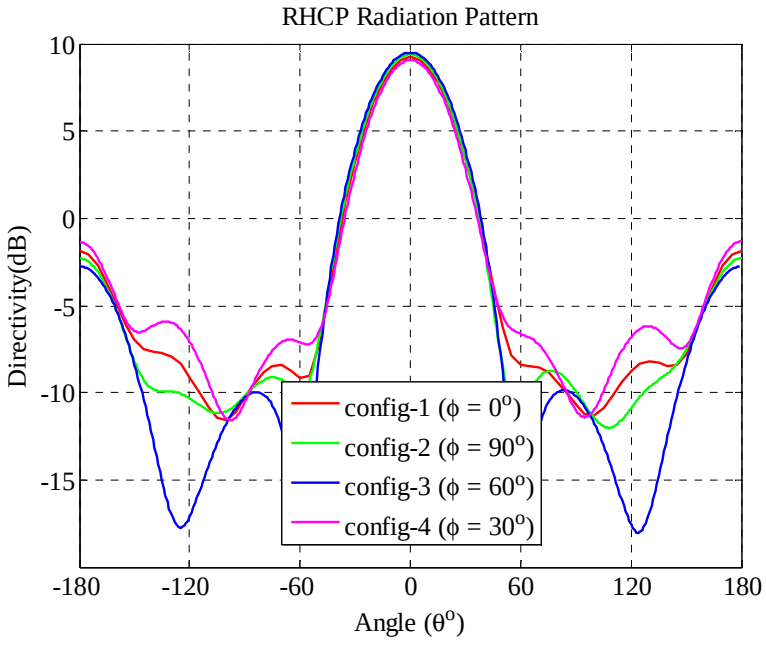

(b)

Figure 3.10: Radiation pattern of the array configurations, (a) LHCP, and (b) RHCP.

Table 3.1: Mutual Coupling and Radiation Pattern Characteristics of The Configurations.

Radiation Properties/ Configuration	**LHCP**			**RHCP**		
	Mutual Coupling S_{21} (dB)	**Radiation Pattern**		**Mutual Coupling S_{21} (dB)**	**Radiation Pattern**	
		Dir (dBi)	**SLL (dB)**		**Dir (dBi)**	**SLL (dB)**
Configuration-1	-17.39	9.12	-10.61	-18.54	9.33	-11.24
Configuration-2	-20.63	9.44	-11.74	-22.52	9.41	-11.68
Configuration-3	-19.29	9.08	-10.93	-20.04	9.54	-12.29
Configuration-4	-17.98	8.82	-9.94	-18.01	9.13	-10.44

It is observed that in both LHCP and RHCP modes, the lowest mutual coupling, S_{21}, is obtained with Configuration-2. In LHCP mode, the highest gain and directivity are obtained with Configuration-2. However, in RHCP mode, the antenna with the highest gain and directivity is Configuration-3. It is noted that the directivity of Configuration-2 is the same in both modes. Moreover, the side lobe level (SLL) of Configuration-2 is low compared to the other configurations. With the lowest coupling level and equal directivity, Configuration-2 is selected for further development.

3.5.1.2 Element Separation

The level of mutual coupling and the radiation pattern of the array in Configuration-2 are shown in Figure 3.11 and Figure 3.12, respectively. The radiation properties of the array for both polarisation modes are presented in Table 3.2. It is observed that the mutual coupling decreases as the separation increases. However, the directivity and the SLL of the array increases with the separation, and this could lead to the occurrence of grating lobes. Meanwhile, the HPBW decreases as the separation increases and the separation also affects the dimension of the array. Therefore, there is a trade off between mutual coupling, array size and the occurrence of grating lobe. Since the targeted mutual coupling at 2.4 GHz is S_{21} < -20 dB, the element separation is set to 0.55 λ. It is also noted that, at this separation, the radiation properties of the antenna are approximately the same in both LHCP and RHCP modes.

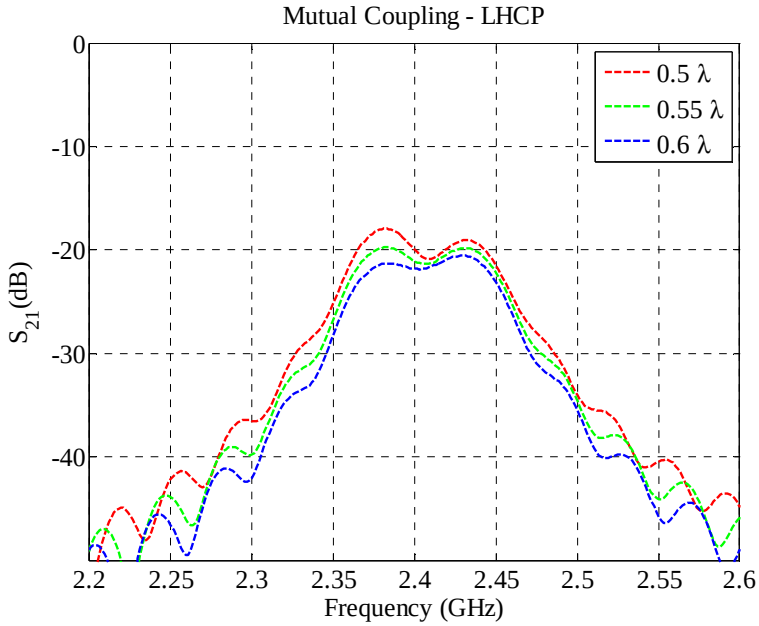

(a)

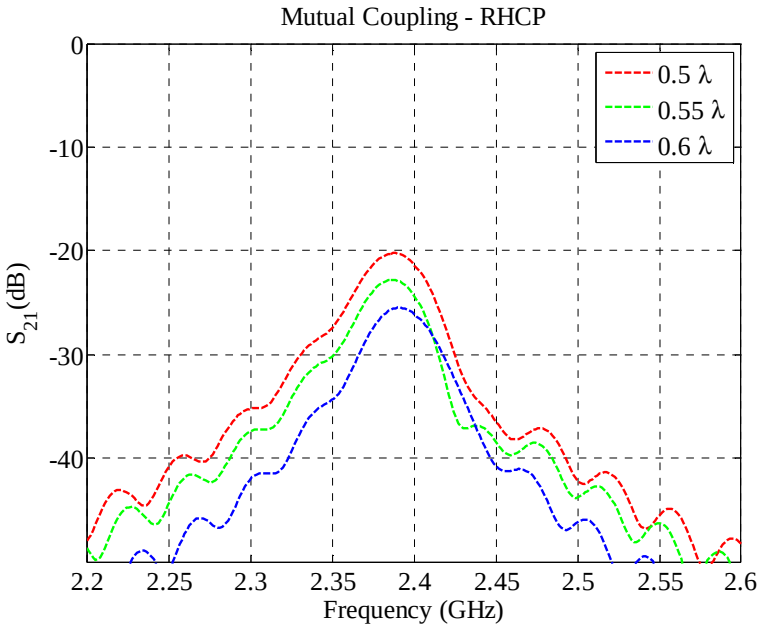

(b)

Figure 3.11: The mutual coupling level of configuration-2 with different element separation, d_p. (a) LHCP, and (b) RHCP.

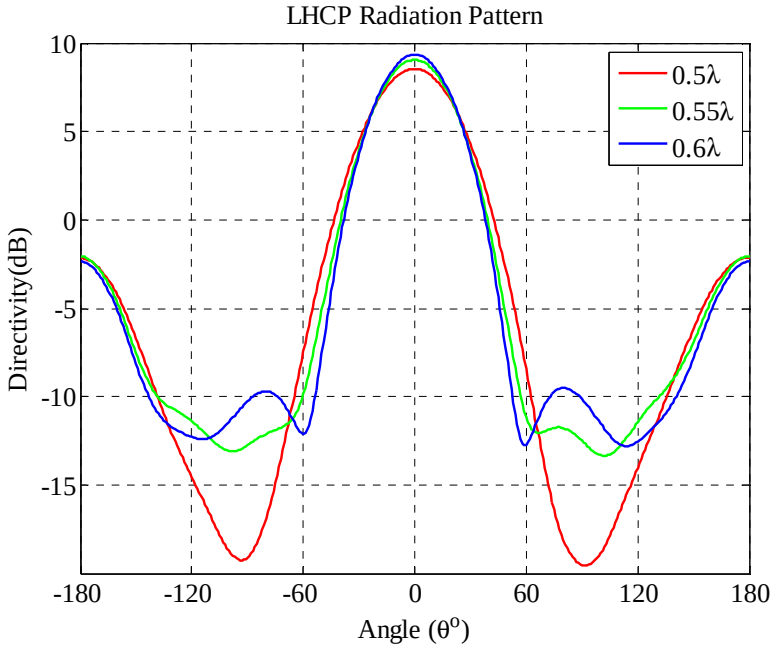

(a)

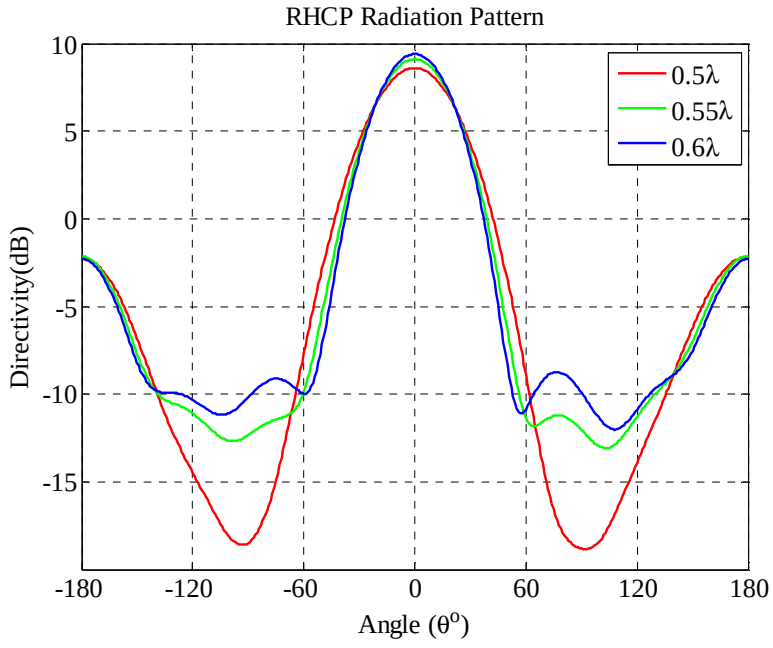

(b)

Figure 3.12: The radiation pattern of configuration-2 with different element separation, d_p, (a) LHCP, and (b) RHCP.

Table 3.2: Radiation Properties Corresponding to The Antenna Separation.

Radiation Properties / Separation d_p (λ)	**LHCP**			**RHCP**		
	Dir (dBi)	**HPBW (°)**	**SLL (dB)**	**Dir (dBi)**	**HPBW (°)**	**SLL (dB)**
0.5	8.5	50.9	- 10.7	8.6	50.4	-10.8
0.55	9.1	45.9	- 11.1	9.1	45.5	-11.2
0.6	9.4	44.2	- 11.7	9.4	43.1	-11.7

3.5.2 Scanning Ranges of the Uniform Linear Array (ULA)

In this section, a geometric approach is used to evaluate the performance of the array. As previously mentioned, the radiation properties of the antenna are approximately the same in both LHCP and RHCP modes. Therefore, from this point onwards, the antennas are set to operate in LHCP mode.

The geometry of the ULA is shown in Figure 3.13.

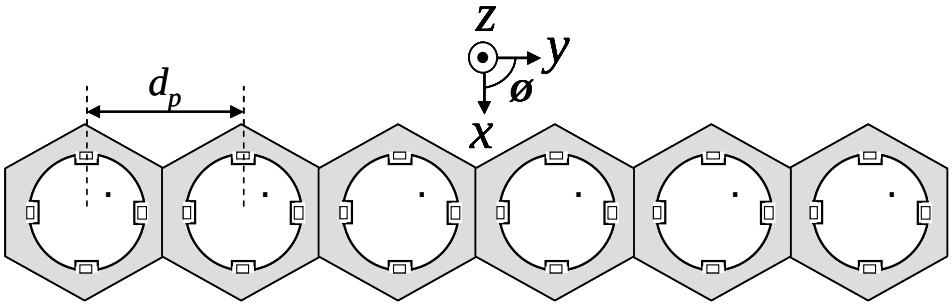

Figure 3.13: Uniform Linear Array.

The scanning range of the array with different number of elements is evaluated and the results are plotted in Figure 3.14 (a). In this simulation, the element separation, d_p, is set to 0.55 λ. The directivity and the scanning range of the array increase with the number of elements. The range increases as the elements are increased from 2-elements ($\theta° = \pm 38°$) to 6-elements ($\theta° = \pm 52°$). Even though the overall directivity of the 10-element array is higher than that of the 8-element array, both arrays have the same scanning range. However, the size and the implementation cost of the array increase as more elements are used.

Next, the scanning range of an 8-element ULA with different element spacing is evaluated and the results are depicted in Figure 3.14 (b). From the results, it is observed that the

scanning ranges achieved when the elements are separated with 0.5 λ and 0.55 λ are approximately the same. However, as the spacing between the elements is increased to 0.65 λ, the scanning range begins to decrease. One reason of this is the appearance of grating lobes. The 8-element ULA with 0.55 λ is modelled in a CST design Suite 2011, and discussed in Section 3.6.

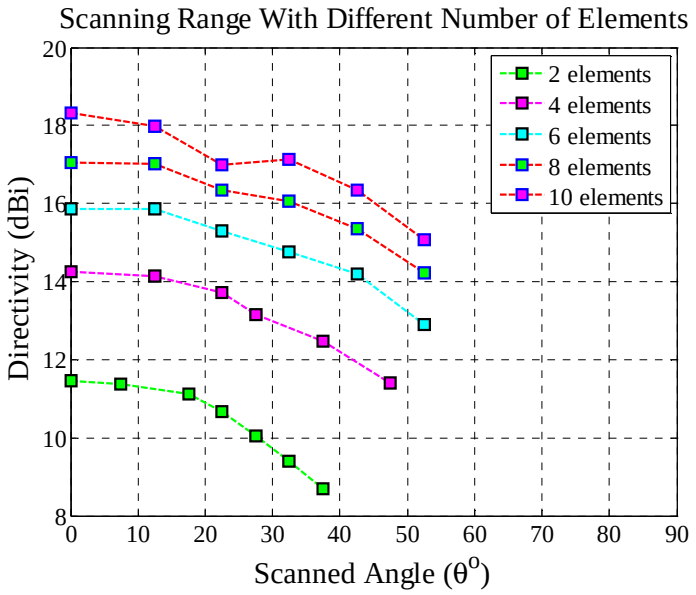

(a)

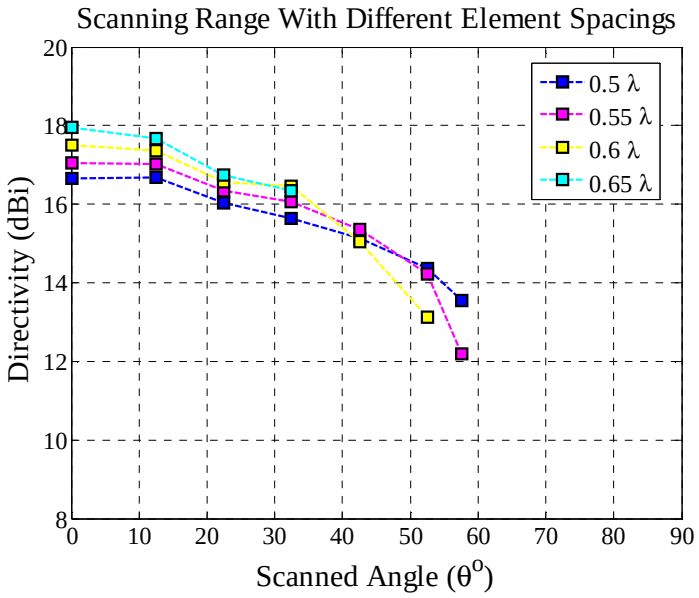

(b)

Figure 3.14: The scanning range of ULA, (a) different number of elements (0.55 λ), and (b) different element separation (8 elements).

3.5.3 Scanning Ranges of the Uniform Circular Array (UCA) and Uniform Concentric Circular Array (UCCA)

The geometry of 8-element UCA and UCCA are shown in Figure 3.15 and Figure 3.16, respectively.

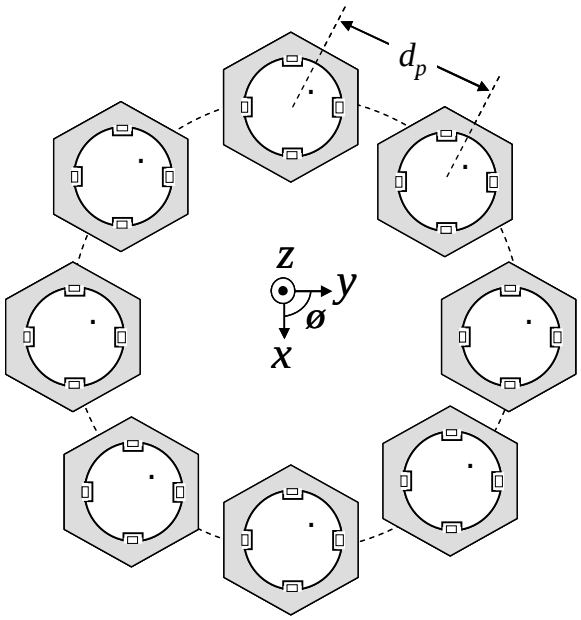

Figure 3.15: Uniform Circular Array (UCA).

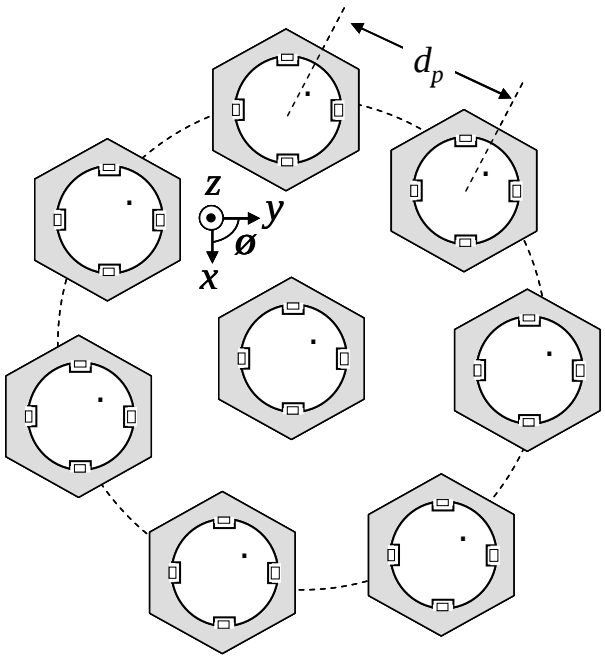

Figure 3.16: Uniform Concentric Circular Array (UCCA).

The scanning ranges of the UCA and UCCA with different element orientations, as shown in Figure 3.17, are evaluated and the directivity is plotted in Figure 3.18. In this simulation, the arrays consist of eight elements and the separations between these elements are fixed at 0.55 λ. From the results, for every element orientation, the directivity of UCCA at boresight is slightly higher compared to the UCA. The widest range achieved by UCA is approximately $\theta° = \pm 42°$ when the elements are oriented at 30° and 60°. On the other hand, the widest scanning range achieved by UCCA is approximately $\theta° = \pm 32°$.

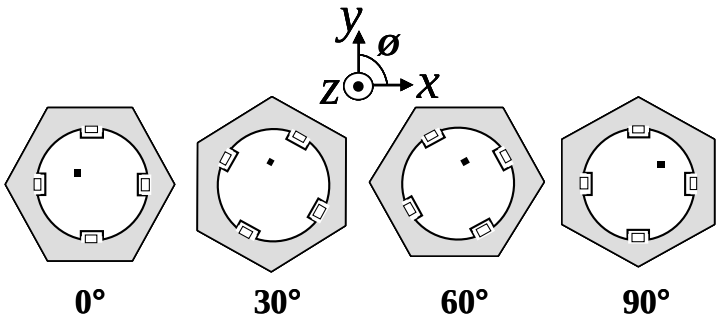

Figure 3.17: Illustration of different element orientation.

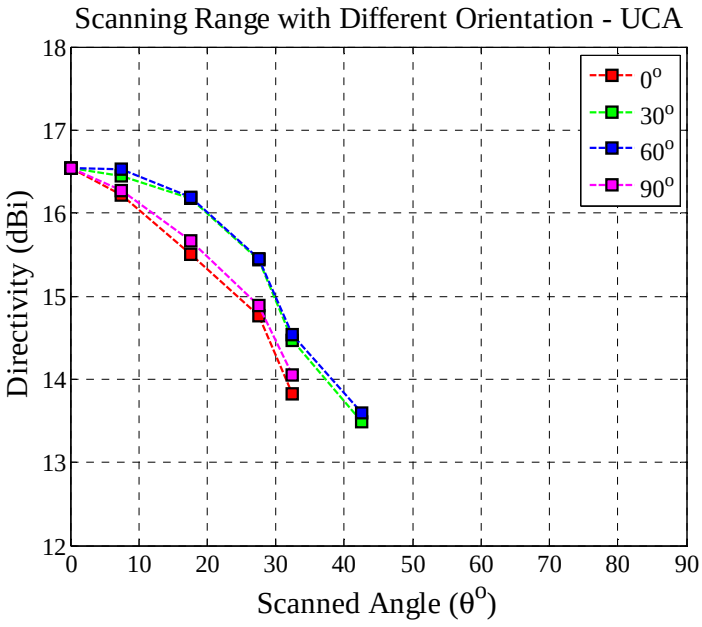

(a)

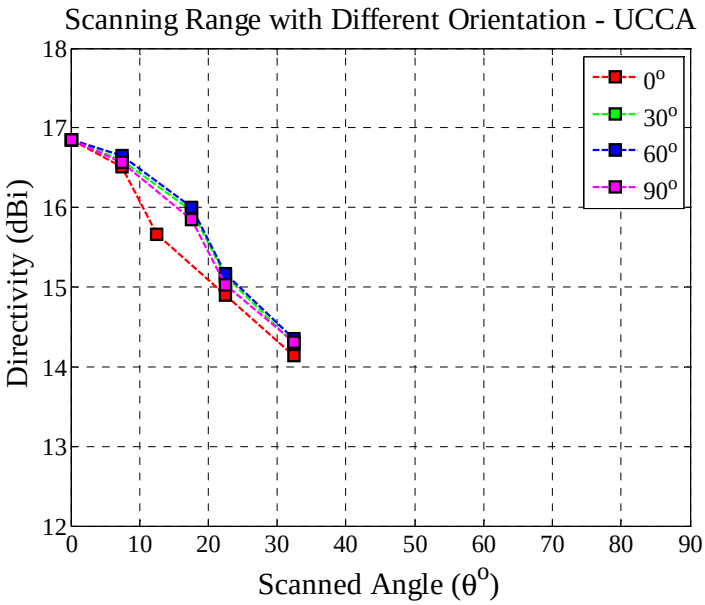

(b)

Figure 3.18: Scanning range with different element orientation, (a) UCA, and (b) UCCA.

Next, the scanning range of the UCA and UCCA corresponding to the different number of elements are plotted in Figure 3.19. In both cases, element separation, d_p, is fixed at 0.55 λ and the orientation at 60°. It is noted that, in both cases, the widest scanning range is achieved with eight elements. However, even with the same number of elements, higher

directivity at boresight is achieved with the UCCA compared to the UCA. This is due to the central element of the UCCA, which focuses a radiation to the centre of the array. Also, the 8-element UCA achieves the highest scanning range of approximately $\theta° = \pm 42°$.

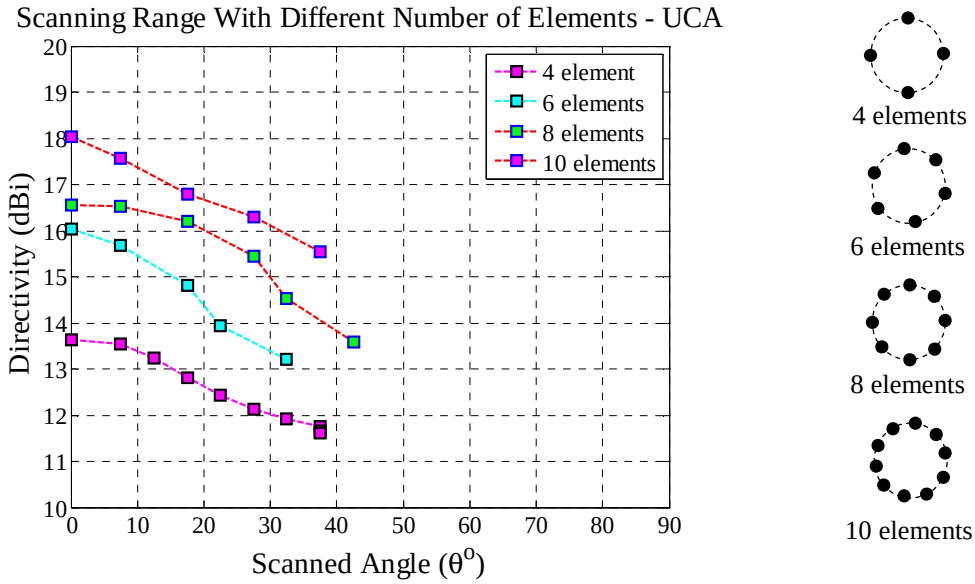

(a)

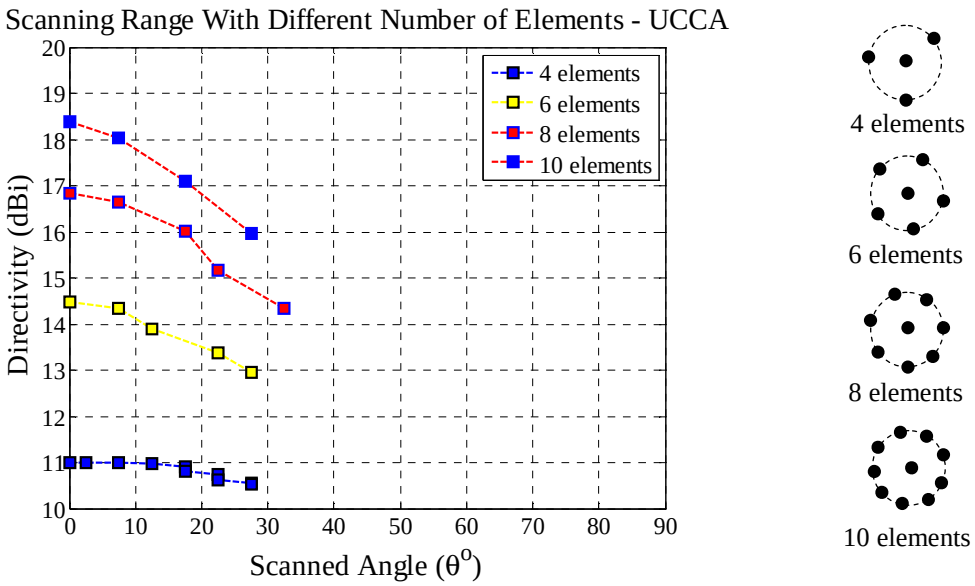

(b)

Figure 3.19: Number of elements and its influence towards scanning range, (a) UCA, and (b) UCCA.

Finally, the influence of element separation on the UCA and UCCA geometry is analysed. In this simulation, 8-element UCA and UCCA with 60° orientation are evaluated and the

scanning ranges obtained are plotted in Figure 3.20. The UCCA has a higher directivity at boresight but a narrower scanning range compared to the UCA. UCAs with element separation of 0.5 λ and 0.55 λ have the widest range at approximately $\theta° = \pm 42°$. However, when the element separation is more than 0.6 λ, the scanning range reduces due to the existence of grating lobes. The grating lobe causes the directivity to degrade as the power from the main beam is transferred to the lobes, and a similar trend is observed with UCCA.

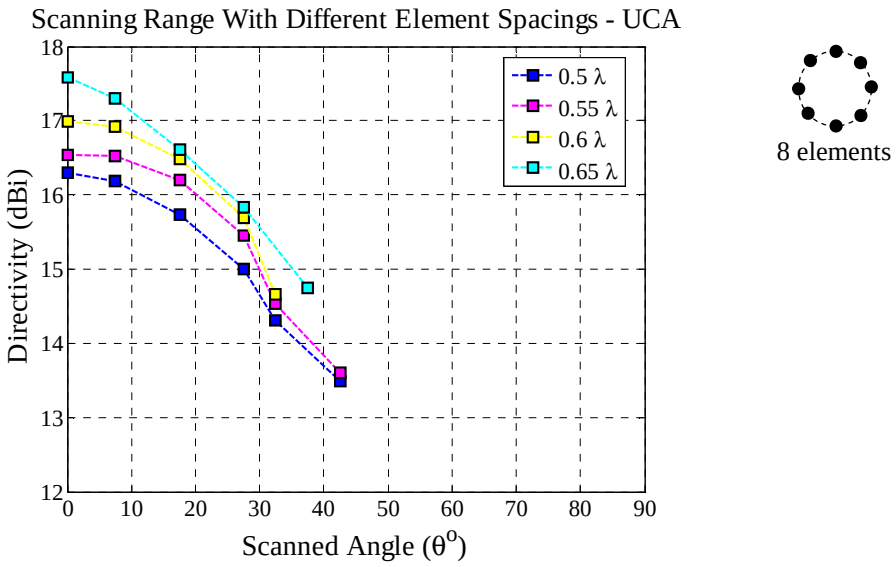

(a)

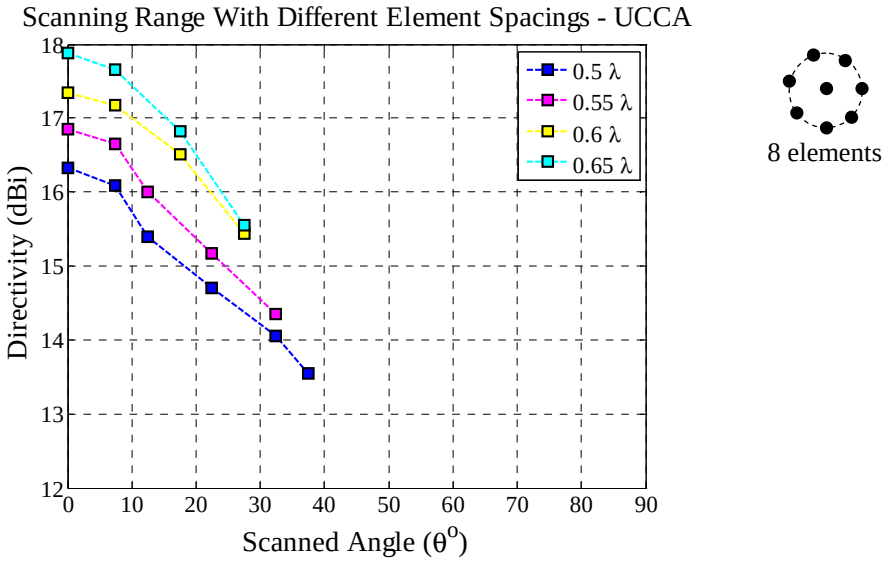

(b)

Figure 3.20: Element separation and its influence towards scanning range, (a) 8-element UCA, and (b) 8-element UCCA.

3.5.4 ULA, UCA and UCCA as Wide Scanning Arrays

Even though the scanning range of the ULA is limited to 1D space, it is observed that a wider scanning range is achieved with ULA compared to the circular arrays. With the appropriate element orientation and element spacing, the widest range achieved by 8-element ULA, UCA and UCCA is approximately $\theta° = \pm 53°$, $\theta° = \pm 42°$ and $\theta° = \pm 38°$, respectively. A wider range is achieved by the ULA as more elements are placed in a row throughout the azimuth region compared to UCA; eight elements for ULA compared to two elements for UCA and three elements for UCCA. Higher scan ranges can be achieved by UCA and UCCA when more elements are used. However, with a limited number of elements, the ULA offers the best solution for further development. The scanning range of the ULA can be increased by having a mean of curvature in its structure.

3.5.5 Faceted Arrays

The advantage of the faceted structure, compared to the cylindrical structure, is that it retains the polarisation properties of the antenna. In this section, 8-element linear faceted-structure array is analysed. Element separation, d_p, is set to 0.55 λ and the elements are arranged in Configuration-2. The geometry of the faceted arrays is shown in Figures 3.21 – 3.24.

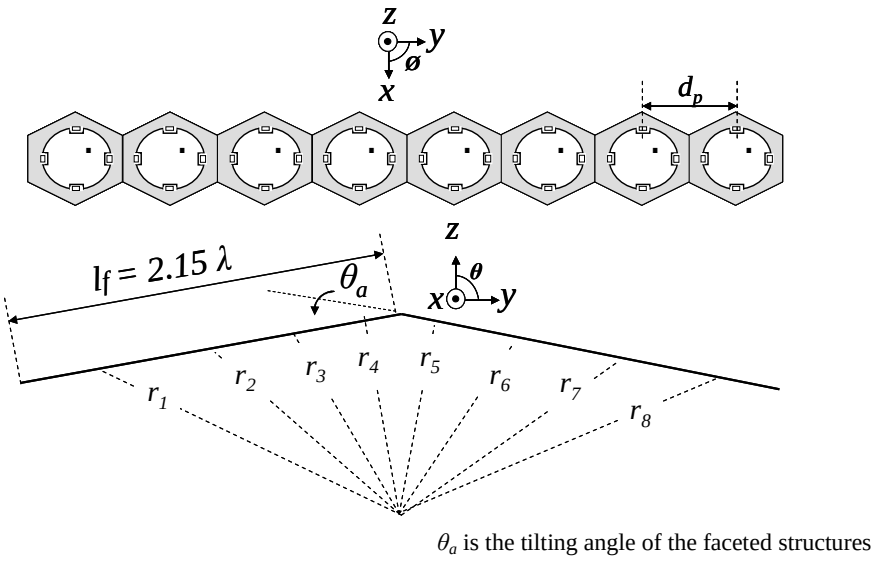

Figure 3.21: The structure of a 2-faceted array.

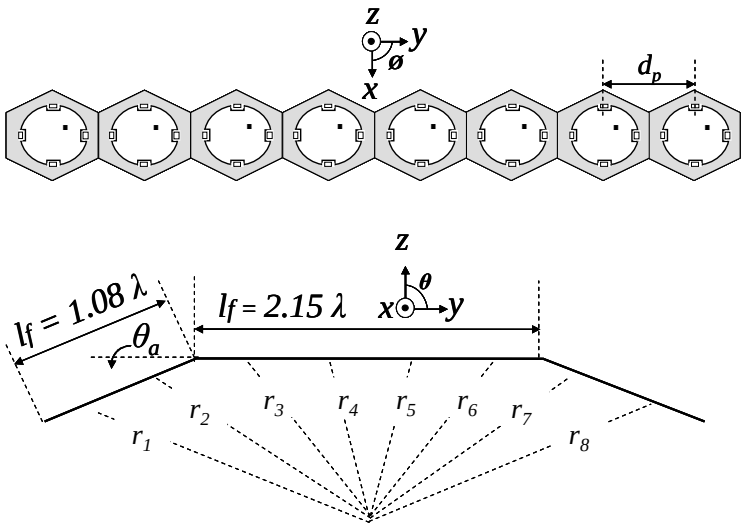

θ_a is the tilting angle of the faceted structures

Figure 3.22: The structure of a 3-faceted array.

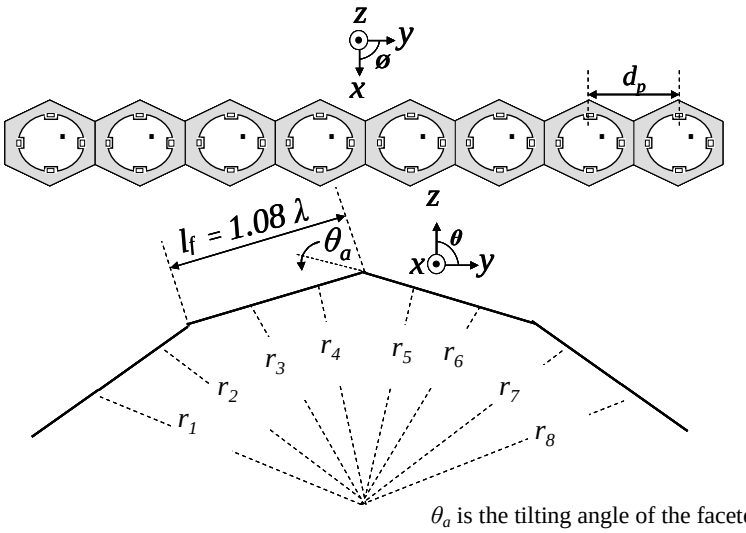

θ_a is the tilting angle of the faceted structures

Figure 3.23: The structure of a 4-faceted array.

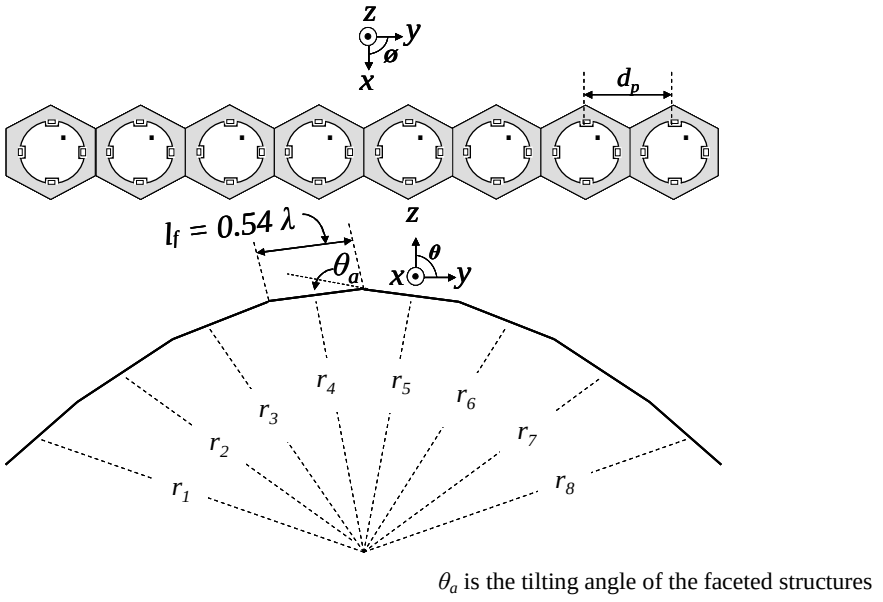

Figure 3.24: The structure of an 8-faceted array.

3.5.5.1 Correction Phase

Due to the tilting structure of the 3-faceted array, elements on the tilted panel have longer radiation paths. For example, as depicted in Figure 3.25, the radiation path of element-1, 2, 7 and 8 is longer compared to elements on the central facet. To compensate for this difference, the phases of the elements on the tilted facets need to be corrected in advance with respect to that of the central panel elements. The correction phase of each tilted element is given by Equation (3.11) [35].

$$corr\_a = k \cdot dist\_a \cdot (\sin\theta_a);\ k = \frac{2\pi}{\lambda} \tag{3.11}$$

where k is the wave number, λ is the wavelength and θ_a is the tilting angle.

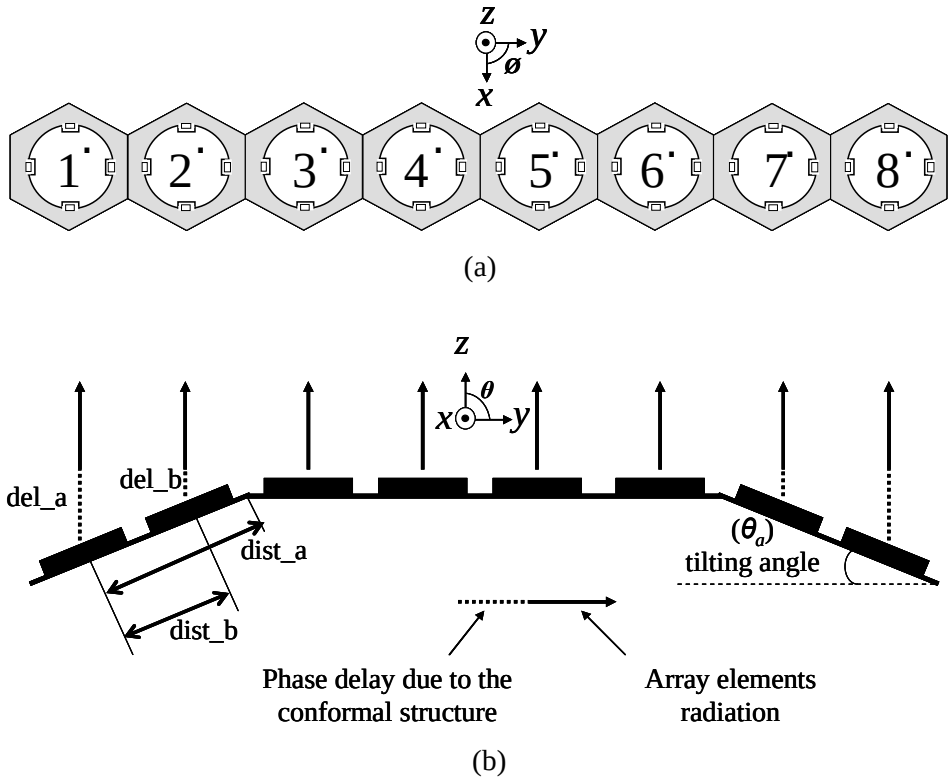

Figure 3.25: Far-field radiation of the 3-faceted array elements, (a) top view, and (b) side view.

3.5.5.2 Faceted Array Synthesis – Height

The volume of the faceted arrays is highly dependent on the tilting angle of the facets. When the tilting angle is 0°, the faceted array forms a uniform linear array. It is noted that, the degree of curvature for the faceted array increases with the tilting angle. This will consequently increase the height of the array when measured from the highest element to the lowest element. The calculation for the height of the faceted arrays is illustrated in Figures 3.25 – 3.28.

$$height_{2-faceted} = l_f \sin\left(\frac{\theta_a}{2}\right)$$

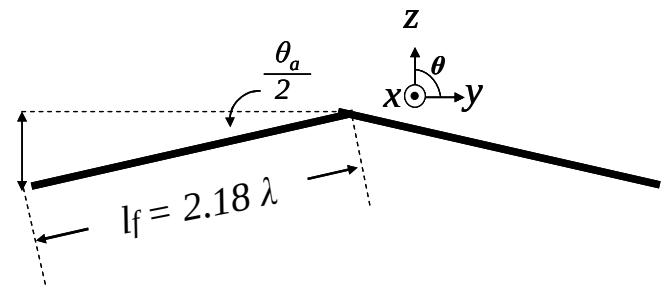

Figure 3.26: The dimension of the 2-faceted array.

$$height_{3-faceted} = l_f \sin(\theta_a)$$

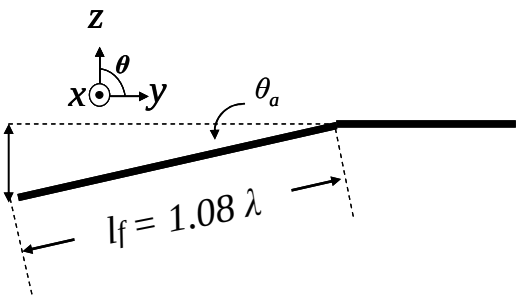

Figure 3.27: The dimension of the 3-faceted array.

$$height_{a4-faceted} = l_f \sin\left(\frac{\theta_a}{2}\right)$$

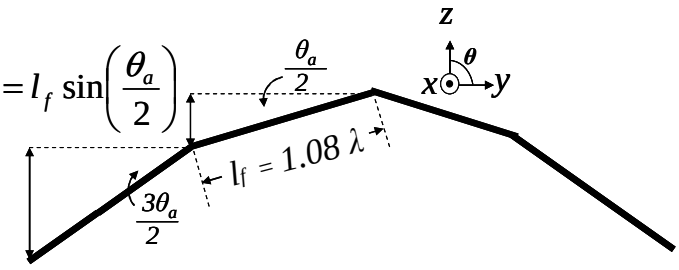

$$height_{b4-faceted} = l_f \sin\left(\frac{3\theta_a}{2}\right)$$

$$height_{4-faceted} = height_{a4-faceted} + height_{b4-faceted}$$

Figure 3.28: The dimension of the 4-faceted array.

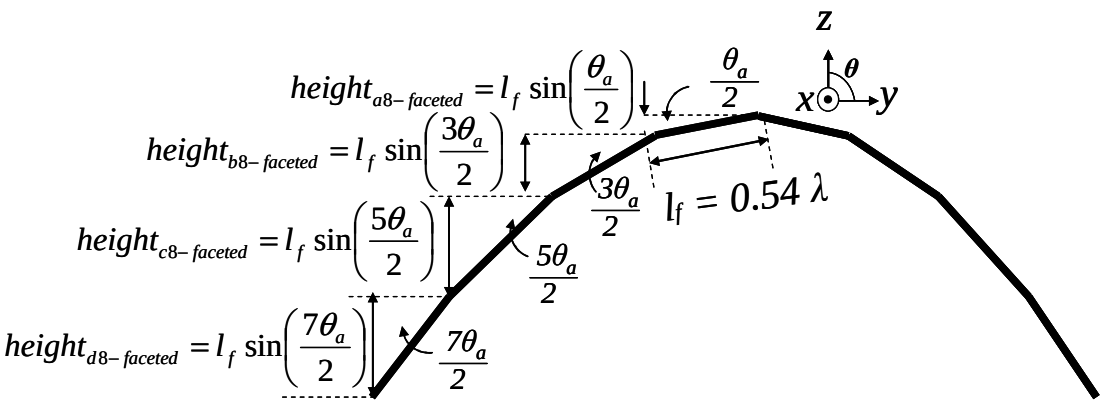

$$height_{8-faceted} = height_{a8-faceted} + height_{b8-faceted} \ldots$$
$$+ height_{c8-faceted} + height_{d8-faceted}$$

Figure 3.29: The dimension of the 8-faceted array.

The relationship between the tilting angle, θ_a, and the array height is plotted in Figure 3.30, where the θ_a is varied from 0° to 50°. The size of the faceted array is influenced by its height, and smaller-sized array is preferred especially for applications in wireless communication systems. Generally, the array height increases with increasing θ_a, and as observed in Figure 3.30, there is a significant increase in the array height for the 8-faceted array. The 2-faceted and 3-faceted arrays have similar array heights and they are less affected by the tilting angle compared to 4-faceted and 8-faceted arrays. It should also be noted that the 8-faceted array forms a complete cylindrical array when θ_a reaches 35°. Beyond this angle, the 8-faceted cylinder becomes smaller, hence reducing its height.

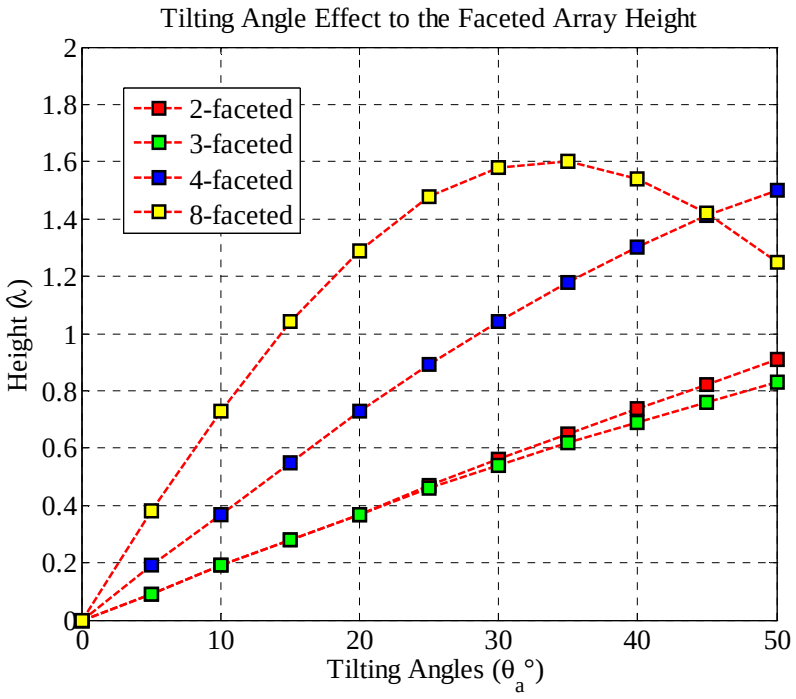

Figure 3.30: Effect of the tilting angle on the array height.

3.5.5.3 Faceted Array Synthesis – Scanning Range

The directivity over the scanning angle for each faceted array with different θ_a is plotted in Figures 3.30 – 3.33. In general, the directivity at boresight decreases as the tilting angle increases, and the decrement is more significant for the 4-faceted and 8-faceted arrays. The directivity also decreases as the main beam is steered away from the boresight.

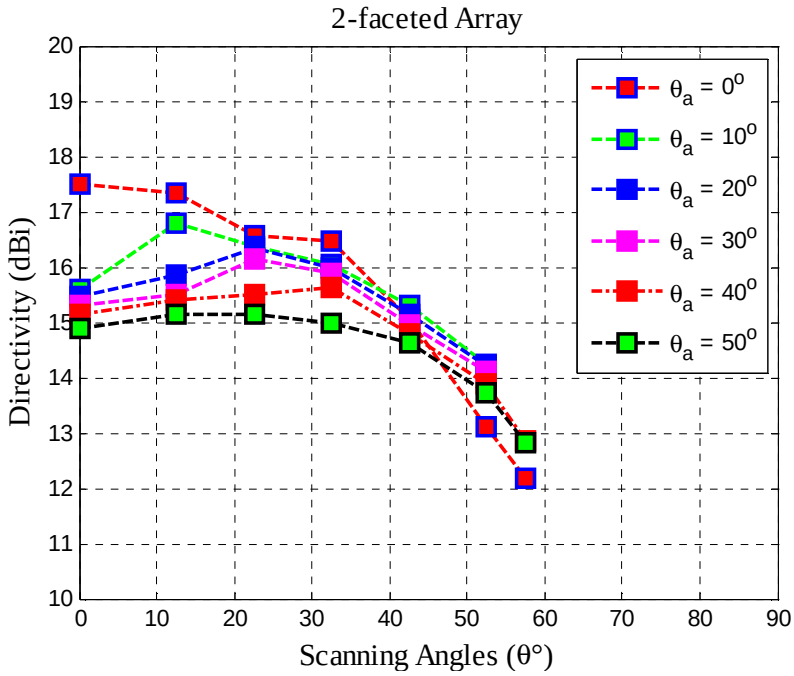

Figure 3.31: Directivity of the 2-faceted arrays with different tilting angles (θ_a).

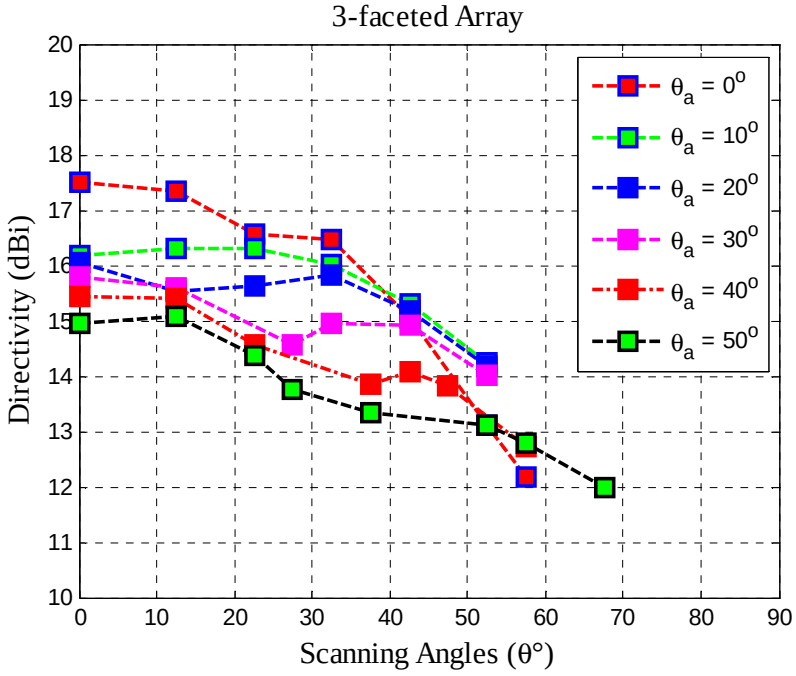

Figure 3.32: Directivity of the 3-faceted arrays with different tilting angles (θ_a).

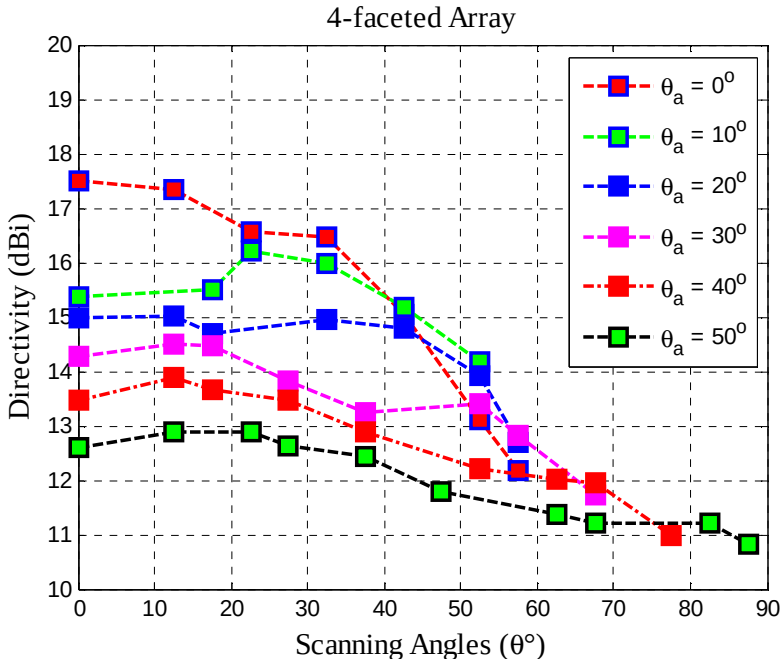

Figure 3.33: Directivity of the 4-faceted arrays with different tilting angles (θ_a).

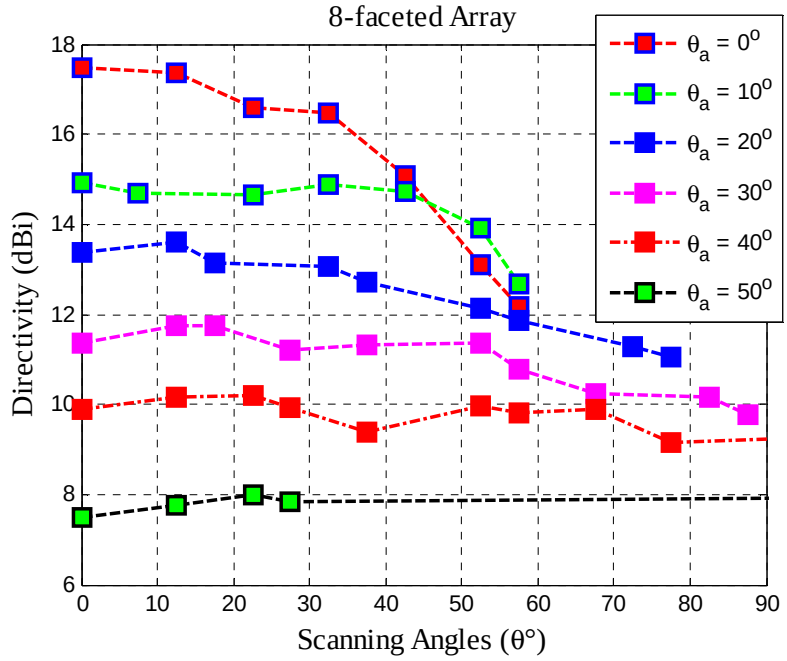

Figure 3.34: Directivity of the 8-faceted arrays with different tilting angles (θ_a).

As seen from Figure 3.31, a minimum scan angle of ±60° cannot be achieved with the 2-faceted array. To achieve a minimum scan angle of ±60°, the 3-faceted, 4-faceted and 8-faceted arrays require a minimum tilting angle of 50°, 30°, and 20°, respectively. Table 3.3

shows the highest scan angle corresponding to the tilting angles and the array heights that can be achieved by the faceted arrays. For example, the 3-faceted array can achieve a ± 62° scan angle with a tilting angle of 50° and an array height of 0.82 λ. Meanwhile, the 8-faceted array can achieve a ± 78° scan angle with a tilting angle of 20° and an array height of 1.30 λ. It is also observed that for higher tilting angles the directivity of the 8-faceted array shows very small variations over the scan angles. However, this can be a huge disadvantage for wireless communication devices as a higher tilting angle will significantly increase the space required by the array.

From these results, it is observed that small arrays can achieve a scan range of ± 60° and beyond by employing faceted structures. For applications that have minimal constraint on the array dimension, the 4-faceted or the 8-faceted array with a high tilting angle can be a good option as it provides scanning stability throughout the scan angles. However, for applications where the array dimension is a major design issue, the 3-faceted array provides the best solution.

Table 3.3: The Tilting Angle and The Array Height Corresponding to The 3 dB Scan Range.

Array	3 dB scan range	Tilt angle (θ_a)	Height (λ)
2-faceted	57°	50°	0.91
3-faceted	62°	50°	0.82
4-faceted	67°	30°	1.04
8-faceted	78°	20°	1.30
ULA	42°	-	-

Next, the directivity over scan angles of the arrays with a fixed height is compared. The heights of the arrays are fixed at 0.18 λ and 0.82 λ, and as in the previous cases, the separation of the elements is fixed at 0.55 λ. Plots of directivity as a function of the scanning angle for the different arrays are shown in Figure 3.35. Also included in these plots is the directivity of a standard uniform linear array on a flat surface. As shown in Figure 3.35 (a), in the case where the height of the array is 0.18 λ and the scanning angle is from 20° to 50°, all arrays have a similar directivity. In addition, none of the arrays are able to scan beyond 60°. When the height is increased to 0.82 λ, only the 3-faceted array is able to scan beyond 60°, as shown in Figure 3.35 (b).

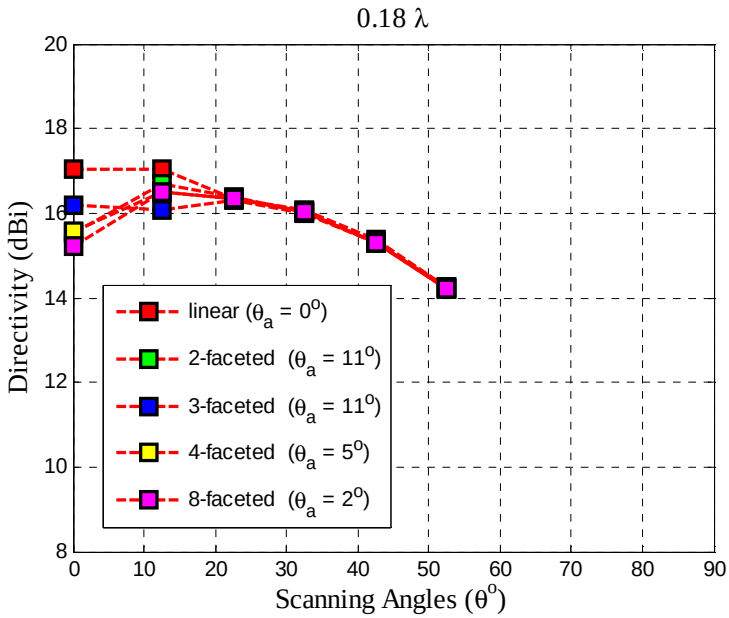

(a)

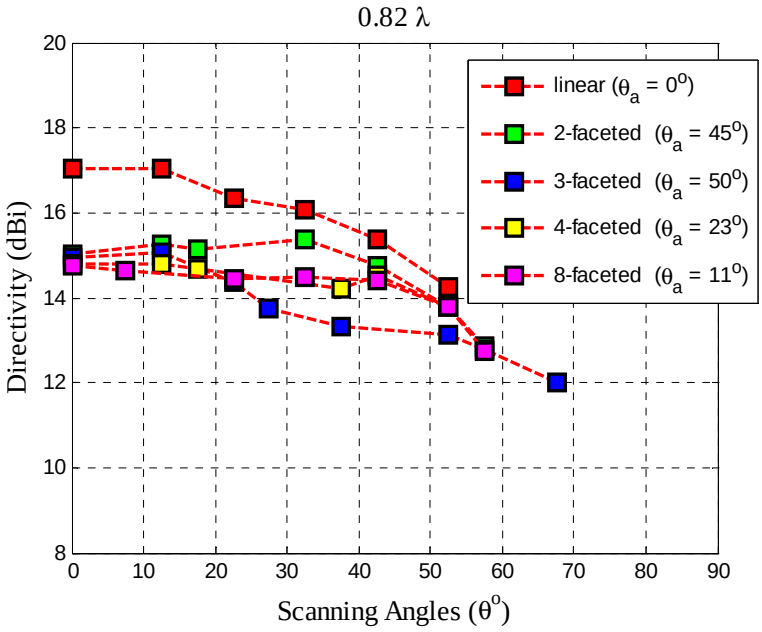

(b)

Figure 3.35: Directivity with a fixed array height (a) 0.18 λ, and (b) 0.82 λ.

3.5.5.4 Variation in 3-faceted Array – Element Separation

In Figure 3.36, the scan range of the 3-faceted array with different element spacing (λ) when θ_a = 50° is observed. It is observed that the 3-faceted array can achieve ±60° scanning range when the element separations are 0.5 λ and 0.55 λ. However, the scanning range reduces when the distance is increased to 0.6 λ. This may be due to the existence of grating lobes, which occur in array with large element spacing [35]. Even though the dimensions of 3-faceted array are smaller and can achieve ±60° scanning range with 0.5 λ compared to the array when the elements are separated by 0.55 λ, its coupling level is higher. The dimensions of the array increase with the increase in the element separation, as shown in Figure 3.36 (b). The separation significantly affects the width of the 3-faceted array compared to its height. This is due to the structure of the array as the central facet of the array is flat.

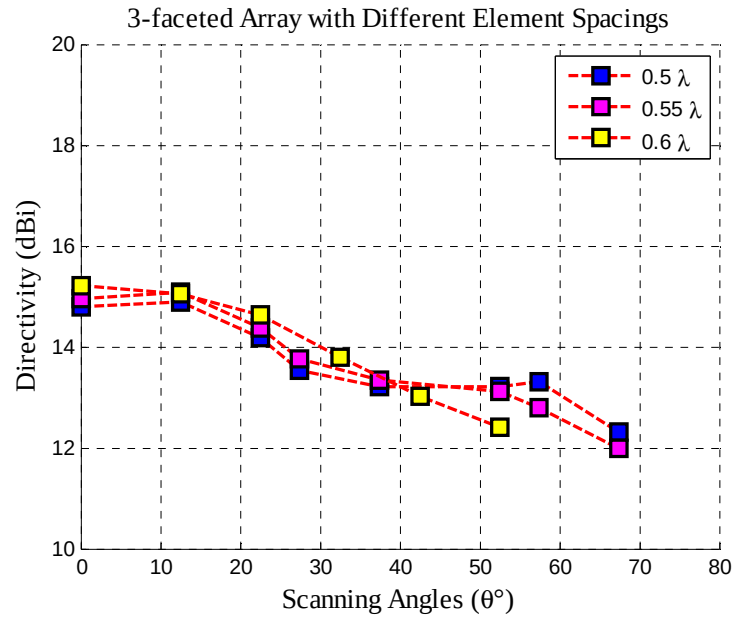

(a)

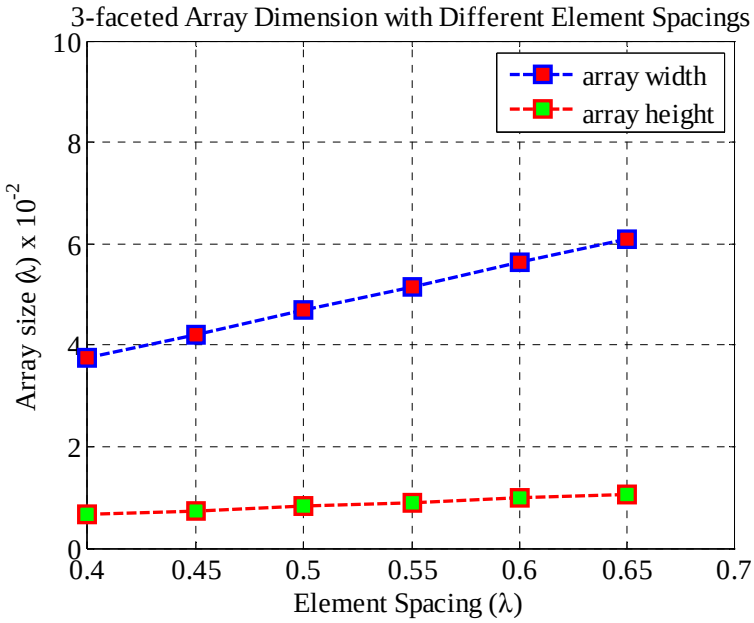

(b)

Figure 3.36: the characteristic of the 3-faceted array with different element spacing when θ_a = 50°, (a) scanning range, and (b) array dimension.

3.5.5.5 Variation in 3-faceted Array – Element Distribution

The variation of element distribution in the 3-faceted array is then observed. In this simulation, the element separation is set to be 0.55 λ and θ_a for each model is maintained at 50°. The scanning range of various 3-faceted array arrangements is plotted in Figure 3.37. From the figure, it is noted that the directivity at boresight is highest for the antenna with the 1:6:1-configuration, followed by the antenna with the 2:4:2- and the 3:2:3-configurations. However, as the main beam is steered away from boresight, the directivity dropped significantly for the 1:6:1-configuration. On the other hand, the directivity of the antenna with the 3:2:3-configuration is within 2 dB of its directivity at boresight throughout the scanning range. This is due to the evenly-distributed element arrangement of the 3:2:3-configuration compared to that of the other configurations. However, the evenly distributed array comes with the expense of increased array height of 1.2 λ (3:2:3-configuration) compared to 0.8 λ (2:4:2-configuration) and 0.4 λ (1:6:1-configuration).

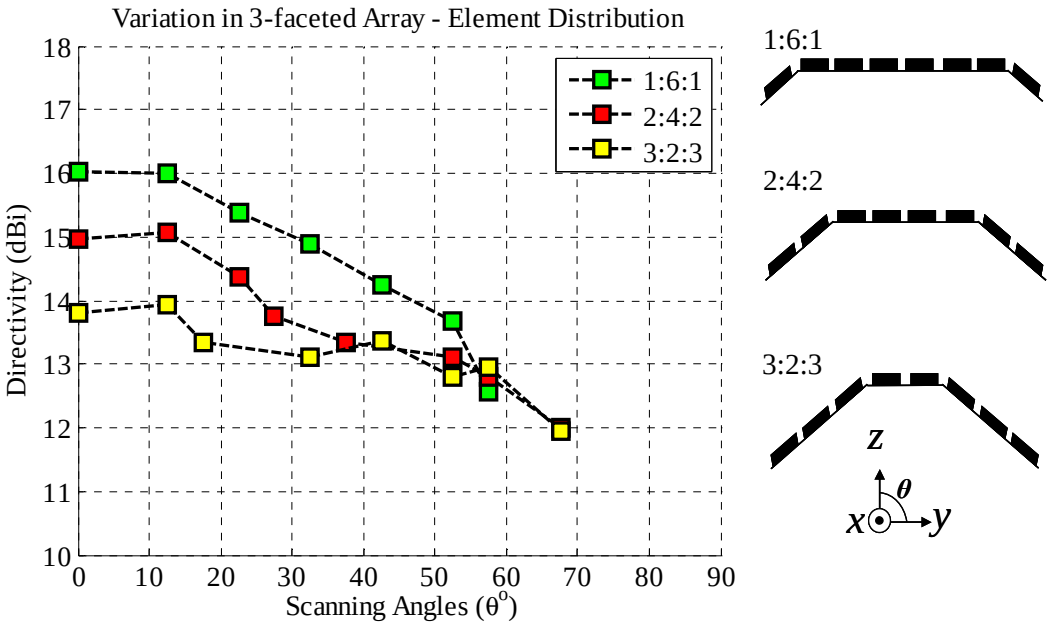

Figure 3.37: Variation of element distribution in the 8-element 3-faceted array.

3.5.5.6 Variation in 3-faceted Array – Number of Elements

The scanning ranges of the 3-faceted arrays with varying number of elements are observed in Figure 3.38. Scanning range with the highest directivity is achieved from the array with 2:6:2-configuration, followed with array 2:5:2-, 2:4:2- and 2:3:2-configurations. This is expected due to the number of elements used in the arrays: 2:6:2-configuration (ten elements), 2:5:2-configuration (nine elements), 2:4:2-configuration (eight elements) and 2:3:2-configuration (seven elements). However, the scanning range achieved by the array with 2:3:2- and 2:4:2-configurations are wider compared to 2:6:2- and 2:5:2-configurations. Higher directivity at boresight is achieved when more elements are concentrated in the central plane. The side panel having fewer elements compared to the central panel and this causes the directivity to reduce significantly when it is steered away from the boresight.

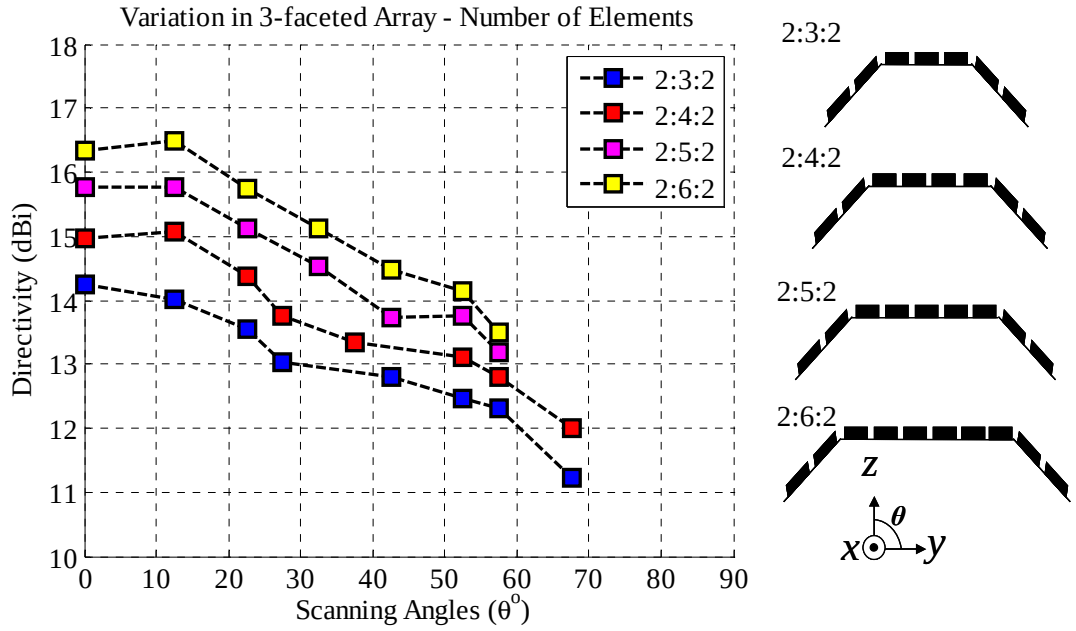

Figure 3.38: Variation of the 3-faceted array with different number of elements.

Based on the simulations of the faceted arrays, it is observed that the 3-faceted array provides the best option in expanding the scanning range of the linear ULA. The 3-faceted array is able to achieve wider scan range with the minimum height compared to the other faceted structures. It is also observed that the 3-faceted array with the 2:4:2-configuration offers the best trade-off between the array dimension and the scanning range. To further the investigation, the 3-faceted array with 2:4:2-configuration is modelled in CST Design Suite 2011 and discussed in the next section.

3.6 Full-wave Analysis of the 3-faceted Array

3.6.1 Input Impedance and Mutual Coupling

The S-parameters of the 3-faceted array when the main beam is at $\theta = 0°$ is shown in Figure 3.39. As observed in Figure 3.39 (a), the input impedance of the elements shifts slightly from the original resonant frequency of 2.4 GHz, due to the coupling between the elements in the array. The antennas induce current into each other which affects their impedance level. Also, mutual coupling between the antennas, as shown in Figure 3.39 (b), is analysed. Mutual couplings between element pairs 1–2, 3–4, 4–5, 5–6 and 7–8 are all approximately equal at -16 dB. However, mutual couplings between element pairs 2–3 and 6–7 are lower, approximately at -21 dB. The coupling levels are influenced by the tilting angle. A higher tilting angle provides more isolation between array elements, which results in much lower coupling levels.

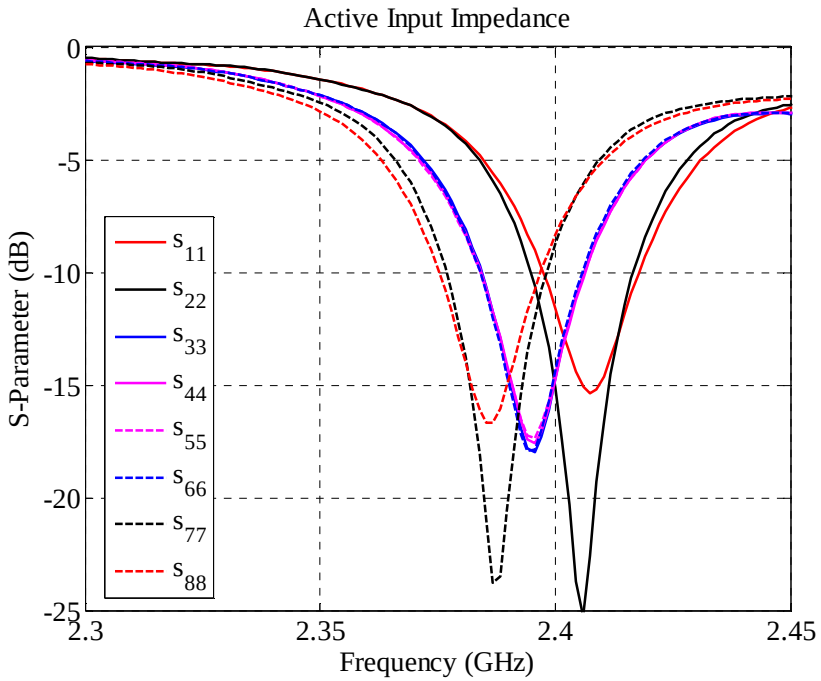

(a)

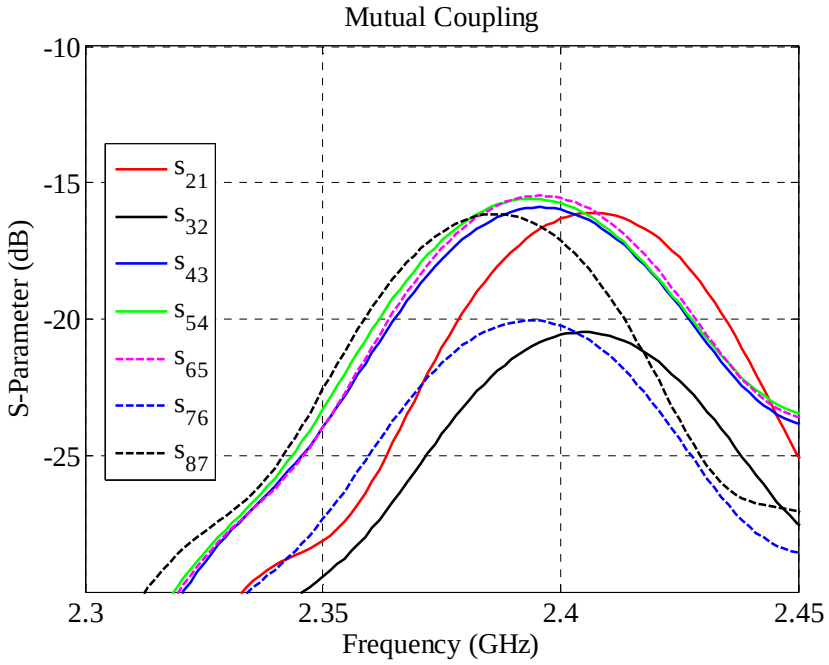

(b)

Figure 3.39: S-parameters for the 3-faceted array, (a) reflection coefficient, and (b) mutual coupling.

3.6.2 3-Faceted Array Scanning Range

The 3D radiation pattern of the 3-faceted array is shown in Figure 3.40. Next, the radiation properties of the 3-facted array are compared against the ULA. The 2D radiation pattern of the flat-surface and the 3-faceted array are shown in Figure 3.41. At boresight, the ULA formed a narrower main beam compared to the 3-faceted array. However, as the scanning reaches 60°, grating lobes start to appear in the ULA. Grating lobes are not desired in adaptive antennas as they expose the system to noise and interference signals coming far from the desired signal. Furthermore, the grating lobe also causes the array to radiate at unwanted angles.

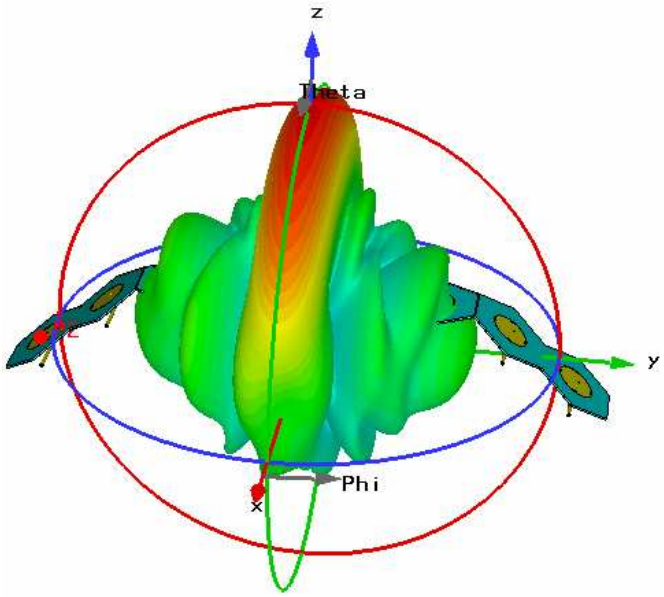

Figure 3.40: 3D radiation pattern of the 3-faceted array.

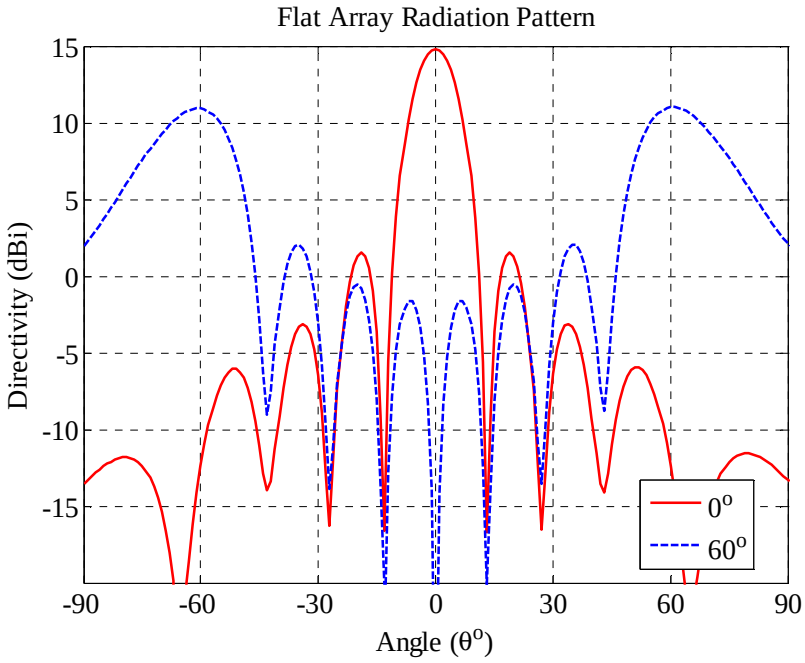

(a)

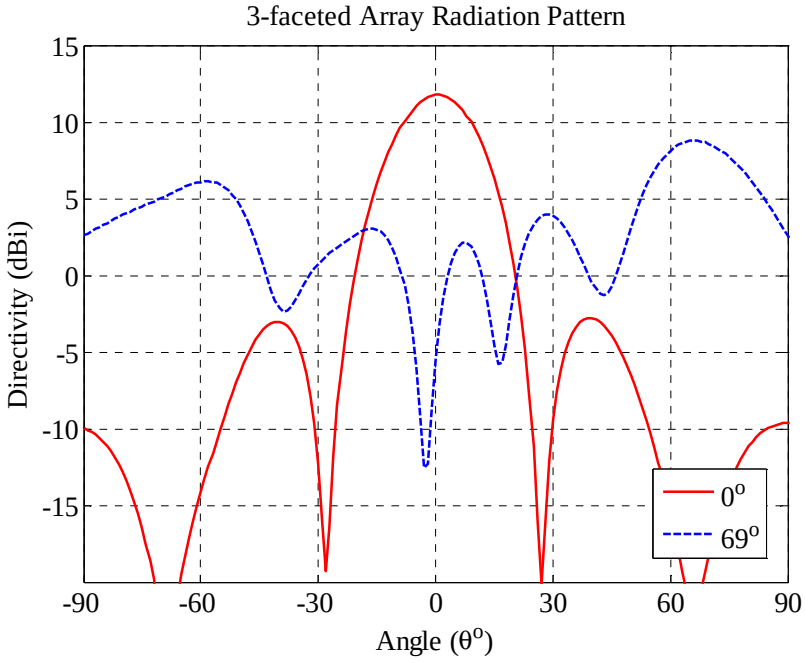

(b)

Figure 3.41: Radiation patterns of the arrays, (a) ULA, and (b) 3-faceted Array.

The scanning ranges for both 3-faceted array and ULA over the scan angle and their corresponding SLL are plotted in Figure 3.42. The directivity of the array is plotted from the boresight to the scan angle at which the directivity is dropped by 3 dB. The phase excitation of each antenna corresponding to the steering angle is tabulated in Table 3.4. As shown in Figure 3.42 (a), the directivity of the ULA is higher than the 3-faceted array throughout the scanning range. However, the 3 dB scanning range of the 3-faceted array reaches ±69° while for the ULA, it only reaches ±56°. In Figure 3.42 (b), the SLL of the arrays corresponding to the position of the main beams is plotted. The SLL of both arrays increases with the scanning range. However, the SLL of the 3-faceted array remains lower than the main beam throughout the scan.

Table 3.4: The Phase Excitation of the Elements.

Phase Excitation (°)								**Main beam**
1	**2**	**3**	**4**	**5**	**6**	**7**	**8**	**direction (θ°)**
3-faceted Array								
280	110	0	0	0	0	110	280	0
100	260	0	30	60	90	10	240	7
65	240	0	60	120	180	122	8	15
350	180	0	150	300	90	170	170	50
350	180	0	120	240	360	210	230	55
350	180	0	90	180	270	230	250	57
350	181	0	60	120	180	250	290	60
8	180	0	150	300	90	312	23	69
Uniform Linear Array								
0	30	60	90	120	150	180	240	0
0	60	120	180	240	300	360	60	9
0	90	180	270	360	90	180	240	18
0	120	240	360	120	240	360	240	27
0	150	300	90	240	30	180	330	37
0	160	320	120	280	80	240	40	52
0	170	340	150	320	130	300	110	56
0	180	360	180	360	180	360	180	60

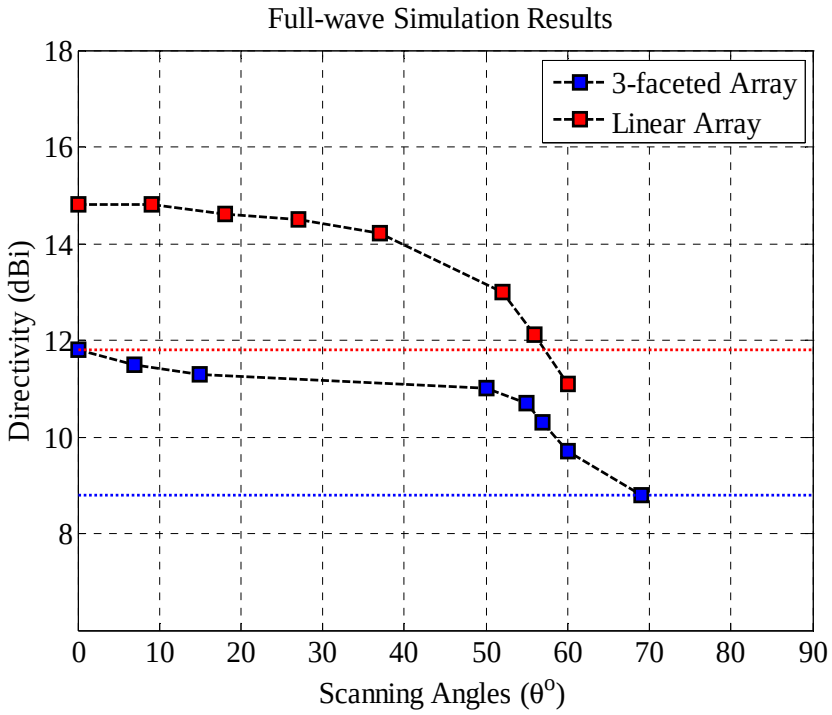

(a)

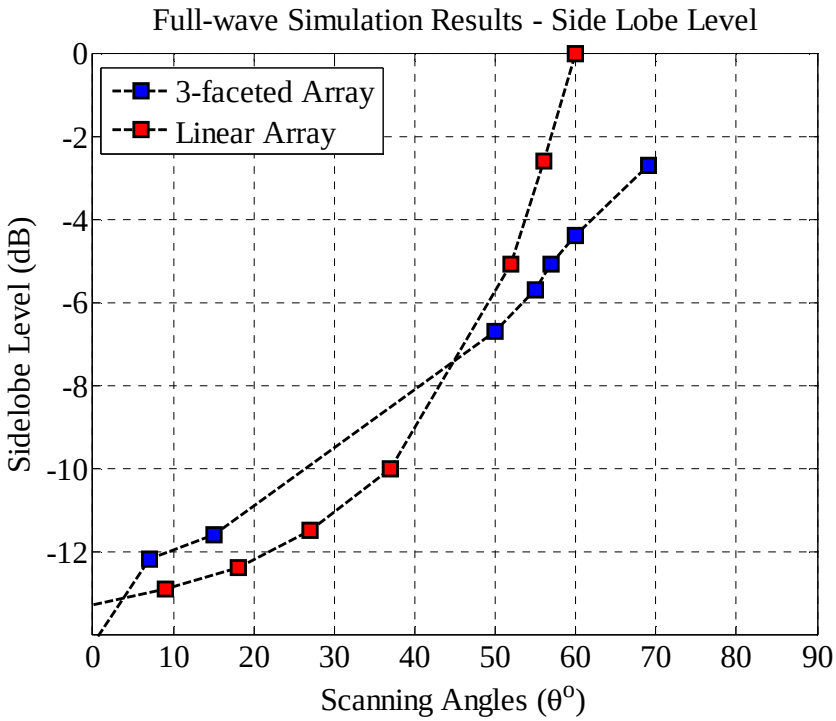

(b)

Figure 3.42: Radiation properties of linear array and 3-faceted array, (a) 3 dB scanning ranges of the arrays, and (b) sidelobe levels of the arrays.

3.7 Low Sidelobe Level Synthesis

As discussed in the previous section, the 3-faceted array achieves the widest scanning range at approximately 70° from boresight. The 3-faceted array, however, generates high sidelobe levels due to its tilting structure.

3.7.1 Amplitude Tapering Method

Adaptive array antennas can be synthesised for low SLL using the amplitude tapering method via the windowing technique. The procedure to synthesise the array is essentially identical to the design process for a FIR filter in digital signal processing (DSP) [23]. The SLL of an adaptive array antenna can be minimised by increasing the radiation intensity from the elements in the centre and simultaneously reducing the radiation intensity from the elements at the edges [23]. The coefficients of an FIR filter and the weightings in an adaptive array antenna are illustrated in Figure 3.44.

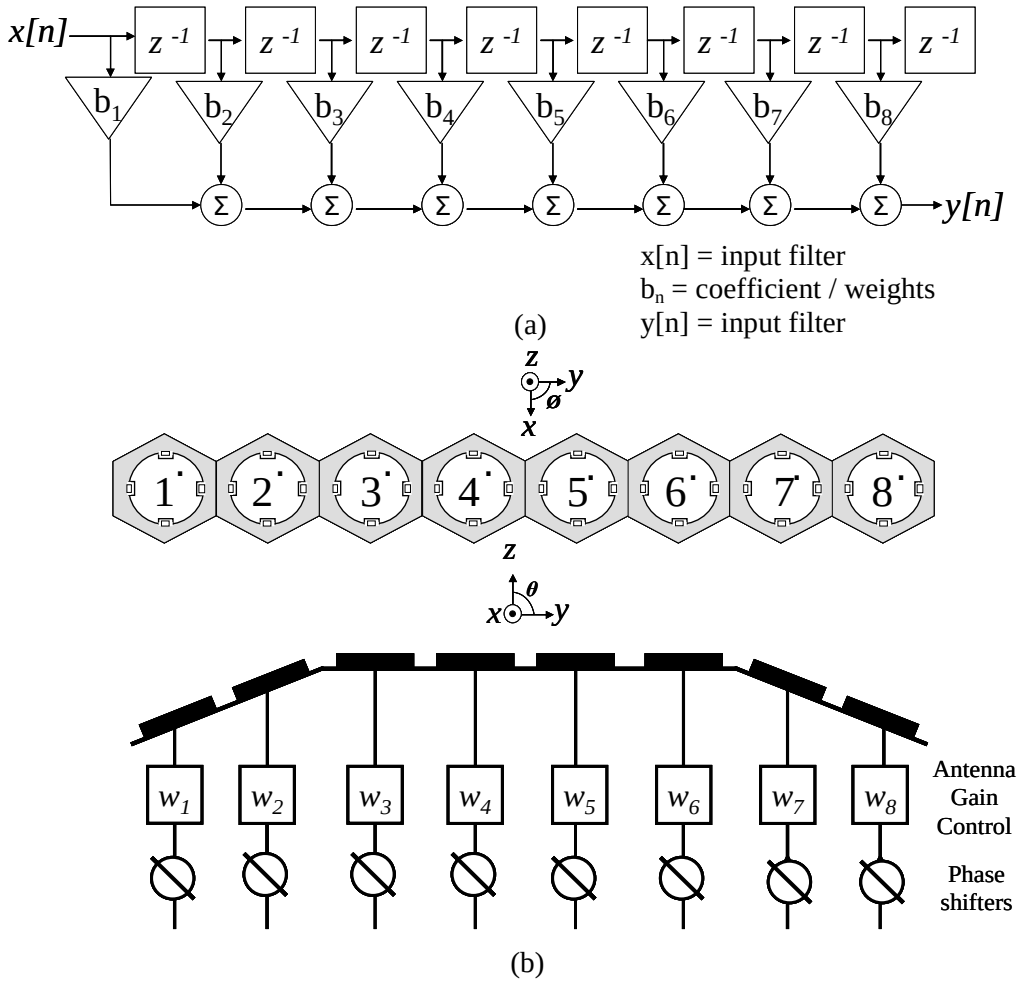

Figure 3.43: Weightings in (a) FIR filters, and (b) Adaptive arrays.

The procedure to synthesise an adaptive array antenna for low SLL using the windowing technique is much simpler than the stochastic optimisation approach, and for arrays with a small number of elements, such as the 8-element 3-faceted array, making the use of the amplitude tapering method is more appropriate. Several windowing techniques for filter design such as Dolph-Chebychev, Gaussian, Kaiser, Hamming and Blackman have previously been used to synthesise adaptive array antennas for low SLLs [23, 35, 46].

For linear arrays, the procedure of using the windowing technique is straight forward as the amplitude excitation of the elements in the array is controlled based on the window coefficients. However, for other kind of array configurations, some steps need to be considered due to the placements of the elements in the array. In [54], techniques to synthesise a uniform circular array (UCA) for low sidelobe levels using the Dolph-Chebyshev Window were proposed, which involved the transformation of the array element space to a mode space. This transformation creates a spatial response of the UCA which is similar to the uniform linear array and enables the use of Dolph-Chebyshev Window.

Unlike planar arrays, variations in the radiation paths of the elements on the faceted array are greater, due to the tilting nature of the antenna structure. By transforming the arrays, the faceted arrays can also be synthesised for low sidelobe levels using the windowing technique. The 3-faceted array is transformed to a linear array by compensating for the phase difference of the elements on the faceted structure. This transformation process has already been discussed as phase correction in Section 3.5.5.1. In this chapter, window functions including Binomial, Taylor, Kaiser and Chebychev are used to synthesise the 3-faceted array for low sidelobe levels. In the following section, this technique is elaborated and analysed. The array consists of eight LHCP antennas, which was proposed in Chapter 2. The height of the 3-faceted array is set to 0.8 λ, the tilting angle (θ_a) is set to 50°. The geometry of the 3-faceted array is illustrated in Figure 3.22.

3.7.2 Low Sidelobe Level Synthesis for the 3-faceted Array

In this section, the 3-faceted array is synthesised for low sidelobe level (SLL). The amplitude tapering method used in the synthesis ranges from the classical window function, such as the Binomial Window, to the tunable windows, such as Kaiser Window.

3.7.2.1 Main Beam at θ = 0°

The 3-faceted array is can be synthesised for low SLL using amplitude weighting techniques. The radiation patterns and the corresponding amplitude distributions for the 3-faceted array

using Blackman, Binomial and Hamming windows are shown in Figure 3.44. The amplitude and phase excitations of the array elements are listed in Table 3.5. As observed from Figure 3.44 (a), the narrowest main beam is obtained with the uniform weighting but at the expense of increased SLL. On the contrary, the Blackman weighting produces a radiation pattern with the lowest SLL but with the widest main beam.

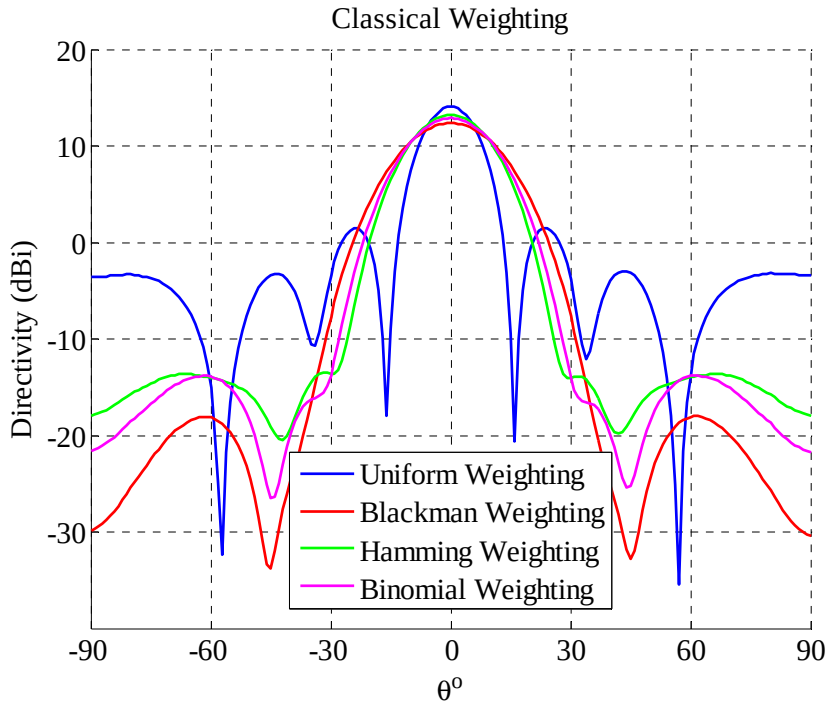

(a)

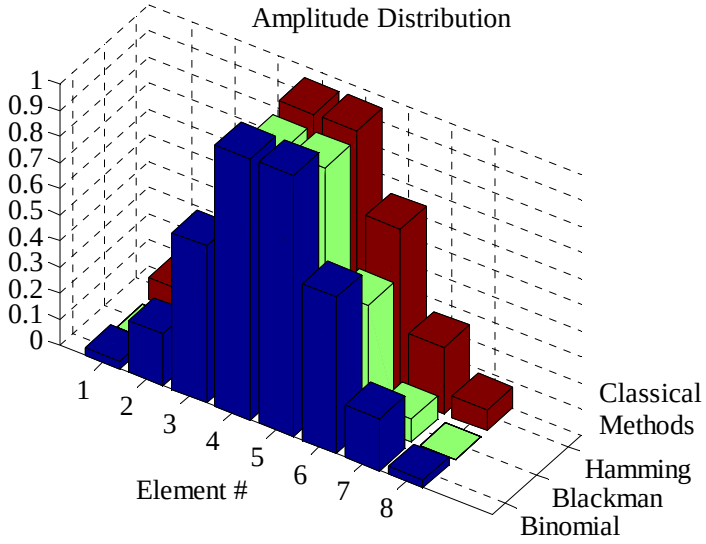

(b)

Figure 3.44: Low SLL technique with Binomial, Blackman and Hamming Windows, (a) radiation pattern, and (b) amplitude distribution.

Another class of amplitude tapering technique is using Kaiser, Taylor and Chebyshev windows. These windows have variable input parameter, which allows the SLL to be customised. The amplitude and phase excitations of the array elements are listed in Table 3.5. In Figure 3.45, the resulting radiation patterns of the 3-faceted array using the Kaiser

Window with different α values are plotted. It can be seen that lowest SLL is obtained with α = 3. On the other hand the narrowest main beamwidth is obtained when α = 1.

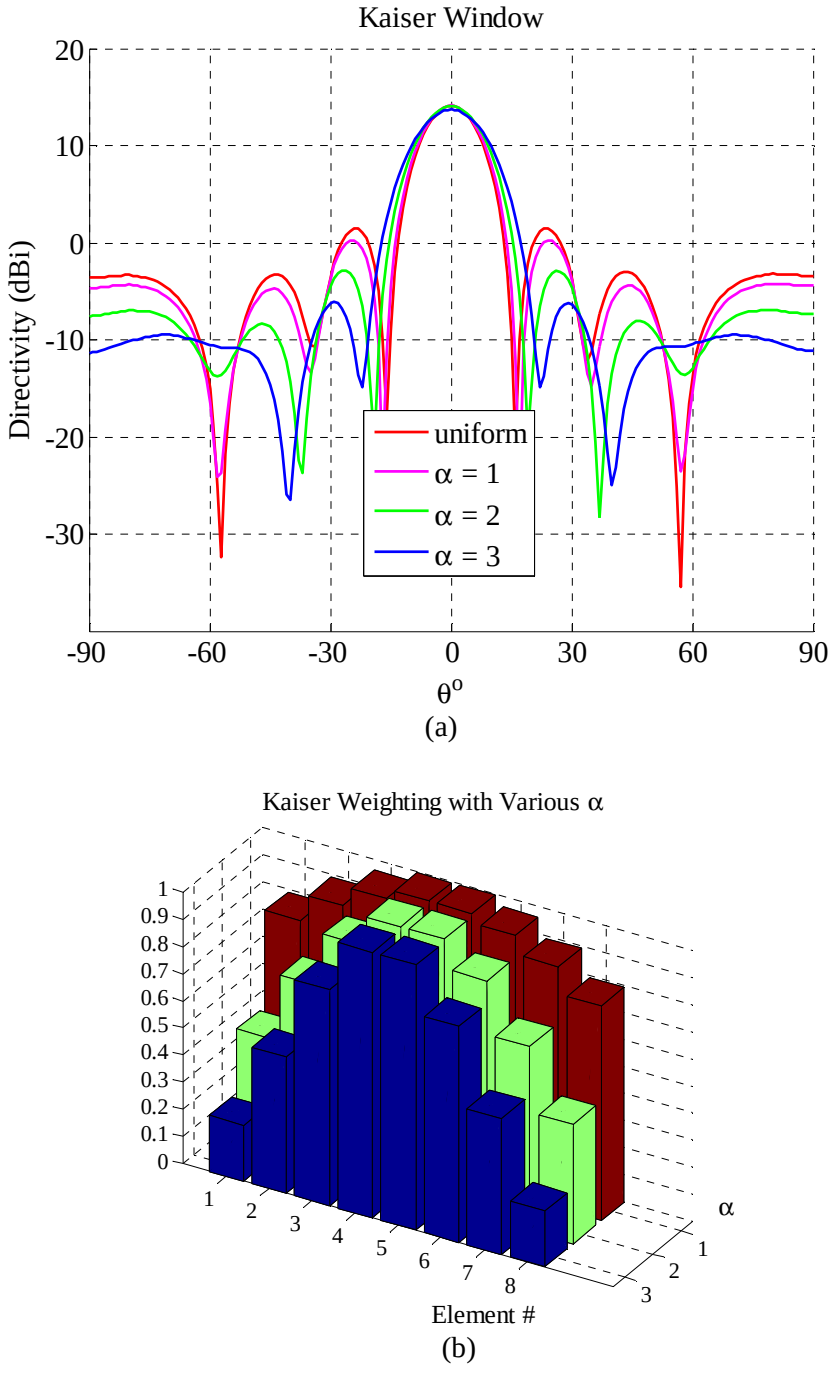

Figure 3.45: Low SLL synthesis using Kaiser Window with different α values, (a) radiation pattern, and (b) amplitude distribution.

The radiation patterns of the 3-faceted array using Taylor and Chebyshev Windows are shown in Figure 3.46 and Figure 3.47, respectively. In both simulations, similar trade-offs are observed, where lower SLLs are obtained at the expense of a broader main beamwidth. The amplitude and phase excitations of the array elements are also listed in Table 3.5.

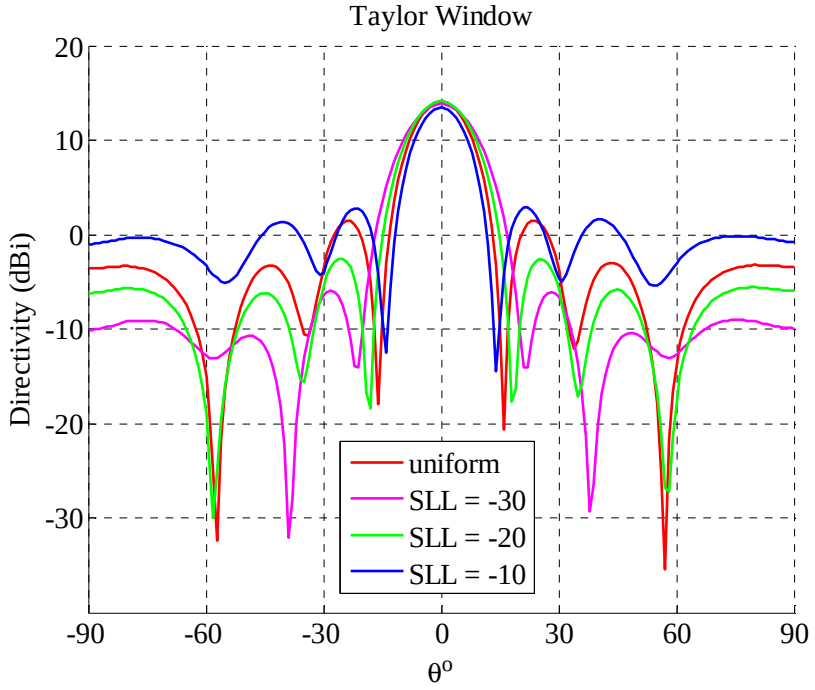

(a)

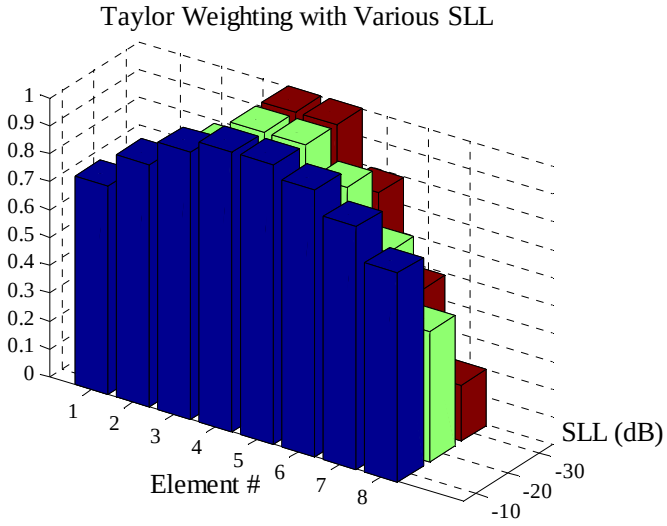

(b)

Figure 3.46: Low SLL synthesis using Taylor Window with different SLL, (a) radiation pattern, and (b) amplitude distribution.

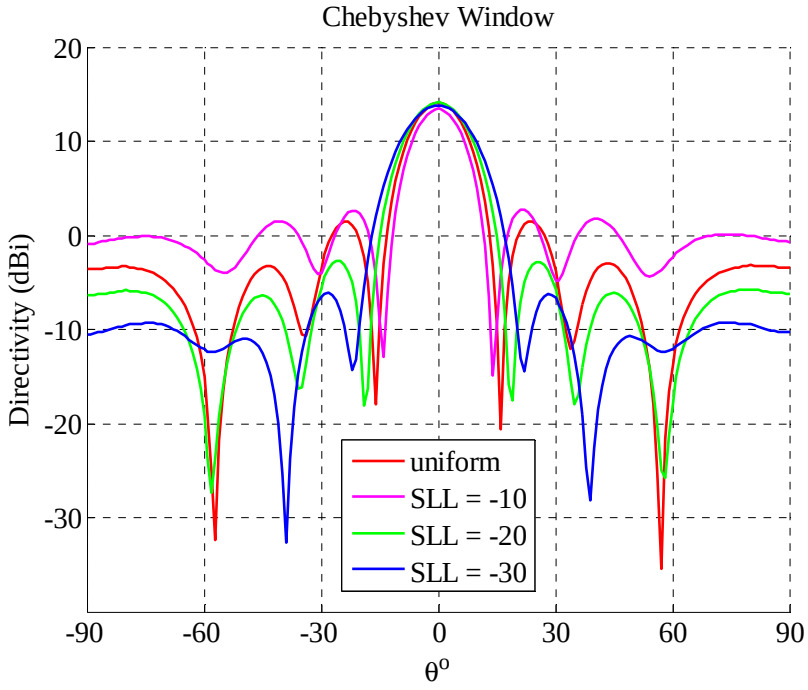

(a)

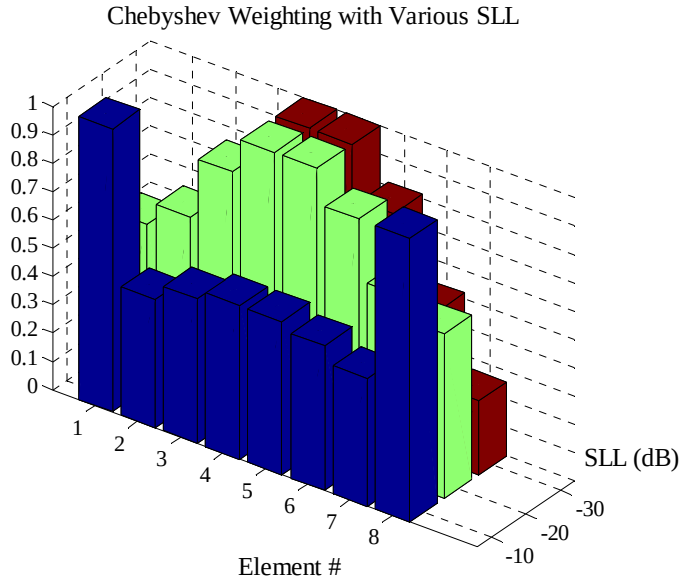

(b)

Figure 3.47: Low SLL synthesis using Chebyshev Window with different SLL, (a) radiation pattern, and (b) amplitude distribution.

The amplitude and phase excitations of the array elements using Blackman, Binomial, Hamming, Kaiser, Taylor, and Chebyshev windowing techniques are listed in Table 3.5.

Table 3.5: Element excitation for the 3-faceted array with Low Sidelobe Levels (Amp < Ø°).

Weighting / Element	1 & 8	2 & 7	3 & 6	4 & 5
Uniform	1.00 < 287°	1.00 < 168°	1.00 < 0°	1.00 < 0°
Binomial	0.03 < 287°	0.20 < 168°	0.60 < 0°	1.00 < 0°
Blackman	0.01 < 287°	0.09 < 168°	0.46 < 0°	0.92 < 0°
Hamming	0.08 < 287°	0.25 < 168°	0.64 < 0°	0.95 < 0°
Kaiser	0.20 < 287°	0.50 < 168°	0.79 < 0°	0.97 < 0°
Chebychev	0.26< 287°	0.52< 168°	0.81< 0°	1 < 0°
Taylor	0.28< 287°	0.53< 168°	0.81< 0°	1 < 0°

3.7.2.2 Main Beam at θ = 60°

Figure 3.48 shows the radiation pattern of the 3-faceted array at two different scan angles, which are 0° and 60°. The array is synthesised for low SLL using four different windows: Blackman, Kaiser (α = 3), Taylor (SLL = -30) and Chebyshev (SLL = -30). The directivity of the array decreases as the main beam is steered away from boresight, and simultaneously, the grating lobes begin to appear. The occurrence of the grating lobe degrades the peak directivity of the main beam. The lowest SLL is achieved with the Blackman window but at the expense of wide beam width. However, the Kaiser, Taylor and Chebyshev tuneable windows give radiation patterns that have lower SLLs than the uniform distribution. With these tuneable windows, the 3-faceted array is able to generate radiation patterns with low SLLs and narrow main lobe width.

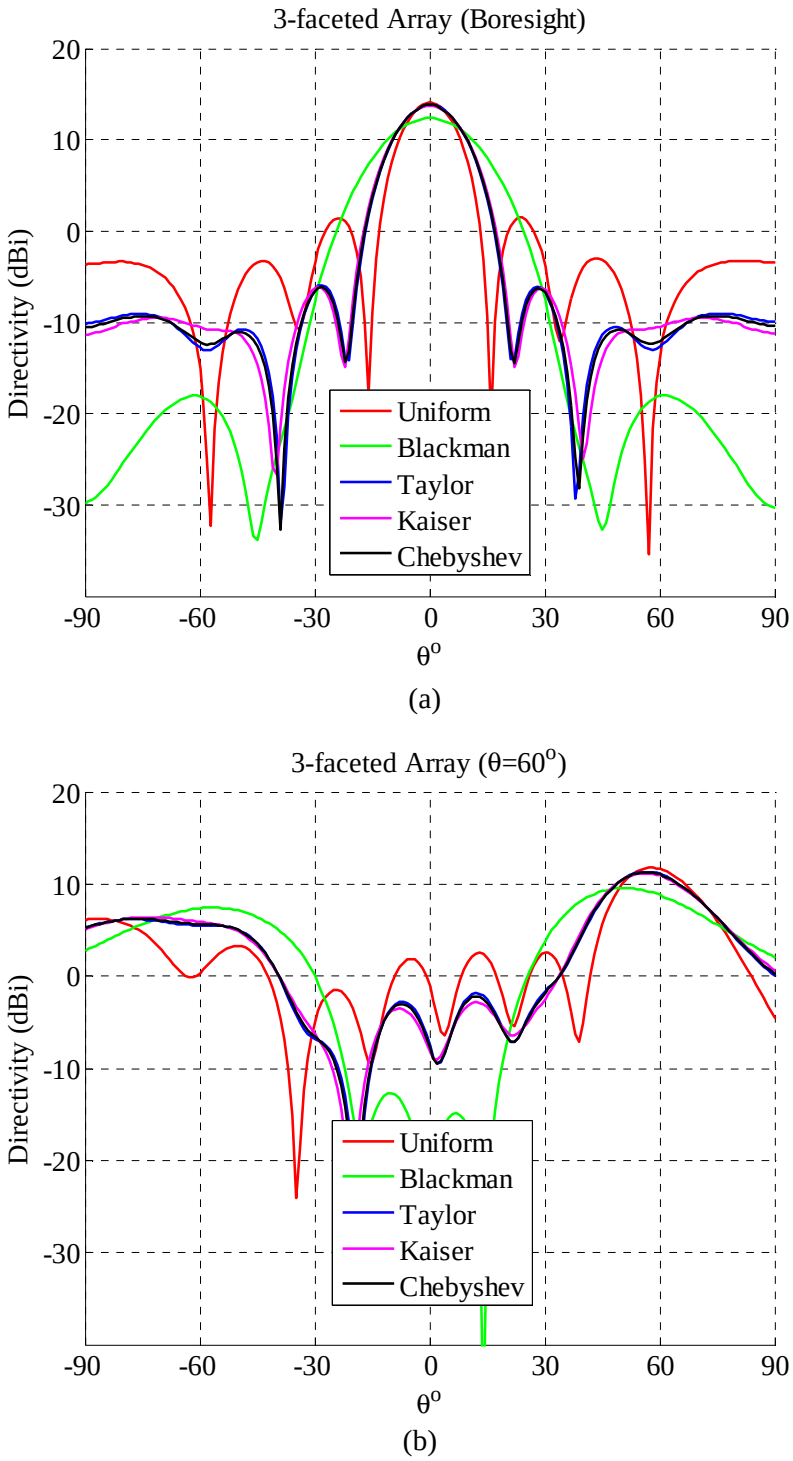

Figure 3.48: Low SLL Synthesis with Windowing Techniques, (a) $\theta = 0°$, and (b) $\theta = 60°$.

3.7.2.3 Low Sidelobe Level Discussion

Due to the degree of curvature of the 3-faceted array, a wider scanning range can be achieved, but it comes at the cost of high sidelobe levels. The tilt in the structure causes the elements of the array to have different far-field radiation paths. By compensating for the phase delays arising from these different paths, the conventional amplitude tapering method that is normally used for uniform linear arrays can be applied to the 3-faceted array. In this chapter, amplitude tapering method using the windowing techniques, which include Binomial, Dolph-Chebychev and Taylor weightings, together with phase corrections are used in order to synthesise the 3-faceted array with low side lobe levels.

The use of a window function with tuneable properties, such as Kaiser, Chebyshev or Taylor allows the SLL of the array to be customised. The radiation pattern generated by these tuneable windows has a similar profile to the uniform amplitude distribution but with a much lower SLL and broader main beam. Overall, Blackman weighting produces the lowest SLL but with the widest beam width, while uniform weighting produces the narrowest beam width but has the highest SLL. The sidelobe levels of the 3-faceted array that is generated using Kaiser Window are 10 dB less than the one using uniform window. Also, the Kaiser window is the best window to use as it balances the trade-off between the SLL and the width of the main beam.

With this technique, not only has the 3-faceted array the benefit of wider scanning range, but also of lower sidelobe levels. In the next chapter, a single port beamforming algorithm will be investigated.

3.8 Summary

In summary, the investigation on the array design with wide scan angle discussed in this thesis is illustrated in Figure 3.49. This chapter addressed the procedure for synthesising of antenna arrays with wide scanning angle where there is a constraint on the number of elements, in particular arrays with fewer than 10 elements. By introducing a mean of curvature to the array structure, such as the faceted array, the scanning range of an array can be increased. In this chapter, the scanning ranges of ULA, UCA and faceted arrays were investigated and the influence of various array design parameters on the 3 dB scanning range was evaluated. Initially, the array orientation with the lowest coupling level is determined and using geometrical approach, the optimum design of wide scanning range array is determined. The 3-faceted array with the 2:4:2-configuration is found to be the optimum array and it is then modelled in a full-wave solver and the results showed that the 3 dB scan

range of the 3-faceted array could reach up to ±70°, which is higher than that of a ULA which is ±56°. It is also noted that mutual coupling levels between the elements of the 3-faceted structure are influenced by the tilting angle. Furthermore, in order to achieve a scan range of more than 60°, the height of the 3-faceted array is lower than the other faceted arrays. Hence, the 3-faceted array was shown to be the optimal solution for applications that have size constraints, such as the wireless communication system. On the other hand, for applications that are not bounded by the array size, the 8-faceted array is a better choice as it can achieve the widest scan range.

To date, design synthesis of faceted array antennas has been targeted on arrays with a large number of elements. This chapter presents a comprehensive analysis on 8-element faceted array antennas, namely 2-faceted, 3-faceted 4-faceted and 8-faceted arrays. The ability of the eight element 3-faceted array to achieve a wide scan range with limited number of elements makes it suitable for a low cost adaptive array antenna for wireless communication systems. Throughout this chapter, the arrays are evaluated in terms of their 3 dB scanning range. In the next chapter, these faceted arrays will be evaluated from the perspective of interference nulling, where the amplitude and phase excitations of the elements are optimised in order to place the main beam at the desired angle and nulls at the interfering angles. In the next chapter, the beamforming algorithms used to optimise the complex excitation of the array elements are discussed. By suppressing the interference, the spatial discrimination of adaptive array antennas is maximised and this allows more communication traffic in the wireless system.

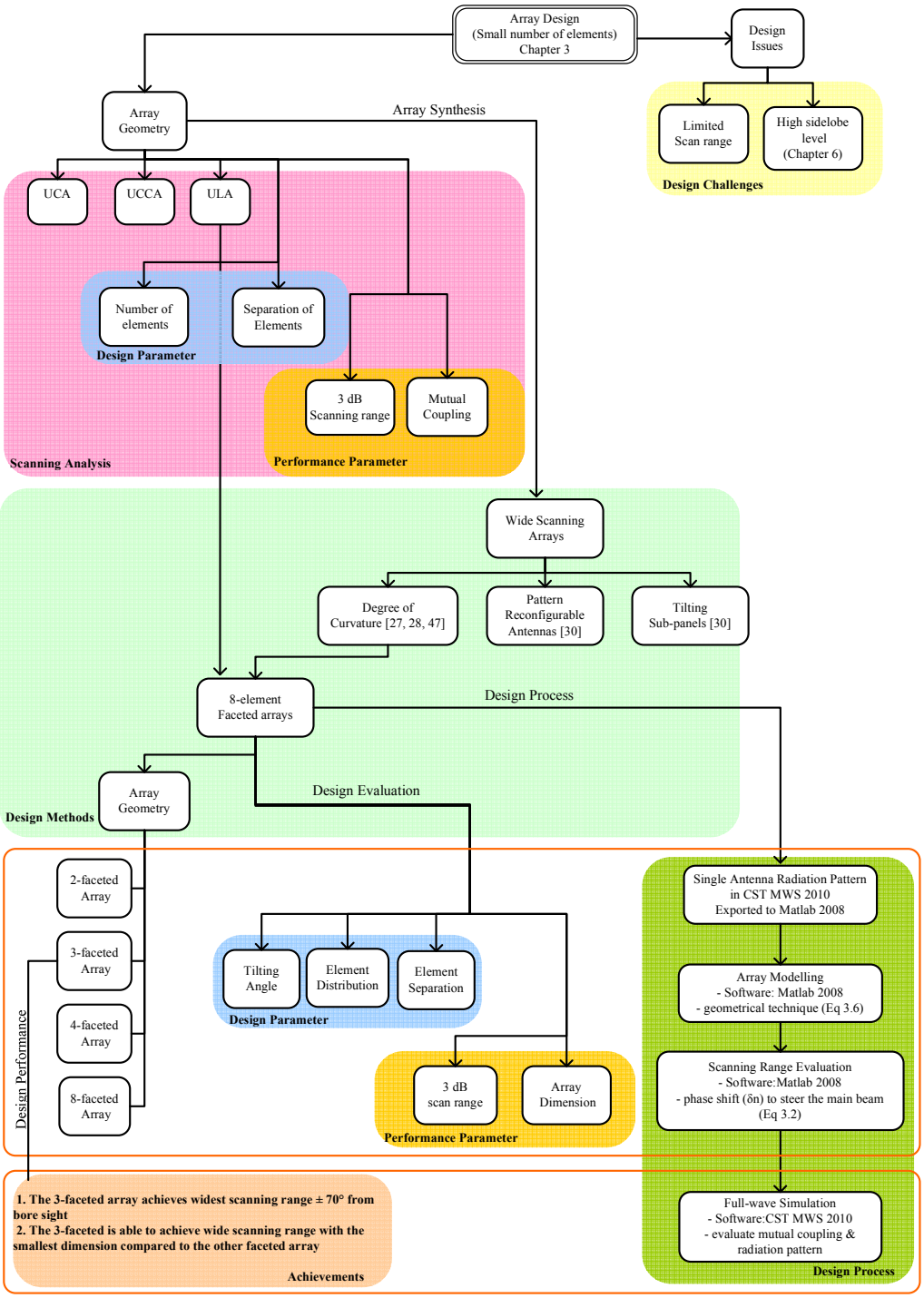

Figure 3.49: The investigation of array design with wide scan angle property.

Chapter 4
Faceted Arrays for Adaptive Beamforming Applications

4.1 Introduction

In Chapter 3, the designs of the adaptive array antenna with wide angle coverage for wireless communication system have been described. By introducing a mean of curvature to the array, such as the faceted structure, the scanning range of the array can be increased. Throughout the design process, the arrays have been evaluated in terms of their 3 dB scanning range, and it is found that the 3-faceted array achieves the widest scanning range. This means that the directivity of the 3-faceted array is maintained within 50 % from the maximum directivity. In this chapter, the 8-element uniform linear array (ULA) and the faceted arrays, namely 2-faceted, 3-faceted, 4-faceted and 8-faceted arrays, will be evaluated from the perspective of adaptive beamforming. Two beamforming approaches will be used, namely, mMSE and mSINR. The spatial usability of the faceted arrays are then compared and analysed.

This chapter is divided into four sections. Section 4.2 presents the theories behind the beamforming techniques Section 4.3 discusses the background study of adaptive array

evaluations for beamforming applications. The comparison of the faceted arrays are presented and discussed in Section 4.4. Finally, Section 4.5 summaries the chapter.

4.2 Beamforming Algorithm

The radiation characteristic of an adaptive array antenna can be tailored in order to optimise the signal transmission and reception properties of a communication system. One aspect of adaptive array antennas is adaptive beamforming, where the complex excitations of the array elements are adjusted in order to place the main beam at the desired angle and nulls at the interfering angles [2, 3, 54-56]. Studies have found that antennas with adaptive beamforming are capable of increasing data rates and maximising the channel capacity in a communication channel [5, 6, 51, 57-61].

In this work, conventional beamforming optimisation techniques such as minimum MSE, maximum SINR and power minimisation are used, in order to evaluate the performance of the faceted array antennas. The discussion on some of the advanced and robust adaptive beamforming can be found in [62-66].

For a narrowband adaptive array antennas, as shown in Figure 4.1, the output of the array can be formulated as in the following Equation (4.1) [67].

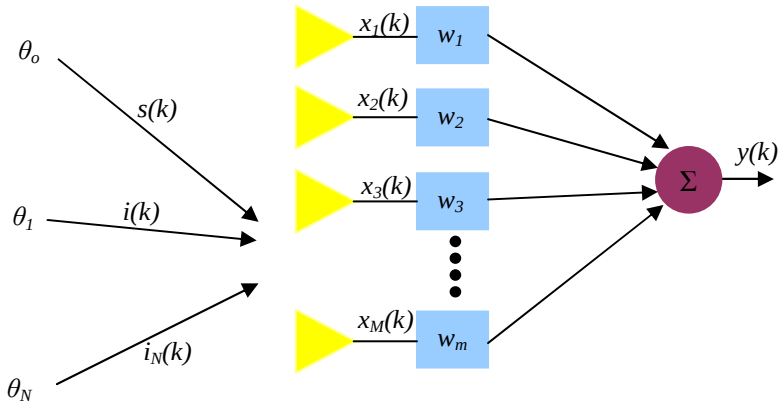

Figure 4.1: Narrowband beamforming structure [67].

$$y(k) = \overline{w}^{H}(k)\bar{x}(k) \tag{4.1}$$

where $\bar{w}^H(k)$ is the Hermitian transpose of the array weight vector and $\bar{x}(k)$ is the vector of the received signals. This signal $\bar{x}(k)$ can be expressed as in Equation(4.2).

$$\bar{x}(k) = \bar{x}_s(k) + \bar{x}_i(k) + \bar{n}(k) \tag{4.2}$$

where $\bar{x}_s(k)$ is the desired signal vector, $\bar{x}_i(k)$ is the interfering signal vector and $\bar{n}(k)$ is the zero mean Gaussian noise for each channel.

4.2.1 Adaptive Beamforming Optimisation Criteria

Adaptive beamforming can be achieved by different optimisation criteria, which includes minimum Mean-Square Error (MSE), power minimisation and maximum Signal to Interference-plus-Noise Ratio (SINR) [3, 46, 63, 65, 67-70]. To accomplish the required criteria, adaptive algorithms, such as Least Mean Squares (LMS), and biologically inspired algorithms, such as Particle Swarm Optimisation (PSO), are used [51, 57, 59, 68, 70-73].

4.2.1.1 Minimum Mean Square Error (MSE)

The illustration of adaptive beamforming using minimum MSE as the optimisation criteria is shown in Figure 4.2 [67]. The array output is subtracted from an available reference signal, *d(k)*, to generate an error signal, *ε(k)*. This error signal is then used to control the array weights, as expressed in Equation (4.3) [67, 74].

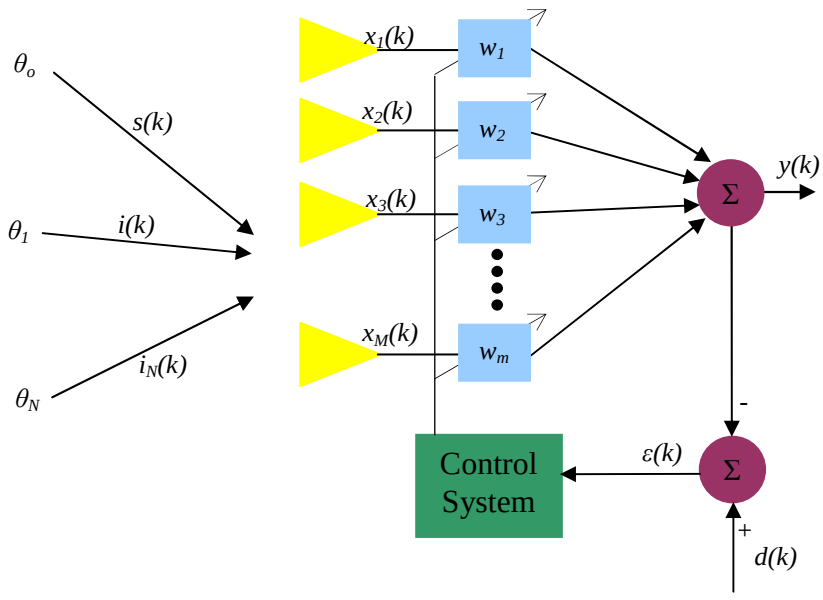

Figure 4.2: MSE based adaptive beamforming algorithm [67].

$$\left|\varepsilon(k)\right|^2 = \left|d(k) - \overline{w}^H \overline{x}(k)\right|^2 \tag{4.3}$$

where $\varepsilon(k)$ is the error of the received signal, $d(k)$ is the desired signal, $\overline{w}^H$ is the Hermitian transpose of the array weight vector and $\overline{x}(k)$ is the vector of the received signals.

4.2.1.2 Maximum Signal to Interference-plus-Noise Ratio (SINR)

Another method that can be used to perform adaptive beamforming is by maximising the SINR of the system [67, 69, 75, 76]. The SINR is described by Equations (4.4) – (4.5) [69, 77].

$$SINR = \frac{\left|\overline{w}^H \cdot \overline{x}\right|^2}{\overline{w}^H \cdot \overline{R}_{xx} \cdot \overline{w}} \tag{4.4}$$

$$\overline{R}_{xx} = \overline{R}_{ii} + \overline{R}_{nn} + \overline{R}_{ss} \tag{4.5}$$

where $\overline{X}$ is the vector of received signals, $\overline{w}$ and $\overline{w}^H$ are the vector of array weights and its Hermitian transpose, respectively, $\overline{R}_{ss}$ is the correlation matrix for the desired signal, $\overline{R}_{ii}$ is the correlation matrix for the interference signal and $\overline{R}_{nn}$ is the correlation matrix for the noise.

4.2.1.3 Power Minimisation

Adaptive beamforming can also be achieved when the output power of the array is minimised towards the direction of interfering signals, termed as power minimisation. The objective function of the power minimisation technique is described by Equation (4.6) [60, 65]. From the function, note that this technique does not require the information of the signal correlations, and this implies that with power minimisation criteria, the existing array architecture can be deployed without additional components such as signal correlators [46].

$$F = \max\left(abs\left[\left|AF(\theta_m)\right| - \sum_{\substack{j=1 \\ j\neq m}}^{M} \left|AF\left(\theta_j\right)\right| \right] \right) \tag{4.6}$$

where AF is the array factor, θ_m is the angle of the desired signal, θ_j is the angle of the interference signals and M is the total number of interfering signals.

4.2.2 Optimisation Method

In time-varying signal environments, such as in wireless communication systems, the signals received by the antenna changes with time. For this kind of environment, a recursive update of the weight vector is needed in order to achieve optimal transmission of the desired signal. This section discusses the common optimisation technique used in adaptive array antennas, which are Least Mean Squares (LMS) algorithm and Particle Swarm Optimisation (PSO) [51, 57, 59, 64, 68, 70-73]. The use of these optimisation techniques depends on the targeted optimisation criteria of the beamforming algorithms such as discussed in the previous section. For example, adaptive algorithm, such as LMS algorithm, is commonly used in beamforming technique that uses linear function, such as minimum MSE, as the optimisation criteria. On the other hand, beamforming techniques with non-linear performance criteria, such as the SINR and the power minimisation, can be solved using biologically inspired techniques, such as the PSO algorithm.

However, the drawback with adaptive algorithms is that they require a receiver at each element of the array in order to calculate the covariance matrix. This introduces extra costs and requires consistent calibrations [57].

The use of power minimisation as the optimisation criteria, discussed in Section 4.2.1.3, on the other hand does not require the signal correlation information, hence offer a cheaper solution to the system. Power minimisation is a non-linear function and stochastic algorithm such as PSO or GA can be used for the optimisation. However, this kind of beamforming scheme comes with a trade-off of a slow convergence rate.

In summary, the choice of the optimisation method for an adaptive array antenna depends on the optimisation criteria and these criteria influences the implementation as well as the performance of the systems [46, 57, 62, 70].

4.2.2.1 Least Mean Squares (LMS)

The LMS algorithm uses steepest descent method, in which a new weight vector is calculated by adding a negative gradient step size to the current weight vector as shown in Equation (4.7) [67].

$$\bar{w}(k+1) = \bar{w}(k) + \mu e^{*}(k)\bar{x}(k) \tag{4.7}$$

where $\overline{w}(k+1)$ is the next complex weight, $\overline{w}(k)$ is the current complex weight, μ is the step size which determines the convergence speed of the algorithm, $e^*(k)$ is the conjugate of the error signal and $\overline{x}(k)$ is the vector of the received signals.

LMS has been widely used in adaptive array antenna applications due to its simplicity [51, 63]. The pseudo-code of the minimised MSE beamforming using the LMS algorithm for adaptive array antenna application is shown in (4.3).

```
while iteration is not reached do
        for each sample of the desired signal, k,
                Calculate the output of the array
                        Equation (4.1)
                Calculate the MSE between the desired signal and array output
                        Equation (4.3)
                Add gradient step size to the current weight
                        Equation (4.7)
        end for
end while
```

Figure 4.3: The pseudo-code of LMS Algorithm.

4.2.2.2 Particle Swarm Optimisation (PSO)

PSO is a stochastic computational technique based on the movements of swarms and is widely used in adaptive array antennas [57, 78-80]. It was developed in 1995 by James Kennedy and Russell Eberhart [81]. A number of agents (particles) are used, representing a swarm moving around in the search space looking for the best solution. The best solution (*fitness*) achieved by each particle is stored and labelled as personal best, p_{best}. PSO will also store the current best value achieved by any particle and label it as global best, g_{best}. After each calculation, p_{best} and g_{best} are compared and stored for future iterations. Each particle tries to modify its position based on its current position, velocity and distance between the current position and p_{best}. This modification is mathematically modelled according to Equations (4.8) and (4.9) [78].

$$v_{PSO(n+1)} = w_{PSO} * v_{PSO(n)} + c_{PSO-1} r_{PSO-1}\left(p_{best,n} - x_{PSO(n)}\right) + \ldots \\ c_{PSO-2} r_{PSO-2}\left(g_{best,n} - x_{PSO(n)}\right) \tag{4.8}$$

$$x_{PSO(n+1)} = x_{PSO(n)} + v_{PSO(n+1)} \tag{4.9}$$

where $v_{PSO(n)}$ and $x_{PSO(n)}$ are the particle velocity and position, respectively. w_{PSO} is the inertia weight that controls the global and local exploration ability of the swarm, c_{PSO-1} and c_{PSO-2} are the scaling constants, while r_{PSO-1} and r_{PSO-2} are random numbers uniformly distributed in (0, 1). The iteration is terminated once a predetermined criterion, usually a good fitness or a maximum number of iterations is reached. In this simulations is the maximum SINR , Equations (4.4), is used as the cost function,

The pseudo-code of PSO algorithm is shown in Figure 4.4 [80].

```
while stopping criteria is not met do
    for each particle in the swarm do
        Pick two random numbers: r_PSO-1 and r_PSO-2
        Evaluate the cost function:
            Equations (4.4)
        Update the particle's velocity:
            Equations (4.8)
        Move the particle to its new position by adding its velocity:
            Equations (4.9)
            if x_PSO < P_best then
                Update particle best known position
            end if
            if x_PSO < G_best then
                update swarm best known position
            end if
    end for
end while
```

Figure 4.4: The pseudo-code of PSO algorithm.

4.3 Array Design for Adaptive Beamforming Applications

Adaptive beamforming essentially is dependent on three aspects, namely, the environment, the complex excitation of the array elements, and the geometry of the array [31]. Recently, researchers have been evaluating the geometry of the arrays based on their adaptive beamforming capabilities [31, 51, 60, 61, 82]. Arrays are evaluated in an environment that

contains various interference signals and a beamforming algorithm is used to calculate the excitation weights for the array elements.

The problem of optimising an antenna array for adaptive beamforming applications is addressed in [31]. The beamforming of the array was achieved by minimising the MSE between a reference signal and the output of the array. With a minimum cut-off of 0.25 λ inter-element spacing, the geometry of the array was optimised using simulated annealing (SA). Arrays of four, five and six isotropic elements were optimised, and the results suggest that optimal array configuration is achieved by concentric circular array arrangement, as shown in Figure 4.5. The study also shows a trade-off between the beamforming performance and coupling level between the elements of the array.

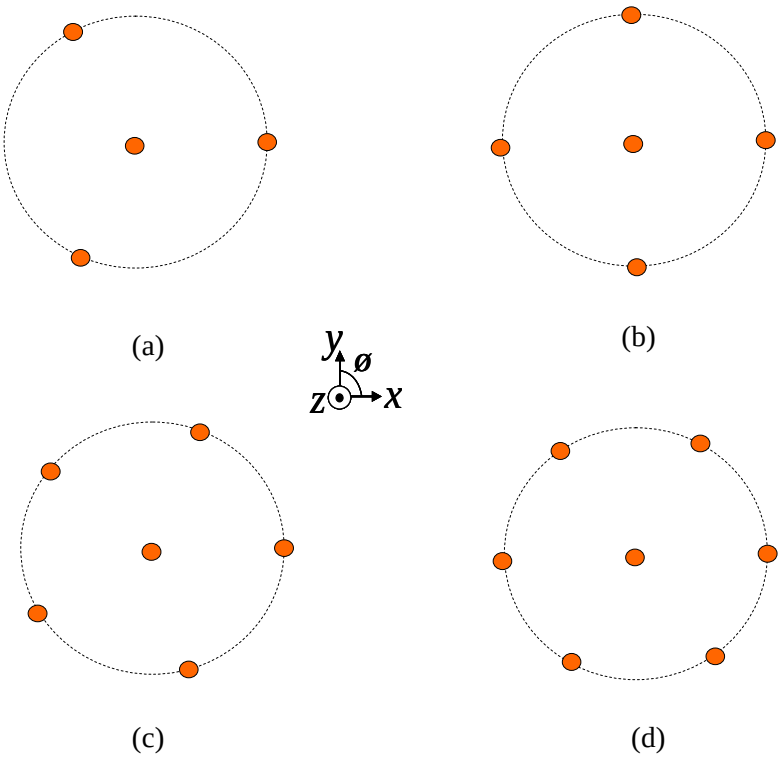

Figure 4.5: Optimal planar arrays for adaptive beamforming, (a) four elements, (b) five elements, (c) six elements, and (d) seven elements [31].

The performances of a uniform circular array (UCA) and a uniform rectangular array (URA) were examined from the context of adaptive beamforming in [51]. Each array consists of 16 isotropic elements as shown in Figure 4.6. The optimised complex excitations for the antenna elements were calculated using the LMS and the RLS algorithms. It was found that despite the deviation in the convergence properties of the adaptive algorithms, the UCA

generates better radiation patterns, in terms of array directivity, main beam width and the depth of the nulls, compared to the URA.

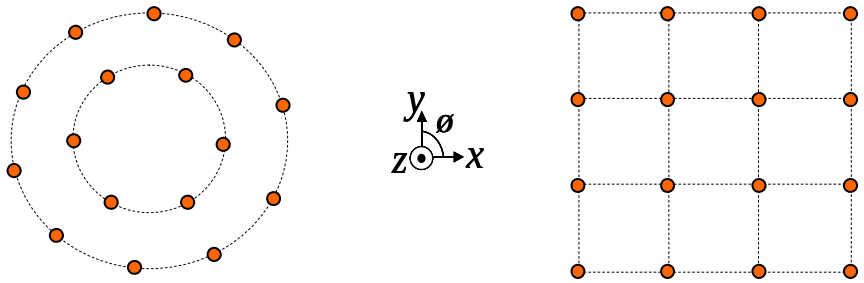

(a) (b)

Figure 4.6: UCA and URA for adaptive beamforming application, (a) UCA, and (b) UCCA [51].

In [60], an 18 element uniform hexagonal array (UHA) and a uniform concentric circular array (UCCA), shown in Figure 4.7, were compared based on their adaptive beamforming performance. The array consists of half-wave dipoles and the PSO algorithm is used to calculate the optimal complex excitations of the array elements in order to maximise the output power towards the desired angle and minimise the output power from the interfering angle. It was found that the resulting radiation pattern of UHA has deeper nulls and higher gain compared to the UCA. Similarly, the performance of UCA is compared against planar uniform circular array (PUCA) [82]. In the comparison, each array consists of 16 half-wave dipoles and the results show that there is a trade-off between the depth of the nulls, the width of the main beam and the physical size of the arrays.

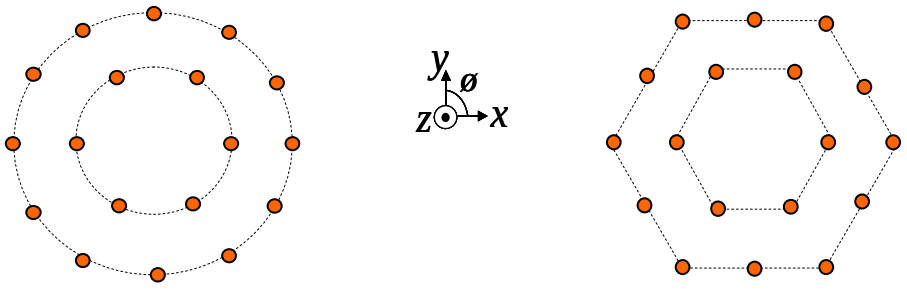

(a) (b)

Figure 4.7: UCCA and UHA for adaptive beamforming application, (a) UCCA, and (b) UHA [60].

Using a similar approach, the performances of the ULA and the faceted arrays, as introduced in Chapter 3, will be evaluated and compared against each other from the perspective of adaptive beamforming. In this evaluation, the height of the faceted array, measured from the highest element to the lowest element, is fixed at 0.8 λ, while the separation between adjacent elements on the array is 0.55 λ. Due to their common usage in adaptive array antennas, the minimum MSE and maximum SINR are used as the performance criteria for the beamforming [26, 51, 63, 69, 75, 76]. The theories behind these beamforming algorithms are discussed in Section 4.2.

4.4 Faceted Array Geometry Evaluation

4.4.1 Configuration for Numerical Experiments

The faceted array consists of polarisation reconfigurable antenna as was proposed in Chapter 2. The antenna operates at 2.4 GHz and is set to LHCP operational mode. The positions of the array elements for the faceted arrays are tabulated in Table 4.1 and the geometries of the faceted arrays are illustrated in Figures 3.21 – 3.24. The beamforming approaches used in this evaluation is summarised in Table 4.2.

Table 4.1: The Positions of Array Elements on the Faceted Array.

Array	**2-faceted**			**3-faceted**		
θ_a	**45°**			**50°**		
	$x(\lambda)$	$y(\lambda)$	$z(\lambda)$	$x(\lambda)$	$y(\lambda)$	$z(\lambda)$
1	0	-1.78	-0.52	0	-1.63	-0.63
2	0	-1.27	-0.31	0	-1.28	-0.21
3	0	-0.76	-0.10	0	-0.82	0
4	0	-0.25	0.11	0	-0.28	0
5	0	0.25	0.11	0	0.28	0
6	0	0.76	-0.10	0	0.82	0
7	0	1.27	-0.31	0	1.28	0.21
8	0	1.78	-0.52	0	1.63	0.63
Array	**4-faceted**			**8-faceted**		
θ_a	**23°**			**11°**		
	$x(\lambda)$	$y(\lambda)$	$z(\lambda)$	$x(\lambda)$	$y(\lambda)$	$z(\lambda)$
1	0	-1.76	-0.63	0	-1.78	-0.62
2	0	-1.30	-0.32	0	-1.32	-0.32
3	0	-0.31	-0.11	0	-0.81	-0.12
4	0	-0.27	0	0	-0.27	-0.01
5	0	0.27	0	0	0.27	-0.01
6	0	0.81	-0.11	0	0.81	-0.12
7	0	1.30	-0.32	0	1.32	-0.32
8	0	1.76	-0.63	0	1.78	-0.62

Table 4.2: Beamforming Approaches for the Faceted Array Evaluation.

Beamforming Approaches	**Optimisation Criteria**	**Optimisation Method**
mMSE	Minimum MSE Equation (4.3)	LMS
mSINR	Maximum SINR Equation (4.4)	PSO

Each array is evaluated in two different scenarios as illustrated in Figure 4.8:

- Case 1 – a desired signal is placed at (θ_d = 0°, $\varnothing_d$ = 0°) and three interfering signals are placed at (θ_1 = -45°, $\varnothing_1$ = 0°), (θ_2 = 30°, $\varnothing_2$ = 0°) and (θ_3 = 60°, $\varnothing_3$ = 0°), and
- Case 2 – the desired signal is placed at (θ_d = 60^o, $\varnothing_d$ = 0°) and two interfering signals are placed at (θ_1 = -55°, $\varnothing_1$ = 0°) and (θ_2 = 10°, $\varnothing_2$ = 0°).

The signal-to noise-ratio (SNR) of both the desired and the interference signals are set to 10 dB.

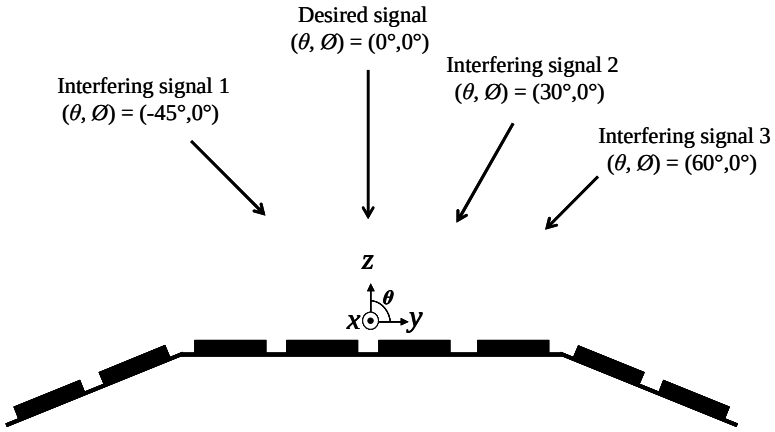

(a)

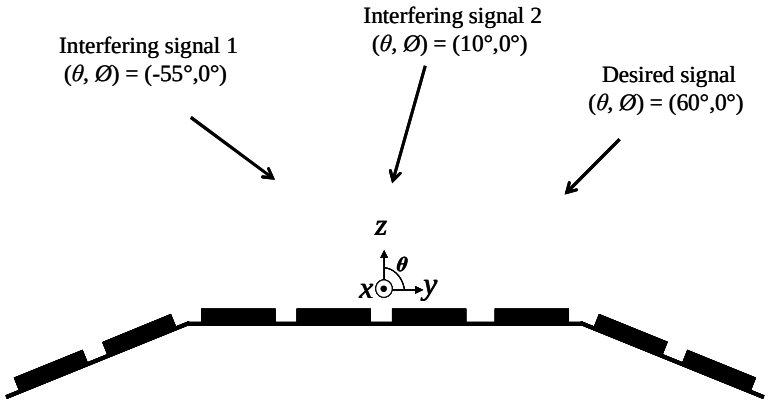

(b)

Figure 4.8: Illustrations of the scenarios for the numerical experiments, (a) Case 1 and (b) Case 2

4.4.1.1 Unit Step (μ)

Figure 4.9 shows the plot of the mean square error with respect to the number of iterations, with different step sizes for the 3-faceted array. In all cases, the LMS algorithm is shown to converge but with different slopes. The algorithm is converged when the MSE between the desired and received signals is nearly to 0, which indicates that the antenna weights approach their optimum values. From the figure, the LMS algorithm requires the least number of iterations with step size μ = 0.05. Thus, in this study, the unit step value (μ) for both LMS

and blind adaptive algorithm is set to be 0.05. The number of iterations for both algorithms is 1000.

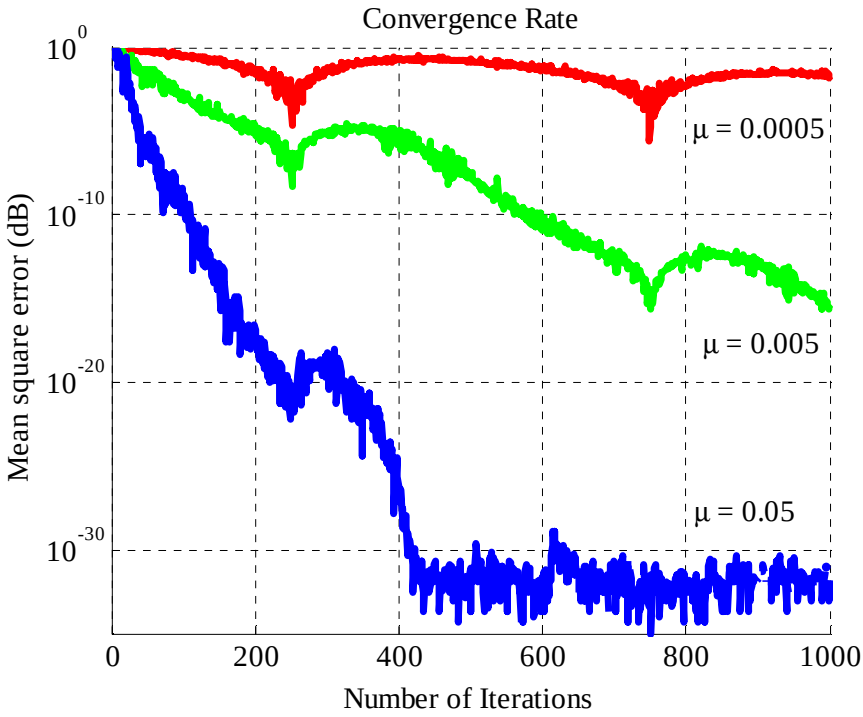

Figure 4.9: Convergence of the LMS algorithm with different step sizes for the 3-faceted array.

4.4.1.2 PSO Parameters

The PSO algorithm is programmed based on the Standard PSO 2007 [83]. The dimension of the PSO is set to 24 particles. The initial positions of the particles are randomly generated inside a search space with a minimum boundary of -1 and a maximum boundary of 1. The weight, w_{PSO} in Equation (4.8) is set to 1.0. Based on the suggested settings in [84], the correction factors, $c_{PSO\text{-}1}$ and $c_{PSO\text{-}2}$ are set to 2.0, the noise power is set to 10 dB, and the stopping criterion for the algorithm is set for a tolerance value of 1×10^{-5}.

4.4.2 Faceted Arrays Evaluation Using mMSE Approach

Using the mMSE approach, the radiation patterns for the two cases are plotted in Figure 4.10. It is noted that in Case 1, as shown in Figure 4.10 (a), the generated radiation pattern from each array has nulls at the incoming angles of the interfering signals. The deepest null is obtained from the ULA at (θ_1 = -45°, $\emptyset_1$ = 0°), and (θ_2 = 30°, $\emptyset_2$ = 0°), but there is a deviation in the null placement of the ULA at the interfering angle (θ_3 = 60°, $\emptyset_3$ = 0°). Also, for all the arrays, the main beams of the arrays are accurately placed at the angle of the

desired signal. It is also noted that the sidelobe levels of the ULA are lower compared to the faceted arrays.

In Case 2, the generated radiation patterns for the faceted arrays show that the nulls are accurately placed at the interfering angles and the main beam is at the desired angle, as shown in Figure 4.10 (b). However, for the ULA, there is a deviation in the main beam position and also the sidelobe levels are higher compared to the faceted arrays. The amplitude and phase excitation for each element in the array are tabulated in Table 4.3.

Table 4.3: The Amplitude and Phase Excitation of Each Element on the Faceted Arrays.

Case 1				
Array	**2-faceted**	**3-faceted**	**4-faceted**	**8-faceted**
1	1∠0°	-4.5∠ 12.6°	-1∠ 0°	2.7∠ -14°
2	-4.2∠-68°	1∠ 5°	-4∠ 30°	2.5∠ 16°
3	-3.3∠-167°	-2.4∠ 22°	-2.5∠ -143°	1∠ 0°
4	-4∠117°	-4.5∠ 146°	-3.15∠ -68°	1.25∠ -36°
5	-4.37∠114°	0.6∠ 18°	-0.7∠ 30°	2.2∠ -89°
6	-2.64∠-158°	-5.6∠ -34°	-2.8∠ 27°	2.1∠ -71°
7	-1.94∠-77°	-4.5∠ -90	-0.9∠ -62°	-0.1∠ -178°
8	-6∠12°	-3∠ 164°	-3.3∠ -1.43°	1.16∠ -173°
Case 2				
Array	**2-faceted**	**3-faceted**	**4-faceted**	**8-faceted**
1	1∠ 0°	2.1∠ 145°	-1∠ 170°	0∠ 0°
2	-1.27∠ 127°	1∠ 0°	192∠ -50°	0.8∠ -169°
3	2.41∠ -139°	-2.5∠ -60°	1∠ 0°	-1.9∠ 167°
4	-3.22∠ -27°	1.1∠ 131°	0.5∠ 165°	0.3∠ -43°
5	-2.73∠ -37°	0.5∠ -60°	-3∠ -22°	1.34∠ -6.4°
6	-2.7∠ 150°	2∠ 161°	-0.6∠ 128°	0.6∠ 77°
7	-0.2∠ -2°	4.2∠ -150°	-0.3∠ -112°	3.1∠ -141°
8	1.52∠ -157°	2.7∠ -71°	1.7∠ 10.35°	2.7∠ -160°

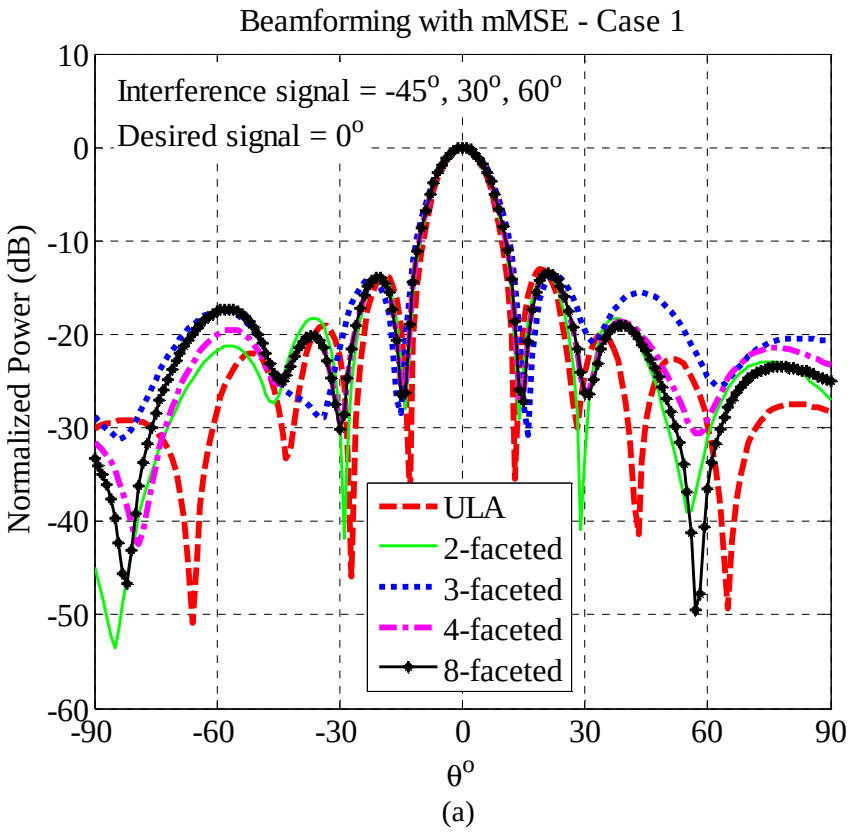

Figure 4.10: The resulting radiation pattern using LMS Algorithm, (a) Case 1, and (b) Case 2.

Table 4.4 shows the directivity of the arrays for the two cases. As shown in the table, the ULA achieves the highest directivity when the desired signal is at the boresight, as in Case 1. However, when the desired beam is shifted to (θ_d = 60°, $\emptyset_d$ = 0°), the directivity of ULA dropped significantly, as much as 4.63 dBi. On the other hand, the directivities of the faceted arrays are maintained within 3 dB for the two cases.

Table 4.4: Directivity of the Faceted Arrays Using mMSE Approach.

Array structure	Case 1 (dBi)	Case 2 (dBi)
ULA	16.99	12.36
2-faceted	15.12	12.52
3-faceted	15.50	12.53
4-faceted	15.13	12.42
8-faceted	15.01	12.39

4.4.3 Faceted Arrays Evaluation Using mSINR Approach

The resulting beam patterns achieved by mSINR approach are shown in Figure 4.11. In Case 1, as shown in Figure 4.11 (a), the generated radiation pattern of each array has nulls at the incoming angles of the interfering signals with the deepest null obtained by the ULA. The main beams are also accurately placed at the angle of the desired signal. The highest main beam is generated by the ULA followed by the 2-faceted, 3-faceted, 4-faceted and 8-faceted arrays.

In Case 2, the generated radiation patterns for the simulation are plotted in Figure 4.11 (b). Similar to the observation in the previous section, the nulls are accurately placed at the interfering angles. However, there is a deviation in the position of the main beam for all of the arrays. The main beam of the 4-faceted array has shifted the most compared to that of the other arrays. It is also observed that the grating lobe appears at (θ = 28°, $\emptyset$ = 0°) in the radiation pattern generated by the ULA. Grating lobes are not desired in adaptive antennas as they cause the peak of an array to appear at unwanted angles. The amplitude and phase excitation for each element in the array are tabulated in Table 4.5.

Table 4.5: The Amplitude and Phase Excitation of Each Element on the Faceted Arrays.

Case 1				
Array	**2-faceted**	**3-faceted**	**4-faceted**	**8-faceted**
1	1∠0°	2∠ -24°	-1∠ 0°	2∠ -8°
2	-2.8∠-64°	1∠ 0°	-0.5∠ -10°	1∠ 0°
3	-3∠-102°	1.5∠ -30°	-2.1∠ -45°	2∠ 46°
4	-3∠148°	0.3∠ -10°	-0.2∠ -27°	2.4∠ -11°
5	0.1∠173°	-4.5∠ -68°	-3∠ 14°	1.8∠ -36°
6	-3.3∠-116°	-8∠ -14°	-2.1∠ -20°	2∠ -40°
7	0.6∠-86°	-6∠ -40	-2∠ -74°	-3.5∠ -104°
8	-0.5∠-46°	-12∠ 44°	-14∠ -114°	-9∠ -80°
Case 2				
Array	**2-faceted**	**3-faceted**	**4-faceted**	**8-faceted**
1	1∠ 0°	0.3∠ -150°	-1∠ 107°	0∠ 0°
2	9.83∠ 165°	1∠ 0°	1.2∠ 0°	-0.3∠ 122°
3	-9∠ -23°	1∠ -63°	1.15∠ -35°	0.2∠ 142°
4	-7.5∠ 83°	-3.4∠ 31°	0.2∠ 98°	-2.8∠ -14°
5	-2.14∠ -70°	0.52∠ -20°	-0.1∠ -60°	0.8∠ 36°
6	-1.4∠ -109°	-0.6∠ -7°	1.4∠ -133°	7.2∠ 73°
7	-1.44∠ 3°	-0.2∠ 178°	1.3∠ -4°	6∠ 34°
8	-3.5∠ -60°	4∠ -46°	3∠ 6°	6∠ 135°

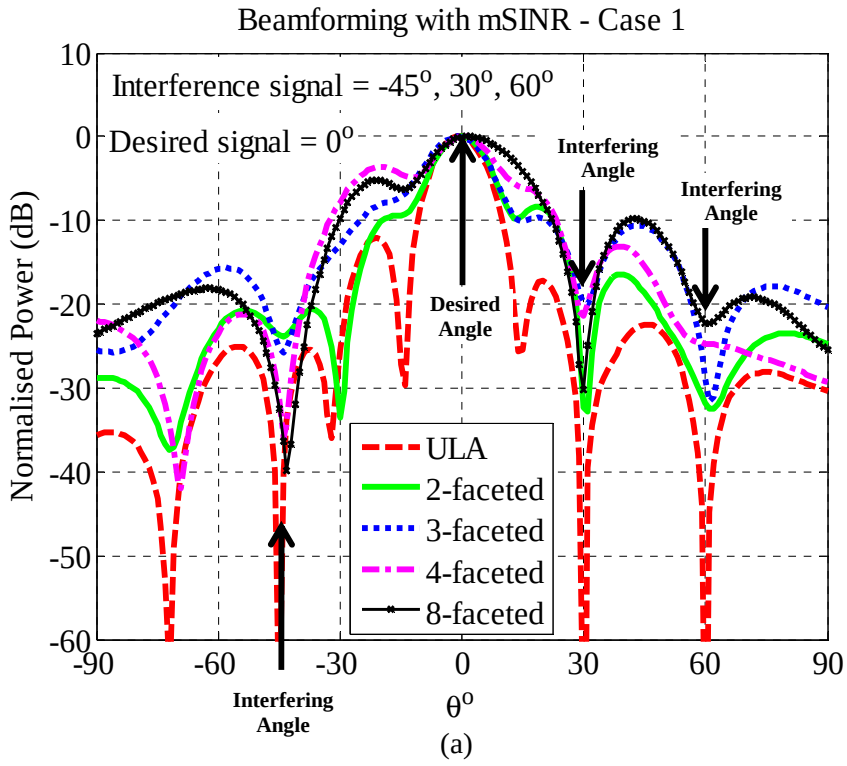

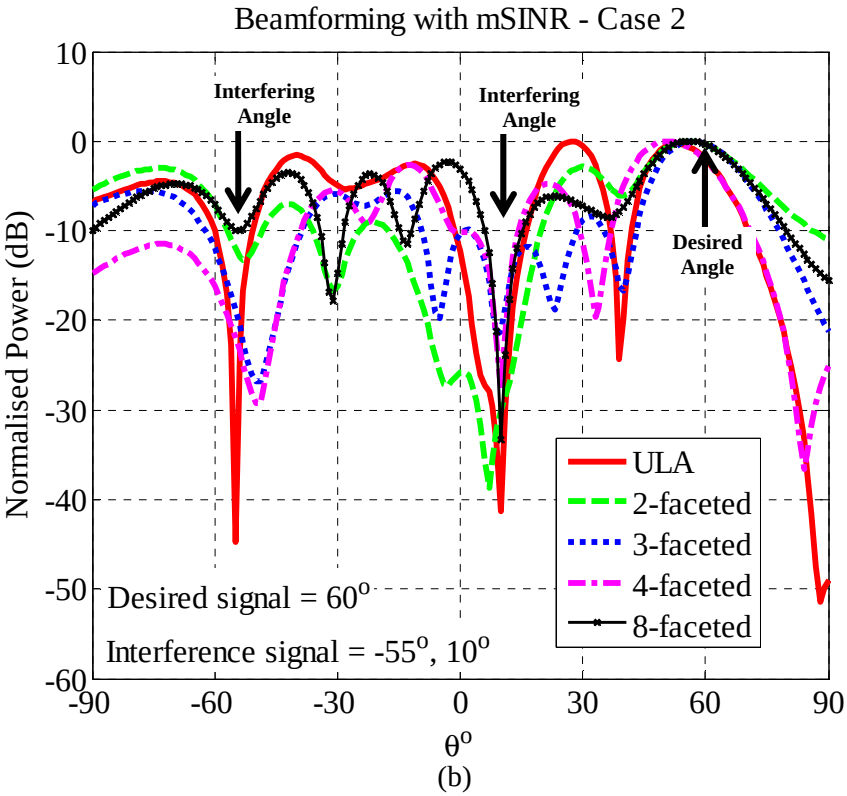

Figure 4.11: The resulting radiation pattern using PSO, (a) Case 1, and (b) Case 2.

Table 4.6 shows the directivity of the different arrays for the two cases. A similar trend is observed as was seen previously when mMSE approach was used in the experiment. As can be seen from the table, ULA achieves the highest directivity when the desired signal is at the boresight (i.e., case 1). However, when the desired beam is shifted to ($\theta_d = 60^o$, $\varnothing_d = 0°$), the directivity of the ULA reduced significantly from 16.94 dBi to 11.25 dBi. On the other hand, comparing Case 1 and Case 2, the directivity of the 3-faceted array degrades the least.

Table 4.6: Directivity of the Faceted Arrays Using mSINR Approach.

Array structure	Case 1 (dBi)	Case 2 (dBi)
ULA	16.94	11.25
2-faceted	13.06	11.04
3-faceted	13.04	12.59
4-faceted	11.54	10.39
8-faceted	13.08	9.00

4.5 Summary

The investigation on faceted array design for adaptive array antenna discussed in this chapter is illustrated in Figure 4.12. The performance of ULA and the faceted arrays, namely, 2-faceted, 3-faceted, 4-faceted and 8-faceted arrays was investigated from the perspective of adaptive beamforming. The complex weights of the elements are optimised using two different approaches, which are mMSE and mSINR. In this evaluation, the elements of the array are separated by 0.55 λ and the height of the faceted array is fixed to 0.8 λ. The

From the results, it is observed that when the desired angle is at boresight ($\theta_d = 0°$, $\varnothing_d = 0°$), ULA outperforms the faceted arrays as it has a higher directivity and lower side lobe levels. On the contrary, as the desired beam is placed away from the boresight, the faceted arrays outperform the ULA, mainly due to the wider scanning range obtained with the faceted arrays. Notably, the 3-faceted array using the mMSE approach outperforms the other arrays as the main beam and nulls are accurately placed at the required angles when the desired angle is further away from the boresight.

Overall, the directivity of the arrays in Case 1 is higher than that of the arrays in Case 2, as the desired angle in Case 2 is further from boresight. It is also noted that the directivity of the 3-faceted array is consistent in both Case 1 and Case 2. On the other hand, the directivity of ULA degrades the most compared to the other arrays. The degradation can be a disadvantage

to the antenna systems, especially in communication devices, as most of the radiated power is not directed to the intended location.

In Case 2, when the desired angle is further from boresight, a grating lobe appears in the radiation pattern of the ULA, which causes the directivity of the array to reduce. The reason for this is that when grating lobe appears in an array, power is transferred from the main beam to the grating lobes [26-28]. Grating lobes are not desired in adaptive antennas as they make the antenna vulnerable to noise and interference signals coming in at angles far from the desired signal. These results suggest that geometry selection is essential for ensuring the optimum performance for an adaptive array antenna, and the 3-faceted array is most suitable for wide-coverage adaptive array applications.

In conclusion, the degree of curvature of the 3-faceted array gives an advantage to the array as a better beamforming is obtained. In the next chapter, the low sidelobe level synthesis procedure for the 3-faceted array will be presented. Amplitude tapering technique on top of the phase correction is used in order to reduce the sidelobe level of the 3-faceted array.

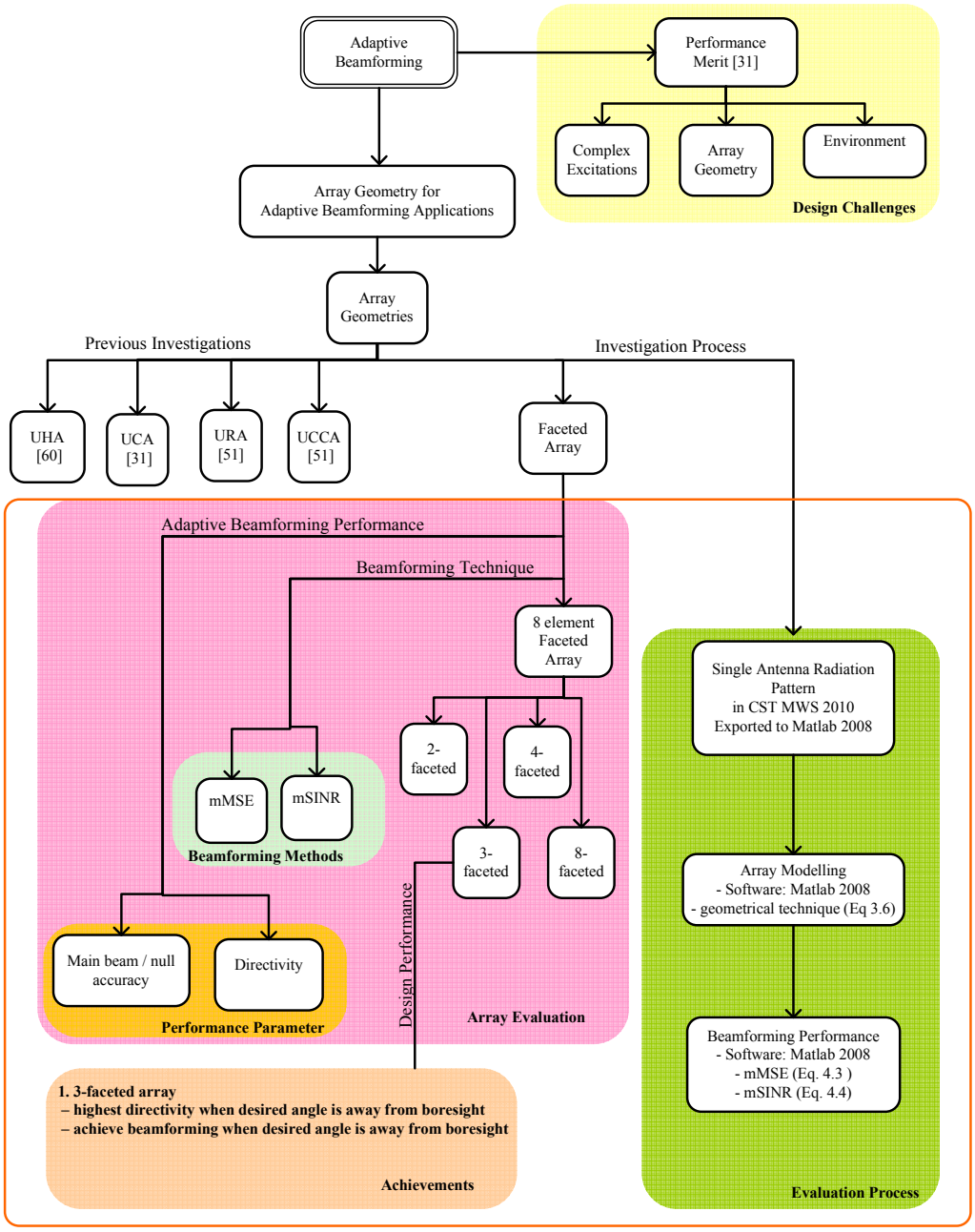

Figure 4.12: The investigation of beamforming for adaptive array antennas.

Chapter 5
Single-port Beamforming Algorithm

5.1 Introduction

The final stage of this research is to decide on the implementation strategy for the adaptive array antenna. Not only will the method of implementation influence the beamforming algorithms that can be used, it will also affect the hardware cost. Migrating from a multi-port beamforming system to a single-port beamforming system is a promising alternative as only a single RF channel is required. A typical RF channel consists of a band pass filter, a low-noise amplifier, a mixer, a low-pass filter and an analog-to-digital converter. This means that with a single-port system, the number of components required for building the system can be significantly reduced. In this chapter, a novel single-port beamforming system for use with a 3-faceted array is proposed. Using the pseudo-inverse function, the signal received at each element is estimated from the combined signal at the single output port. With the estimated values, the weighting for each array element can be then calculated using conventional beamforming algorithms as discussed in Chapter 4. With the reduced number of components and hence cost, the adaptive array antenna has a good potential to be deployed in commercial wireless communication devices.

This chapter is divided into five sections. Section 5.2 describes the beamforming architecture and the Section 5.3 discusses the proposed single-port beamforming method. The results obtained are then presented and discussed in Section 5.4. Finally, Section 5.5 summaries the chapter.

5.2 Beamforming Architecture

The beamforming of an adaptive array antenna can be implemented at different stages and the commonly used structures are microwave beamformer and local beamformer and digital beamformer [33].

5.2.1 Microwave Beamformer

The microwave beamformer is sometimes referred as analog beamforer [33]. In this structure, the beamforming is achieved after retrieving and combining the information received from each element. The combination of the signals means fewer components are needed in implementing the microwave beamforming, leading to reduced cost and lower power consumption of the adaptive phased array antenna. An example of a study that was conducted with microwave beamforming is found in [85], where the beamforming system is achieved using a microwave sampling technique. The signals of the array elements are sampled in the microwave frequency using pulses with adjusted time delay and duty cycles. The structure of the beamformer is shown in Figure 5.1.

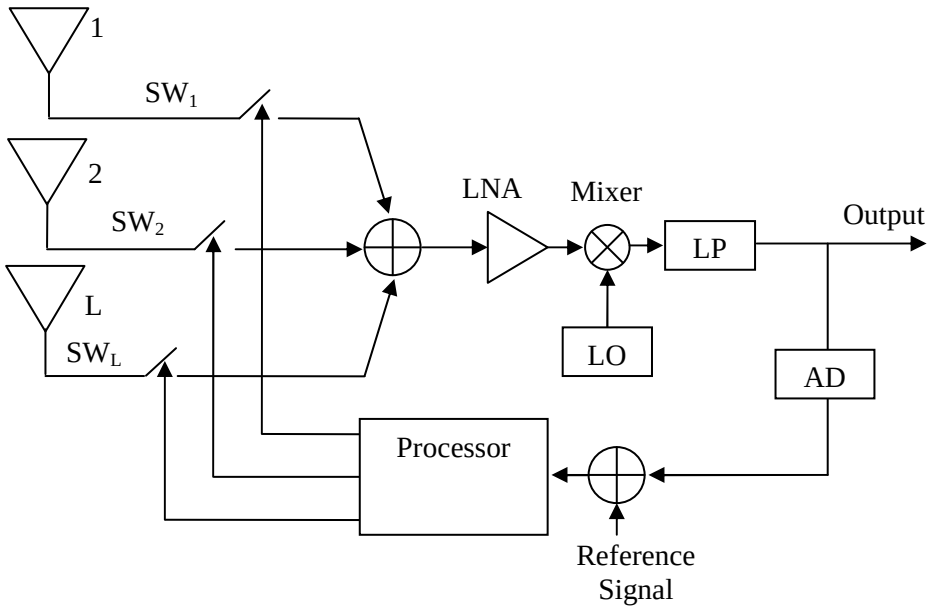

Figure 5.1: Microwave sampling beamforming structure [85].

The proposed beamformer consists of electronic switches, a power combiner, a low-noise amplifier (LNA), a mixer, an LPF, an ADC and a processor. The phase shifters, commonly used in adaptive array antennas, are replaced by reconfigurable switches and the required weightings to control the switching circuits are calculated in digital domain. With this structure, the hardware components required are reduced as only single RF channel is used. However, the spatial information of the signals is lost as the signals are combined before the RF channel. Without this information, further signal processing applications for adaptive array antenna such as the adaptive beamforming is difficult to achieve.

5.2.2 Local Beamformer

In a local beamformer, the weighting is achieved through local oscillators, which means the weighting is achieved only by phase control, without any gain control. In [71], phase-only adaptive nulling with a genetic algorithm (GA) was proposed. An illustration of this beamforming scheme is shown in Figure 5.2. In this approach, the amplitude weightings of the array elements are fixed. The phase weightings are determined based on the total output power of the array. Similar to the microwave beamformer mentioned above, this beamformer also uses a single RF channel, hence reducing the required hardware in the array implementation. However, phase only beamforming has a slow convergence rate and reduced beamforming resolution [29, 71].

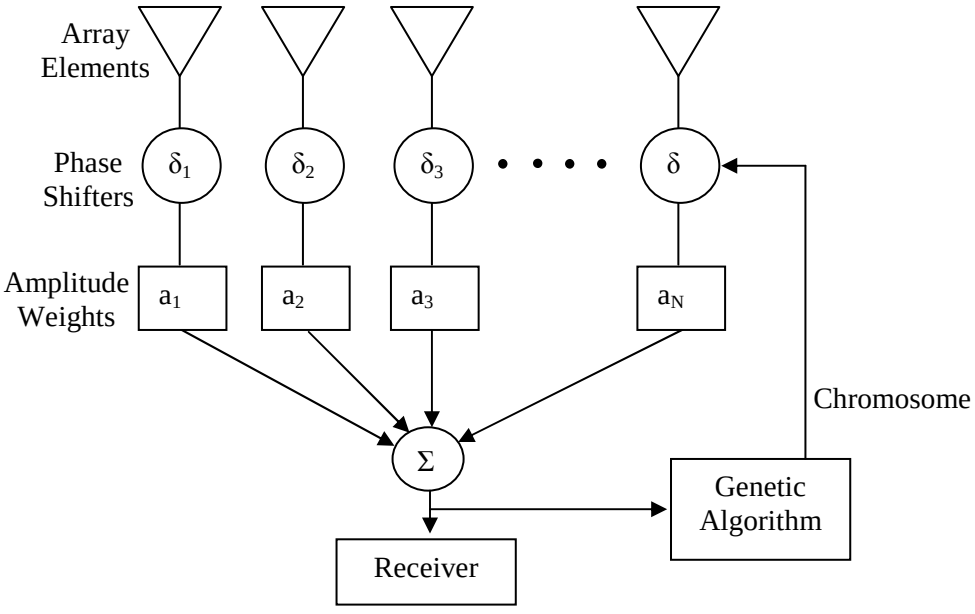

Figure 5.2: Phase-only beamforming with GA [71].

5.2.3 Digital Beamformer

In a digital beamformer, as illustrated in Figure 5.3, the beam is formed at the digital state. The signals received by each element are first down-converted, sampled and are then used to obtain the beamforming. This means the number of RF channel required is proportional to the number of elements in the adaptive array antenna. Apart from its ability of fine steering with a high-resolution ADC, the advantage of this scheme is that it suited most of the adaptive beamforming algorithms as was discussed in Chapter 4 [63, 86-89]. However, due to a large number of components required, this beamformer is costly and has mainly been limited to military applications [9].

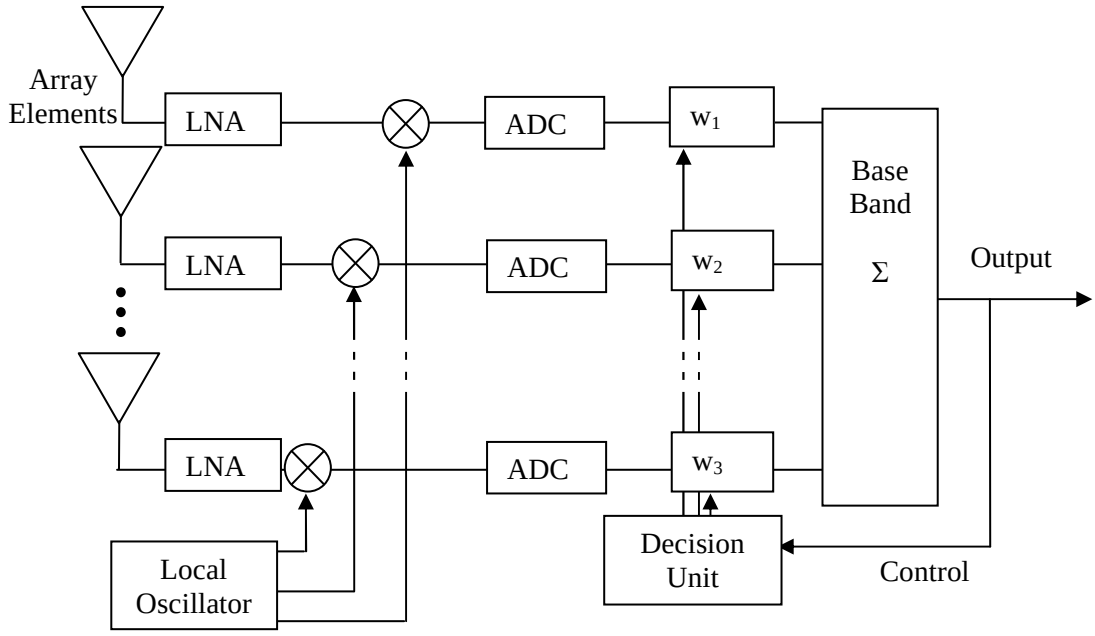

Figure 5.3: Digital beamformer [33].

5.2.4 Single-port Beamformer

The cost of an adaptive array antenna can be reduced by implementing a single-port beamformer as it requires only one RF channel and several techniques using single-port beamforming techniques have been proposed [32, 90, 91].

Single-port techniques without having information of the received signal at each array element have been used in [32, 92, 93]. In these techniques [92, 93], also termed perturbation algorithms, the weightings of the array elements are constantly changed and the resulting array outputs are monitored. Adaptive beamforming is then achieved using the parameters derived from the gradient of the output variance. In [32], a similar beamforming approach

was used but with fewer weight changes. The proposed algorithm was implemented on a Sample-Matrix-Inversion (SMI) adaptive beamformer. However, in spite of its fast convergence behaviour, the SMI algorithm is computationally expensive [87] and this has a big impact on its implementation cost [89, 94]. Apart from that, without the spatial information of the received signals, the use of conventional beamforming algorithms is still limited.

Alternatively, single-port beamforming can be achieved by estimating the lost information of the received signals [90, 91, 95, 96]. With the estimated signals, advanced beamforming techniques such as adaptive beamforming using minimum MSE and maximum SINR can be applied. In [91], the signal of each element is obtained by de-multiplexing the combined signal of the array output. The concept uses Spatial Multiplexing of Local Elements (SMILE), is illustrated in Figure 5.4. The signals from each element are multiplexed into a single LNA and mixer, similar to the time division multiple addressing (TDMA) scheme. The signal is then amplified and de-multiplexed at the baseband level in order to retrieve the original signal at each element. These signals can be fully established, as long as the initial signals are sampled at the Nyquist rate. However, even though the use of LNAs and mixers is reduced in this technique, the number of LPFs and ADCs is still proportional to the number of elements in the array. This does not give much reduction in the implementation cost of the array.

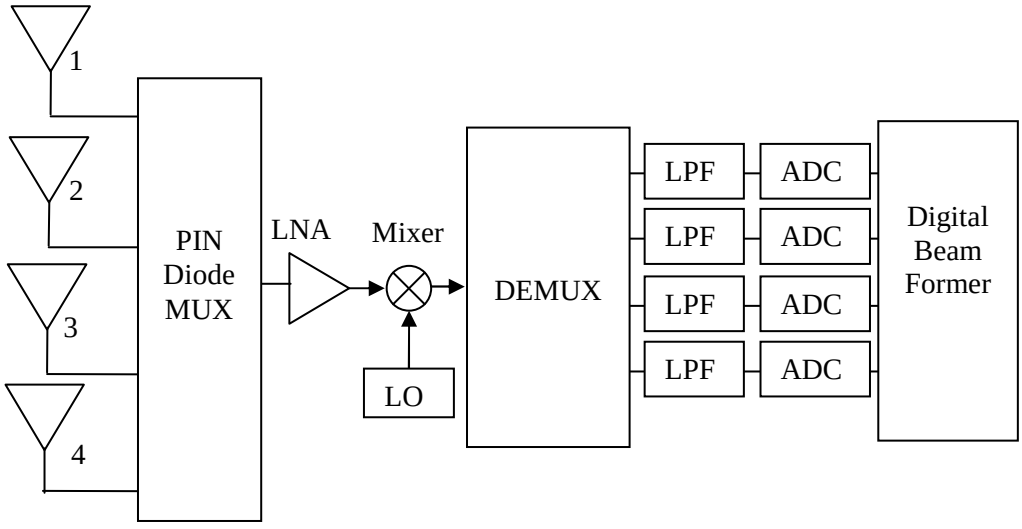

Figure 5.4: SMILE system [91].

To further reduce the amount of hardware, a single-port digital beamforming scheme based on the time sequence phase weighting (TPSW) was used in [90, 95, 96]. The block diagram of the technique is shown in Figure 5.5 [96]. The beamformer consists of phase shifters (0°/180°), power dividers, a single RF channel and a digital beamformer.

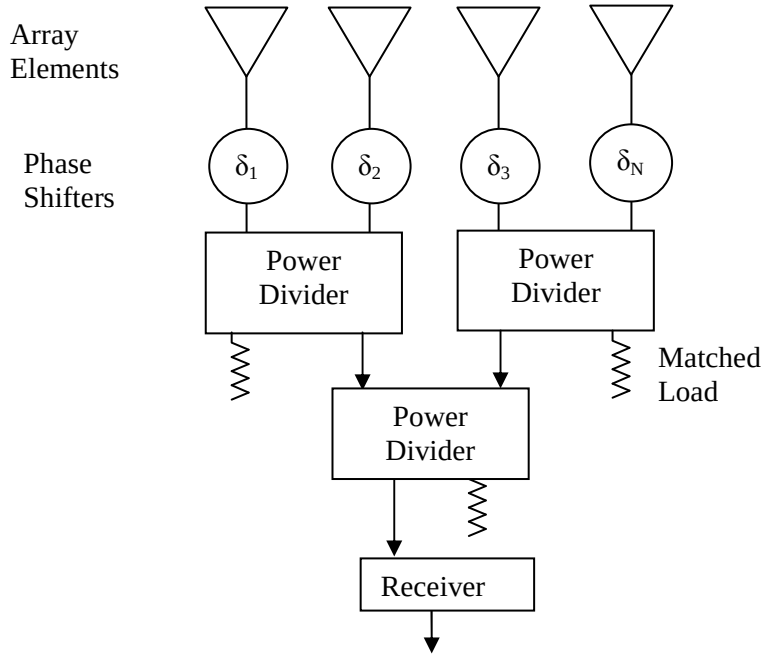

Figure 5.5: TPSW system [96].

In this technique, the signal at each aperture is given by Equation (5.1).

$$X' = \begin{bmatrix} x_1 & x_2 & x_3 & x_N \end{bmatrix} \tag{5.1}$$

where N is the number of elements in the array.

In the proposed system, the output is given by Equation (5.2).

$$Y = \frac{1}{\sqrt{N}} WX' \tag{5.2}$$

where W is the weighting matrix for the array.

X is then defined as Equation (5.3).

$$X = \frac{X'}{\sqrt{N}} \tag{5.3}$$

General relationship between the output of an array and the signals received at each element is described by Equation (4.1) is then rearranged to be as:

$$X = W^{-1}Y \tag{5.4}$$

The weighting matrix is then choose to be represented by a Hadamard matrix, $W = H_N$. Based on the property of Hadamard matrix,

$$W = H_N = H_2 \otimes H_{\frac{N}{2}} \tag{5.5}$$

$$W^{-1} = \frac{1}{N} H_N \tag{5.6}$$

where $\otimes$ denote the Kronecker product and for N = 4,

$$H_4 = H_2 \otimes H_2 = \begin{bmatrix} 1 & 1 & 1 & 1 \\ 1 & -1 & 1 & -1 \\ 1 & 1 & -1 & -1 \\ 1 & -1 & -1 & 1 \end{bmatrix} \tag{5.7}$$

The signal at each array element is then recovered by inversing the phase weighting using the Walsh-Hadamard matrix that consists of either +1 or -1, as shown in Equation (5.7), which can directly be represented as 0° or 180° phase difference [96]. Also, this feature simplifies the hardware implementation as only phase shifters are required as opposed to the conventional method which requires additional amplitude gain control. However, in most of the high performance beamforming algorithms, the weightings of the beamformer are complex values, where both amplitude and phase perturbation are required [29].

5.3 Single-port Beamforming Technique

In this section, a single-port beamformer that uses the signal estimation technique is discussed. The signal from each element is estimated using the pseudo-inverse function. The technique is applied to the beamforming schemes that use minimum MSE as the

performance criteria. The beamforming schemes for this implementation is summarised in Table 5.1

Table 5.1: Beamforming Schemes for the Single-port Implementation.

Beamforming Approaches	**Optimisation Criteria**	**Optimisation Method**
mMSE	Minimum MSE Equation (4.3)	LMS

5.3.1 Single-port vs. Multi-port system

The block diagrams of the multi-port and single-port beamforming systems are shown in Figure 5.6. In the multi-port system, shown in Figure 5.6 (a), the signals from the receivers are passed through the RF channels for further signal processing. In the single-port system, shown in Figure 5.6 (b), the signals received at each antenna element are coherently combined using a power combiner before going through the single RF channel.

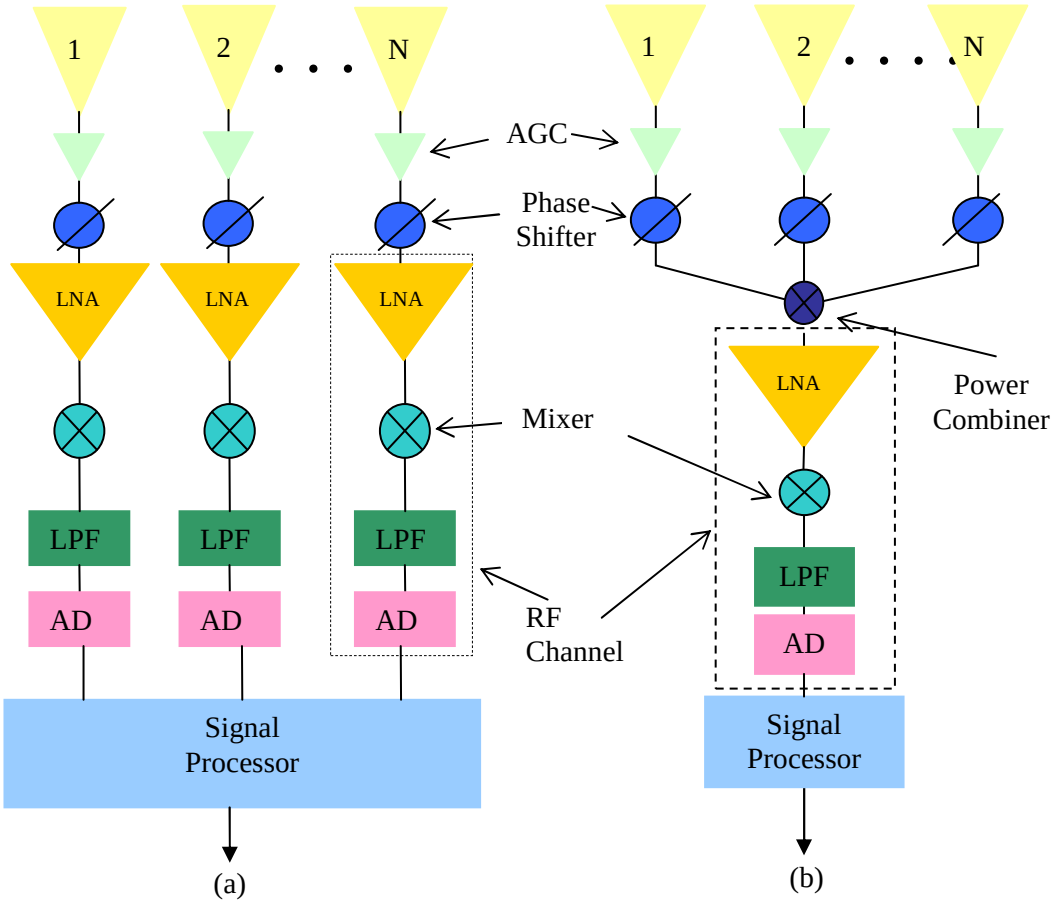

Figure 5.6: Component blocks of the beamformer, (a) multi-port, and (b) single-port.

For beamforming schemes that are based on minimum MSE, the complex weightings of the antenna elements are calculated by minimising the mean square error of the received signals, and this calculations require the use of the received signal vectors, $\bar{x}(k)$. Unlike the multi-port beamformer, as illustrated in Figure 5.6 (b), only the combined signal is accessible in the single-port beamformer. This means that the processor has no prior information of the signals at each of the antenna element, $x_n(k)$.

5.3.2 Single-port Adaptive Beamforming

The relationship between the output of the array, the weightings of the array elements and the received signals corresponding to the steered angle is discussed in Section 4.2.

Based on the relationship between the output of an array and the signals received at each element, as described by Equation (4.1), a set of array weightings is derived. For example, a weighting database of an array with eight elements for 10 different angles of arrivals (AoA), θ_p, is described by Equation (5.8).

$$\begin{bmatrix} y_{5^o} \\ y_{10^o} \\ y_{15^o} \\ y_{20^o} \\ y_{25^o} \\ y_{30^o} \\ y_{35^o} \\ y_{40^o} \\ y_{45^o} \\ y_{50^o} \end{bmatrix} = \begin{bmatrix} w_{1(5^o)} & w_{2(5^o)} & w_{3(5^o)} & w_{4(5^o)} & w_{5(5^o)} & w_{6(5^o)} & w_{7(5^o)} & w_{8(5^o)} \\ w_{1(10^o)} & & & & & & & \bullet \\ \bullet & \bullet & & & & & & \bullet \\ \bullet & & \bullet & & & & & \bullet \\ \bullet & & & \bullet & & & & \bullet \\ \bullet & & & & \bullet & & & \bullet \\ \bullet & & & & & & & \bullet \\ \bullet & & & & & \bullet & & \bullet \\ \bullet & & & & & & \bullet & \bullet \\ w_{1(50^o)} & w_{2(50^o)} & w_{3(50^o)} & w_{4(50^o)} & w_{5(50^o)} & w_{6(50^o)} & w_{7(50^o)} & w_{8(50^o)} \end{bmatrix} \begin{bmatrix} x_1 \\ x_2 \\ x_3 \\ x_4 \\ x_5 \\ x_6 \\ x_7 \\ x_8 \end{bmatrix} \tag{5.8}$$

Based on the relationship between array weight vector, $\bar{w}^H(k)$, and the array output, $y(k)$, the signals at each array element, $\bar{x}(k)$, can be estimated by multiplying $y(k)$ with the matrix inverse of $\bar{w}(k)$, as expressed in Equation (5.9).

$$\bar{x}(k) = \bar{w}^{-1}(k) \cdot y(k) \tag{5.9}$$

where $\bar{w}^{-1}(k)$ is the inverse array weight vector and $y(k)$ is the output of the array.

However, since $\overline{w}(k)$ is not square, its direct inversion does not exist. Hence, the use of pseudo-inverse function to obtain the inverse of $\overline{w}(k)$ is proposed. The pseudo-inverse function has been used in spectral reconstruction [97], image reconstruction [98] and recently in signal reconstruction [99].

For example, for the case of AoA, θ_p = 15°, the signal at each element can be estimated using Equation (5.10).

$$\begin{bmatrix} x_{1(15^o)} \\ x_{2(15^o)} \\ x_{3(15^o)} \\ x_{4(15^o)} \\ x_{5(15^o)} \\ x_{6(15^o)} \\ x_{7(15^o)} \\ x_{8(15^o)} \end{bmatrix}' = p\_inv\left[w_{1(15^o)} \quad w_{2(15^o)} \quad w_{3(15^o)} \quad w_{4(15^o)} \quad w_{5(15^o)} \quad w_{6(15^o)} \quad w_{7(15^o)} \quad w_{8(15^o)}\right]\left[y_{(15^o)}\right] \quad (5.10)$$

With the estimated $\overline{x}(k)$ values, the mMSE beamforming approach can be carried out the pseudo-code for the approach is shown in Figure 5.7.

```
Generate a database of possible array weight for 10 desired scan angle
Retrieve the array output y(k)
Retrieve the AoA information of the desired and interfering signals
Estimate the signal of each array element x_N(k) using Equation (5.10)
    while iteration is not reached do
        for each sample of the desired signal, k,
            Calculate the output of the array
                Equation (4.1)
            Calculate the MSE between the desired signal and array output
                Equation (4.3)
            Add gradient step size to the current weight
                Equation (4.7)
        end for
    end while
Update array weights
```

Figure 5.7: The pseudo-code of the single-port mMSE beamforming.

5.4 Simulation Results and Discussion

In this section, the performance of the proposed estimation technique for adaptive beamforming applications is evaluated. The proposed polarisation reconfigurable antenna and the 3-faceted array are used as the platform for the comparison. The antenna is set to LHCP mode and operated at 2.4 GHz. The geometry of the 3-faceted array is set as follows; the height of the 3-faceted array is set to 0.8 λ, the separation between the two elements is 0.55 λ, the tilting angle (θ_a) is 50° and the length of the side facets and central facets are 1.08 λ and 2.16 λ, respectively. The geometry of the 3-faceted array is illustrated in Figure 3.22. The 3-faceted structure is chosen due to its wide scanning range as discussed in Chapter 3. As illustrated in Figure 5.8, the array is simulated in an environment with:-

- a desired signal placed at (θ_d = 20°, $\emptyset_d$ = 0°), and
- an interfering signal coming from (θ_i = -10°, $\emptyset_i$ = 0°).

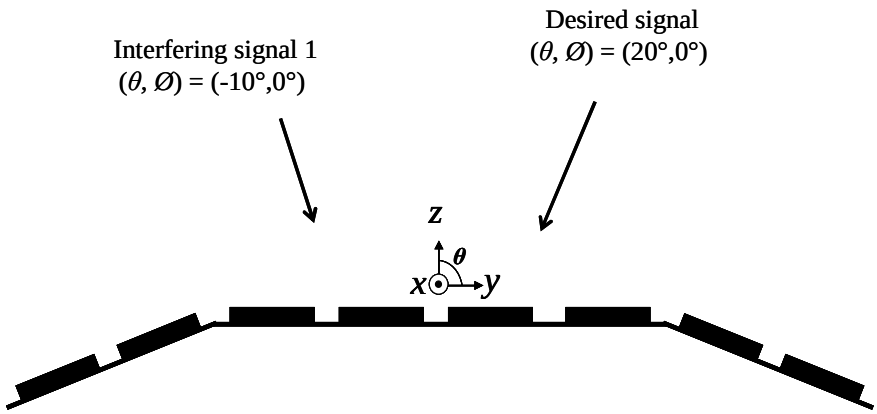

Figure 5.8: An illustration of the simulated environment.

The signal-to noise-ratio (SNR) of both the desired and the interference signals are set to be 10 dB.

5.4.1 Single-port mMSE

With μ = 0.05 and 3000 iterations, the phase and amplitude excitations of each element are calculated using the proposed single-port mMSE beamforming and the resulting radiation pattern is analysed. The required complex excitation of each element and the resulting radiation patterns of the arrays are shown in Figure 5.9 and Figure 5.10, respectively.

As seen from Figure 5.10, the main beams of the radiation patterns for both single-port and multi-port systems are placed at the desired angle (θ_d = 20°, $\emptyset_d$ = 0°) and the nulls are correctly placed at (θ_i = -10°, $\emptyset_i$ = 0°). However, the null from the proposed single-port algorithm is deeper than that produced by the multi-port algorithm. The proposed single-port algorithm also showed a faster convergence rate than the multiple-port algorithm, as shown in Figure 5.11, hence it requires less execution time than the multi-port system as tabulated in Table 5.2.

Table 5.2: Multi-port and Single-port Beamforming Execution Time - mMSE.

Method	Single-port	Multi-port
mMSE	21.9 ms	30 ms

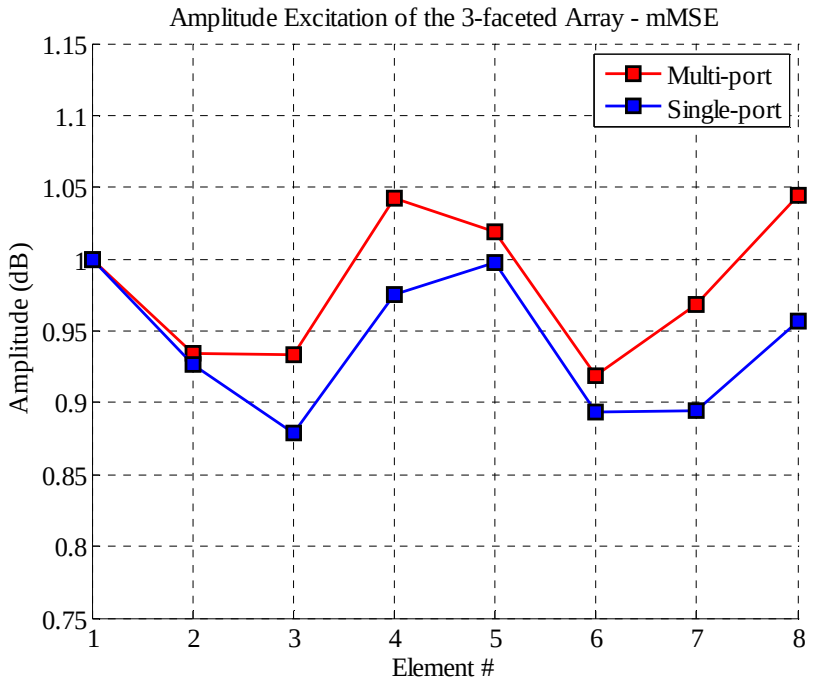

(a)

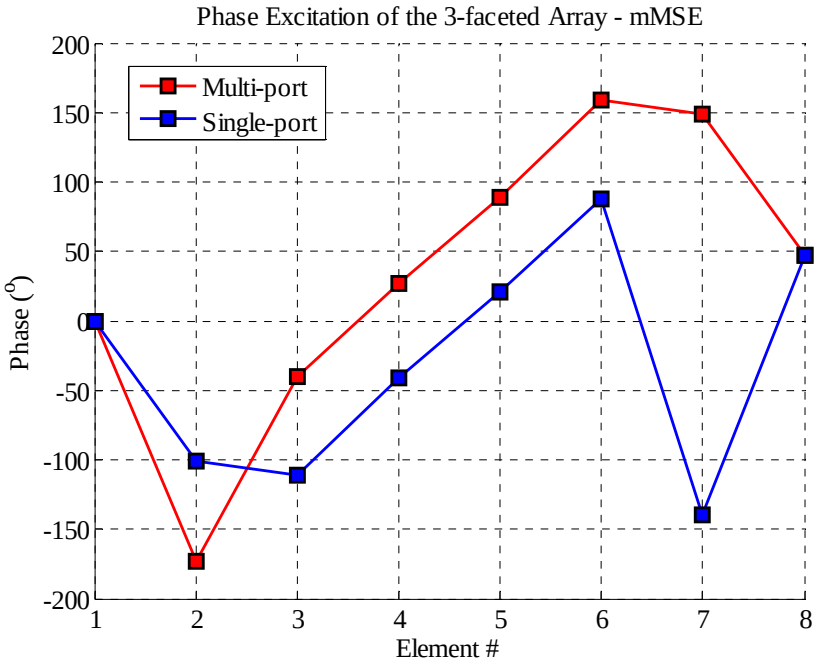

(b)

Figure 5.9: The complex excitation of each element of the 3-faceted array to obtain the desired radiation pattern, (a) amplitude, and (b) phase.

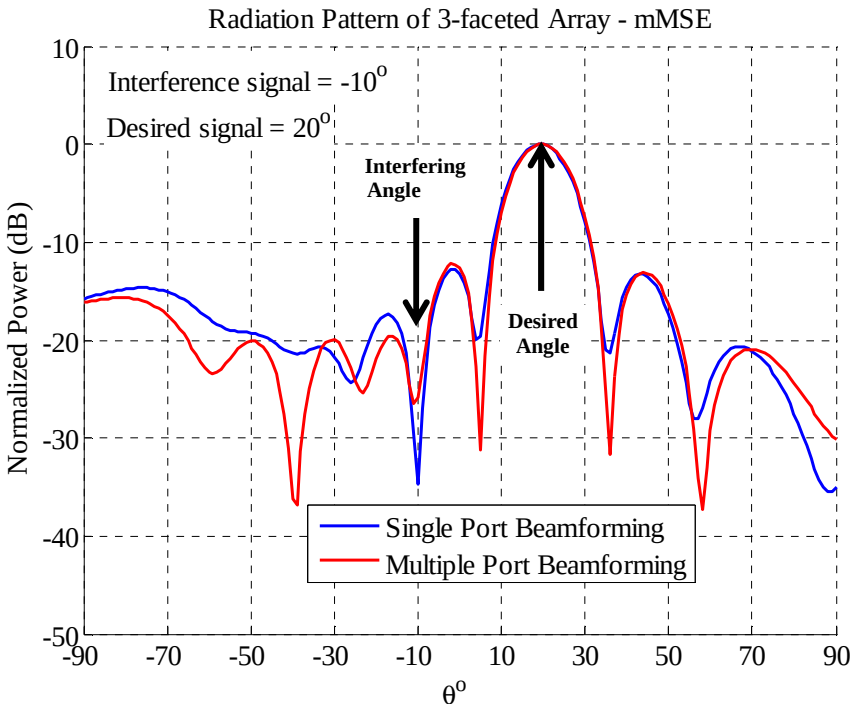

Figure 5.10: The resulting radiation pattern of the multi-port and single-port system using mMSE.

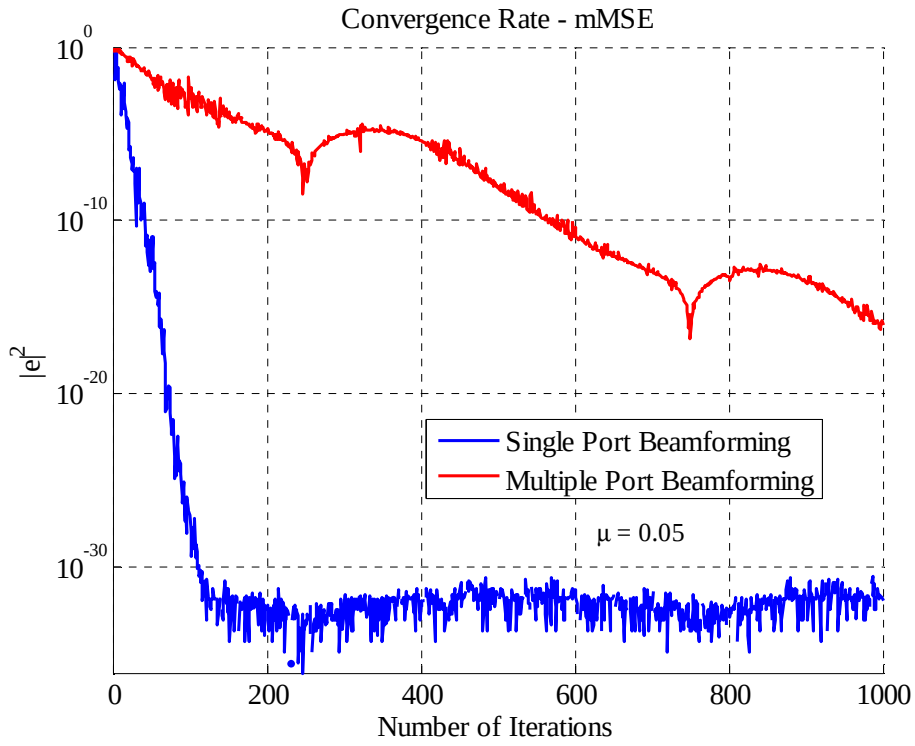

Figure 5.11: The convergence rate of the proposed single-port and multi-port mMSE.

5.4.2 Sensitivity of the Single-port Technique

In this section, the sensitivity of the mMSE single-port algorithm is observed. Figure 5.15 shows the radiation pattern of the 3-faceted array for three different cases. In this simulation, as shown in Figure 5.12, three situations are considered:-

- Case 1 – Signal separation by 30° – a desired signal at θ_d = 20° and an interference signal at θ_{i1} = -10°,
- Case 2 – Signal separation by 20° – a desired signal at θ_d = 20° and an interference signal at θ_{i2} = 0°, and
- Case 3 – Signal separation by 10° – a desired signal at θ_d = 20° and an interference desired signal at θ_{i3} = 10°.

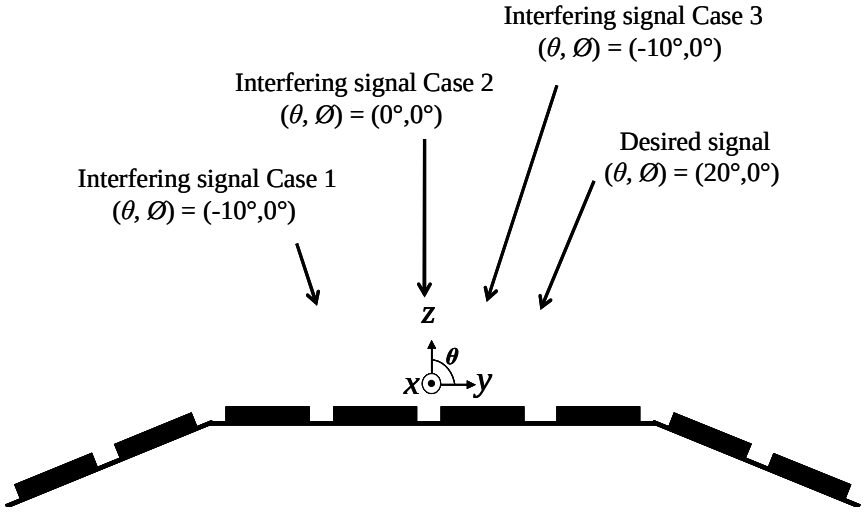

Figure 5.12: An illustration of the simulated environment for sensitivity analysis.

The results are shown in Figures 7.15 – 7.17. From the results, both the multi-port and the single-port techniques generate accurate radiation patterns when the interference and desired signals are separated by 30° and 20°, as shown in Figure 5.13 and Figure 5.14, respectively. However, for the case with 10° separation, shown in Figure 5.15, the radiation pattern of the single-port technique deviates by 5°. On the other hand, the radiation pattern of the multi-port technique is accurately generated.

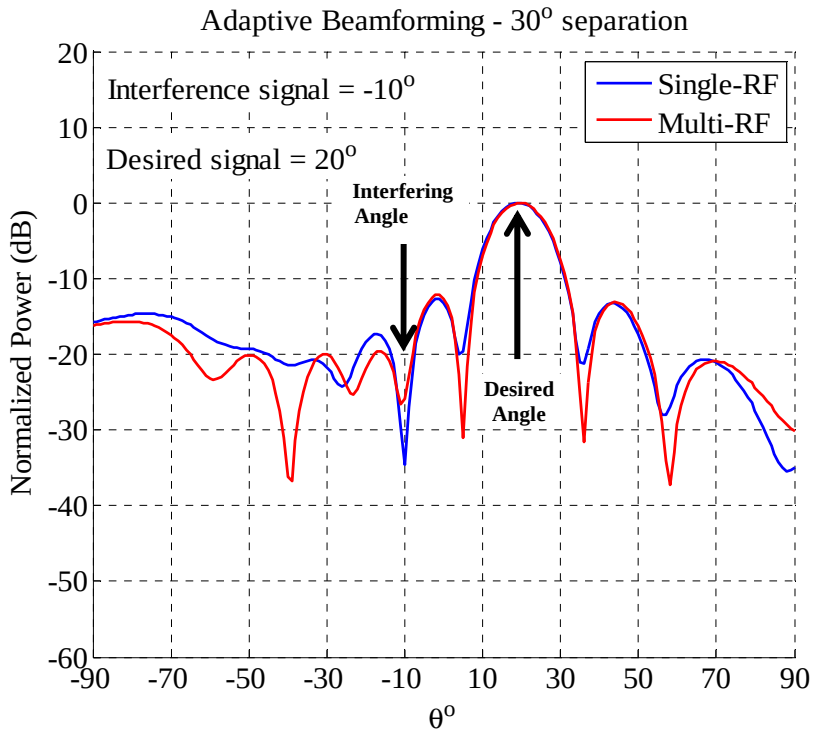

Figure 5.13: The radiation pattern of the 3-faceted array for Case 1.

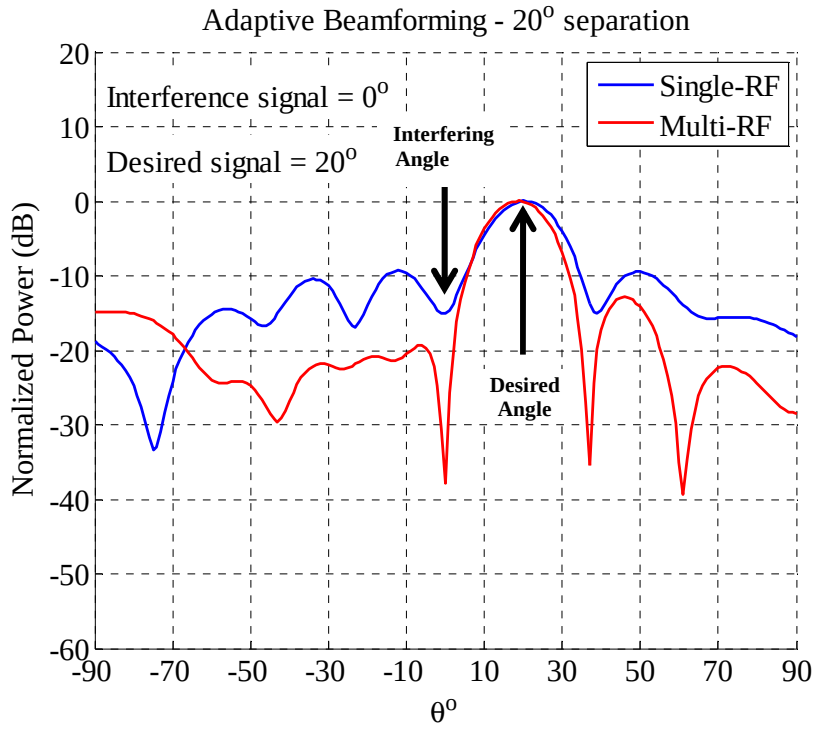

Figure 5.14: The radiation pattern of the 3-faceted array for Case 2.

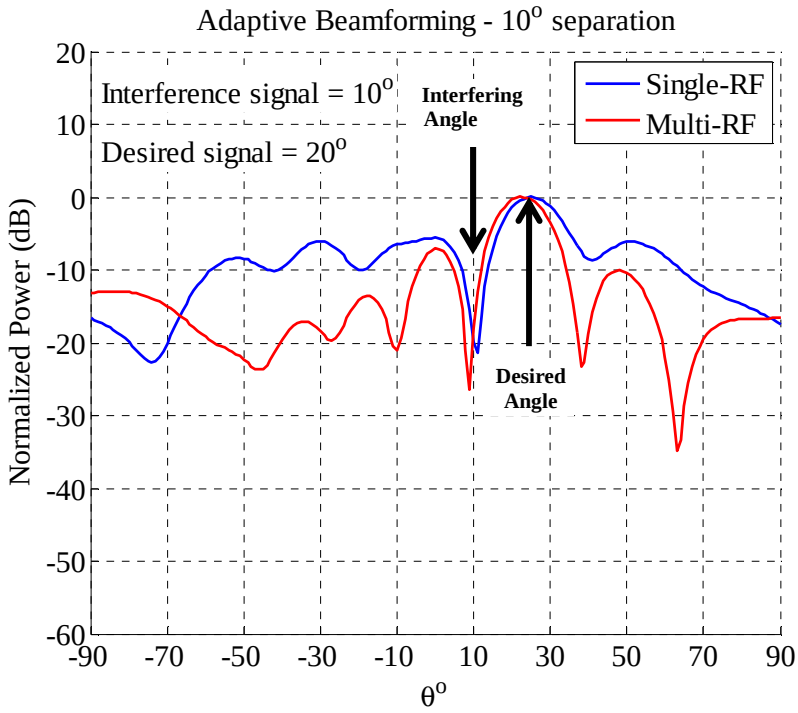

Figure 5.15: The radiation pattern of the 3-faceted array for Case 3.

Next, for the case with 10° separation (θ_d = 20°, θ_i= 10°), the single-port technique is simulated with different number of iterations and the resulting radiation pattern is plotted in Figure 5.16. It is noted that the main beam and the null of the radiation pattern are accurately placed when the single-port algorithm is simulated with 8000 iterations, compared to the multi-port algorithm which requires only 3000 iterations. These results demonstrate the limitation of the proposed single-port technique as it requires of at least a separation of 20° between the desired and the interference angles.

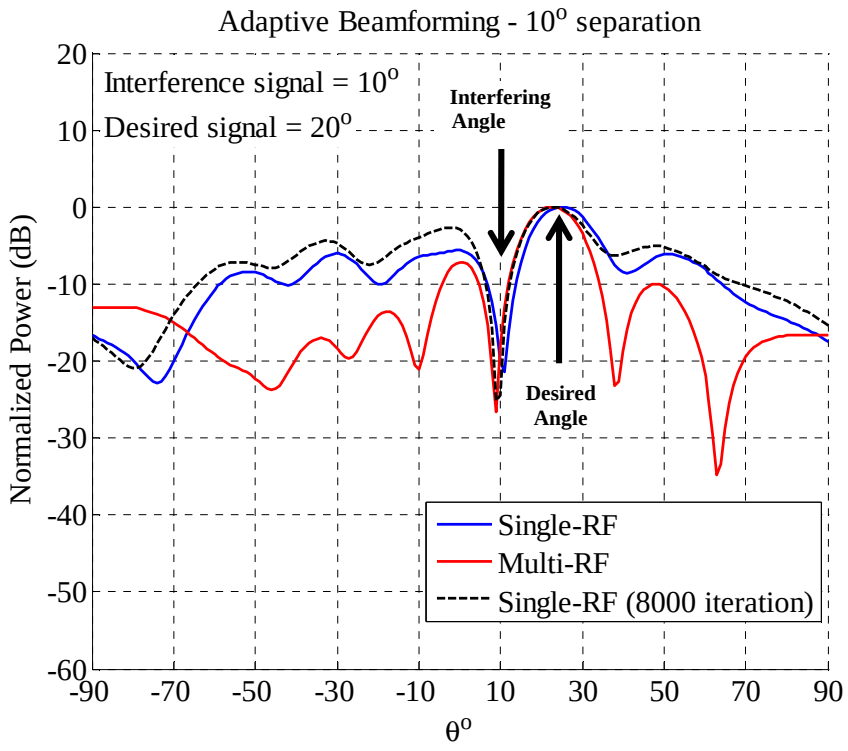

Figure 5.16: The radiation pattern of the 3-faceted array using mMSE for the case of 10° separation between a desired signal and an interference signal.

5.4.3 Single-port Beamforming with Different Number of Elements

Another aspect of the proposed single-port beamforming algorithm is its performance when different number of elements is used in the 3-faceted array. The resulting radiation patterns for 4-, 8- and 16-element 3-faceted arrays are presented in Figure 5.17. As seen from the results, all arrays have the main beam and null placed correctly at the desired and interference angles, respectively. However, for the 4-element array, there is a slight shift in the main beam placement by 6°. Also, it is noted that the beam width of the 16-element array is the narrowest while the 4-element array is the widest, with HPBW of 10° and 28°, respectively. This is due to the directivity and the scanning resolution of the adaptive array antenna, which increases with the number of elements in the array.

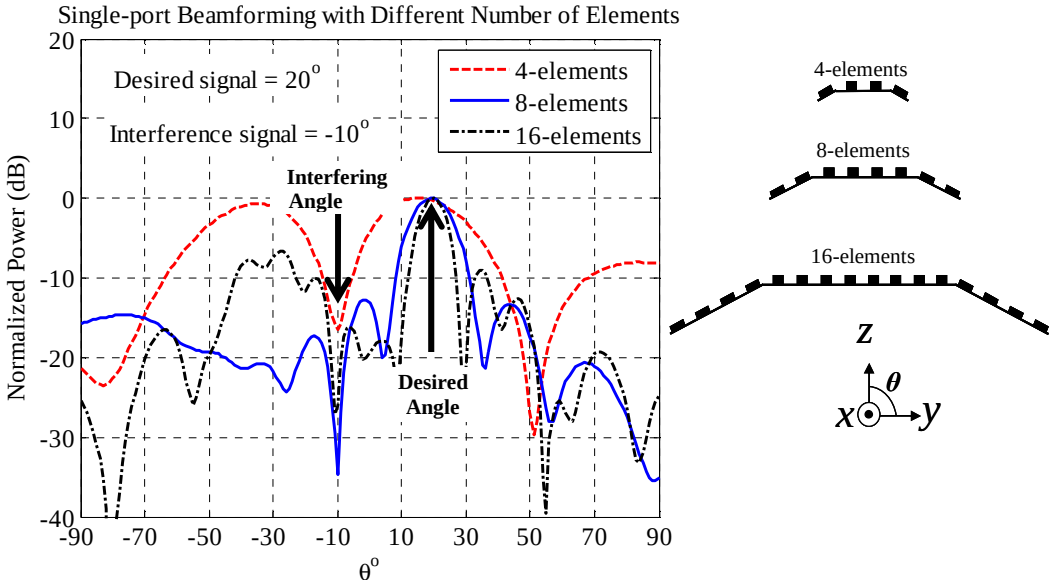

Figure 5.17: Single-port beamforming with different number of elements.

The results show that adaptive beamforming can be achieved with the proposed pseudo-inverse estimation technique. However, the algorithm requires more iteration when the interference and null are closely separated. With the proposed single-port beamforming technique, redundant RF front-end components in the system are eliminated. This means that an adaptive array antenna with a single-port beamformer can be implemented with significantly reduced hardware and hence lower cost than an equivalent multi-port beamformer.

5.5 Summary

In this chapter, a single-port beamforming technique has been proposed and summarised in Figure 5.18. The algorithm was simulated on a 3-faceted array consisting of eight microstrip antennas. Using pseudo-inverse technique, the signal from each antenna is estimated. The estimated signal is then used to optimise the complex excitation of the array elements. From the results, it has been observed that the proposed single-port beamforming was able to produce the desired radiation pattern in less time than the multi-port system. Using this single-port technique, the adaptive array antenna can be implemented with significantly reduced hardware and lower cost than an equivalent multi-port beamformer. This reduction is achieved by the elimination of redundant RF front end components from every single element. Next, the approaches towards a low cost adaptive array antenna for communication systems will be summarised and discussed.

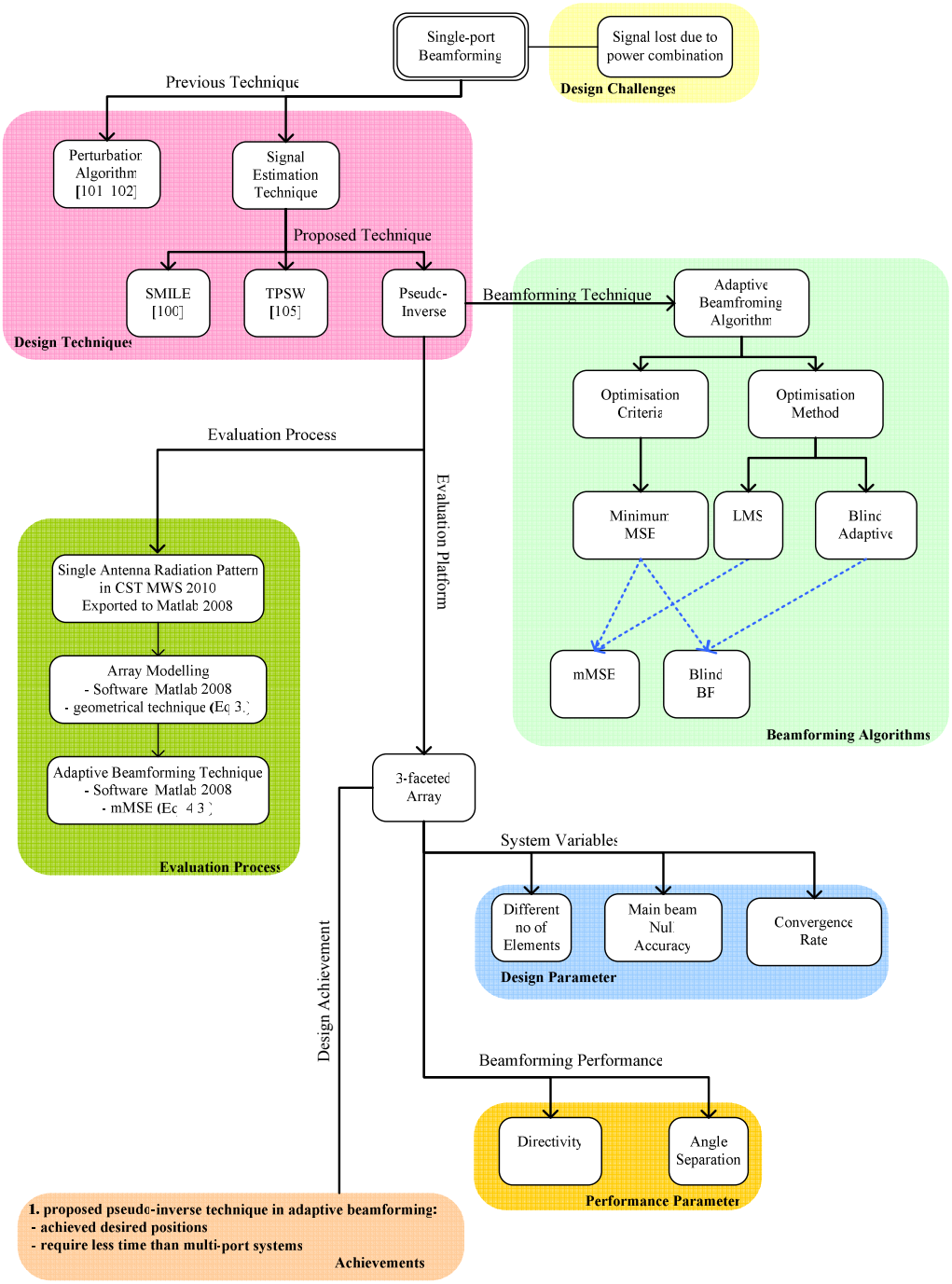

Figure 5.18: The summary of single-port beamforming algorithm for adaptive array antenna.

Chapter 6
Conclusions

6.1 Introduction

This thesis presents several novel aspects in adaptive array antennas for wireless communication systems, which are a polarisation reconfigurable antenna design, a wide scanning array design and a single-port beamforming technique. This chapter summarises the study presented in this thesis. The main objectives of each chapter are reviewed and the goal of the research is assessed and evaluated. The main achievements are then highlighted and future developments that could follow on from this study are suggested. This chapter is organised as follows. Section 6.2 discusses the conclusion of each chapter in the thesis and the main contributions of the thesis are highlighted in Section 6.3. Section 6.4 suggests future work and development based on the research presented in this thesis and, finally, Section 6.5 concludes the chapter.

6.2 Chapter Summary and Conclusion

Chapter 2 discusses the designs of a polarisation reconfigurable antenna. Various key dimensions of the antenna are observed in order to understand their effects on the radiation of the antenna. Microstrip antennas are used as they have a low-profile structure and a directional radiation characteristic. The proposed single-feed antenna structure is compact and simple, making it suitable to be implemented in wireless communication devices. Polarisation diversity is achieved by controlling the connections between the antenna and parasitic elements. The antenna has high radiation efficiency (91.5 % - LHCP and 86.9 % - RHCP) and good axial ratio (< 3dB at 2.4 GHz) in both RHCP and LHCP operational modes. The reconfiguration also has minimal effects on the operating frequency of the antenna. Reconfigurable antennas are cost-effective in terms of structure re-use as their radiation properties can be altered and still use the same radiating structure. The use of reconfigurable antennas also increases the functionality of the adaptive array antenna and this is highly desirable especially in modern communication systems.

Array designs for the adaptive array antenna are then described in Chapter 3. The cost of an adaptive array antenna is proportional to the number of elements in the array. However, arrays with a small number of elements have limited scan range. In this chapter, various array configurations are synthesised for a wide scanning range. Throughout the design process, the arrays were evaluated in terms of their 3 dB scanning range. It is noted that, in order for a ULA to achieve a reasonable scanning range, at least four antennas are required in an adaptive array and the range increases with the number of elements in the array. One method to increase the scanning range of an adaptive array antenna is by introducing curvature to the structure. 8-element array antennas with different faceted structures, namely, 2-faceted, 3-faceted 4-faceted and 8-faceted were analysed. It is concluded that the 8-element 3-faceted array offers the best trade-off between the dimension and the scanning range of the array. The array could reach up to ±70° scanning range, which is higher than that of a flat-surface array at ±56°. It is essential for adaptive array antennas to have a wide scanning range, especially in wireless communication systems, as the transmission link is not always within the boresight of the antenna.

However, faceted arrays suffer from high sidesobe levels. The faceted structure causes the elements of the array to have different far-field radiation paths. By compensating for the phase delays arising from these paths, the conventional amplitude tapering method that is normally used for uniform linear arrays can be applied to the 3-faceted array. It was shown

that the sidelobe levels of the array that is less by 10 dB, compared to uniform weighting, when Kaiser Weighting is used. Also, the Kaiser weighting ($\alpha = 3$) provides the best result as it balances the SLL and the main beam width and allows a trade-off between them. With this technique, not only the adaptive array has a wide scanning range, it also has reduced sidelobe levels.

A useful property of an adaptive array antenna is the adaptive beamforming, where the main beam of the array could be placed at the desired angle while nulls are placed at the interfering angles. This feature enables the adaptive array antenna to maximise its spatial usability and channel capacity. In Chapter 4, adaptive beamforming techniques using different optimisation criteria, which include minimum Mean-Square Error (MSE), power minimisation and maximum Signal to Interference-plus-Noise Ratio (SINR) are discussed. The performance of the faceted arrays is then evaluated in the context of adaptive beamforming. The arrays are simulated under two different situations: Case1 - a desired signal at boresight, and Case2 - a desired signal away from boresight. It is observed that the 3-faceted array outperforms the other arrays in the case where the desired beam is placed away from the boresight, ($\theta_d = 60°$, $\emptyset_d = 0°$). The directivity of the 3-faceted array is consistent in both cases which suggest the suitability of the 3-faceted array for wide-coverage adaptive array applications. It was also concluded that careful geometry selection is essential as it influences the beamforming of the adaptive array antenna.

Single-port beamforming algorithms are explored in Chapter 5. In a single-port beamformer, signals coming from each element are combined before going through the RF-channel. However, as a result of the combination, the spatial information of the signal is lost, hence limiting the use of conventional beamforming algorithms. In this chapter, a signal estimation technique for adaptive array antennas is proposed using a pseudo-inverse function. The algorithm is simulated on the 3-faceted array and the results are compared to the one from multi-port system. It was shown that the single-port beamforming algorithm with pseudo-inverse function is able to produce the desired radiation pattern. However, for high resolution cases, where the desired and interference signals are 10° separated, the proposed technique requires nearly three times more iterations than the multi-port technique.

However, the approaches discussed above are bounded to certain trade-off as shown in Table 6.1.

Table 6.1: The Trade-off between the Performance and the Low Cost Approach for the Adaptive Array Antenna.

Low Cost Approach	Advantage	Disadvantages
Polarisation Reconfigurable Antenna Design	1. The adaptive array antenna can radiate either LHCP or RHCP wave. 2. The number of array element can be reduced as a single antenna can be reconfigured to transmit different radiation properties.	1. The switching mechanism required in the reconfiguration process influences the radiation properties of the antenna 2. Complex circuitary required for the reconfiguration process increases the physical dimension of the antenna.
3-Faceted Array Structure for Adaptive Array Antenna with Small Number of Elements	1. The scanning range of the array can be increased up to ±70° compared to the conventional linear array, ±56°. 2. The cost of the adaptive array antenna is reduces as less elements is required by the array in order to achieve wide scanning range.	The overall dimension of the array is increased compared to the conventional linear array.
The use of inverse array weight to estimate signals for Single-port Beamforming	1. The cost of adaptive array antenna is reduced as no redundant RF channel is required, as opposed to multi-port beamforming, in the system. 2. Conventional beamforming algorithms that require the information of signals at each antenna can be applied to the single port beamforming structure.	When the interference and desired signals are close (±10°), this single-port approach requires more iteration than the multi-port beamforming.

Overall, it is concluded that the required adaptive array antenna performance can be achieved using the polarisation reconfigurable antenna, the 3-faceted array antenna and the single-port beamforming technique. Therefore, it is possible to reduce the cost of an adaptive array antenna without compromising its performance, which suggests its potential to be deployed commercially, especially in wireless communication industry. The goal and achievements of this thesis are illustrated in Figure 6.1.

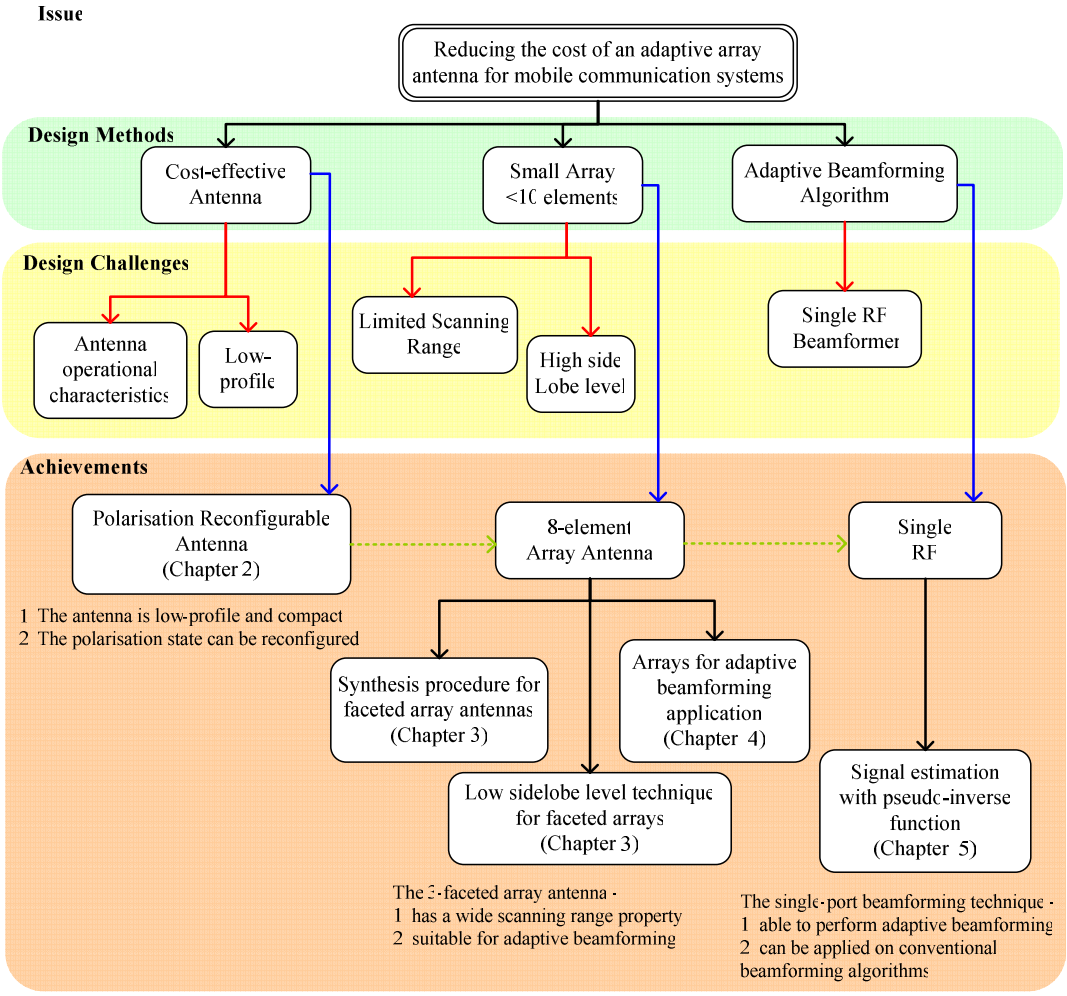

Figure 6.1: Summary of the areas and the challenges addressed in the thesis.

6.3 Summary of Contributions

The implementation cost of adaptive array antennas can be kept to a minimum by using reconfigurable antennas in the array, reducing the number of elements in the array and implementing single-port beamforming techniques. This thesis has developed several techniques for the design of adaptive array antennas which will enable their cost effective adoption in wireless communication systems. These techniques are as follows:

- **The design of an adaptive array antenna with wide scanning range property:** Adaptive array antennas with small number of elements have a limited scanning range and this scanning range can be increased by introducing a mean of curvature to the array structure. To date, design synthesis of faceted array antennas has been targeted on arrays with a large number of elements. This thesis presents a comprehensive analysis on 8-element faceted array antennas, namely 2-faceted, 3-faceted 4-faceted and 8-faceted arrays (Section 3.5.5). The proposed 3-faceted array achieves a wide scanning range of ± 70° from boresight (Section 3.6).

- **The design of a faceted array antenna for adaptive beamforming applications in wireless communication systems:** In literature, the geometries of adaptive array antennas have been evaluated based on their adaptive beamforming capabilities. The array geometries that have been evaluated include uniform linear array (ULA), uniform circular array (UCA), uniform hexagonal array (UHA) and uniform rectangular array (URA). In this thesis, the 8-element faceted array antennas, namely 2-faceted, 3-faceted 4-faceted and 8-faceted array are evaluated from the perspective of adaptive beamforming (Section 4.4). The proposed 3-faceted array achieves optimum results as it has high directivity and the main beam and nulls are placed accurately at the desired and interference angles, respectively, even when the desired signal is away from boresight ($\theta = 60°$).

- **The procedure for synthesising a 3-faceted array antenna for low sidelobe level:** One of the techniques used to reduce the sidelobe level of an adaptive array antenna is amplitude tapering using windowing technique. This synthesise method is essentially identical to the design process for an FIR filter in digital signal processing (DSP). For a ULA, the procedure is straight forward as the amplitude excitation of the elements in the array is controlled based on the window coefficients. In this thesis, the use of phase correction matrix is proposed, which

allows the 3-faceted array to be synthesised in the same way as a ULA. With this technique, not only the adaptive array has a wide scanning range, it also has reduced sidelobe levels.

- **A single-port beamforming technique:** Single-port beamforming techniques include the use of perturbation algorithm, Spatial Multiplexing of Local Elements (SMILE) and Time Sequence Phase Weighting (TPSW) using Walsh-Hadamard matrix. However, in all of these methods, the spatial information of the signals is not fully recovered and this limits the use of conventional adaptive beamforming algorithms. This thesis has proposed a signal estimation technique using pseudo-inverse function for the single-port beamformer (Section 5.3). The radiation patterns generated by the proposed single-port beamforming have main beam and nulls placed accurately at the intended angles. With the proposed single-port beamforming technique, redundant RF front-end components in the system are eliminated.

6.4 Future work

This thesis points to several areas that require further investigation:-

1. Polarisation Reconfigurable Antenna Design

    a. Switching mechanism

The proposed antenna achieves its polarisation reconfiguration with switched connections between the parasitic elements and the main radiating structure. The next step is to integrate the design with a reliable switching mechanism. Issues regarding the antenna and switch integrations include the design of bias network for PIN diodes and the power handling requirement of the RF MEMS switches. The additional structures needed to allow the polarisation reconfiguration may interfere with the performance of the antenna. This switching technology presents its own challenge as well as introducing an additional cost to the adaptive array antenna.

    b. Antenna miniaturisation

Future work with the proposed design is to miniaturise the structure. A miniaturised version of the proposed polarisation reconfigurable antenna is desirable especially as wireless communication devices are getting smaller. Techniques such as using high permittivity substrates, slot loading and shorting pin can be explored. The challenge will be to maintain the polarisation reconfiguration while applying those miniaturising techniques.

2. Array Design

    a. Evaluate the performance of faceted arrays for DoA estimation

In this thesis, the performance of the faceted array is evaluated from its 3 dB scanning range and its adaptive beamforming ability. Another important aspect of adaptive array antennas is the ability to estimate the DoA of a signal. Future studies will evaluate the performance of the faceted array in estimating the DoA using algorithms such as Bartlett, Capon and MUSIC.

    b. Faceted arrays with non-identical elements

The faceted arrays in this thesis were synthesised for wide scanning range and these arrays consist of directional elements. Future work on this topic would be to evaluate the scanning ranges of faceted arrays that consist of elements with different radiation characteristics such as bi-directional, omni-directional elements or a possible combination of these elements.

3. Beamforming Algorithm

    a. Performance criteria and optimisation algorithm

Various beamforming performance criteria, such as minimised MSE, maximised SINR and power minimisation, were investigated in this thesis. To achieve the criteria, standard versions of LMS and PSO algorithms were used. Future work in this area would be to use the advanced versions of these algorithms to accomplish different beamforming performance criteria.

    b. Hardware implementation of the beamforming algorithm

Beamforming strategies for the 3-faceted array using different optimisation criteria were explored in this thesis. Future studies will be to verify these beamforming strategies experimentally. FPGA or ARM processors can be used as the platform for the hardware implementation. Following this, the proposed single-port beamforming technique using the pseudo-inverse signal estimation method can then be evaluated from a hardware point of view.

    c. Simulation of signals with different power levels

The signal estimation method using pseudo-inverse function was simulated in an environment with a desired signal and an interference signal. The signal-to noise-ratio (SNR) of these signals was set at be 10 dB. Future work will be to analyse the proposed technique with different SNR levels.

4. Adaptive Array Antenna Prototype

The ultimate aim is to fabricate the optimised adaptive array antenna and measure its performance. This involves the integration of various adaptive array components such as the antennas, impedance matching circuits, power splitter and the beamformer.

6.5 Final Comment

Today's extensive use of wireless technology requires efficient and reliable antenna systems. Adaptive array antennas can be an attractive solution to meet these requirements as they have the ability to produce highly directive radiation and the radiation pattern can be electronically controlled to adapt to the environment. However, the complexity and cost of the antenna has limited its widespread application in the commercial sector. This thesis proposed several techniques to overcome these problems.

The future will see more applications of wireless technology in our daily life. The demand for more reliable wireless devices will require manufacturers to produce commercially attractive adaptive array antennas. This thesis proposes a number of solutions that will help to achieve this goal.

References

[1] M. Chryssomallis, "Smart antennas," *IEEE Antennas and Propagation Magazine*, vol. 42, pp. 129-136, Jun 2000.

[2] S. Bellofiore, C. A. Balanis, J. Foutz, and A. S. Spanias, "Smart-antenna systems for mobile communication networks. Part 1. Overview and antenna design," *IEEE Antennas and Propagation Magazine*, vol. 44, pp. 145-154, 2002.

[3] C. A. Balanis and P. I. Ioannides, *Introduction to Smart Antennas*: Morgan & Claypool Publishers, 2007.

[4] M. G. J. Spencer, "Smart antennas in handsets for improving 3G performance," in *4th International Conference on 3G Mobile Communication Technologies*, 2003, pp. 53-57.

[5] L. C. Godara, "Application of antenna arrays to mobile communications. II. Beam-forming and direction-of-arrival considerations," *Proceedings of the IEEE*, vol. 85, pp. 1195-1245, 1997.

[6] P. Ioannides and C. A. Balanis, "Uniform circular arrays for smart antennas," *IEEE Antennas and Propagation Magazine*, vol. 47, pp. 192-206, Aug 2005.

[7] M. Greene, "Adaptive Antenna on Mobile Handsets," Radiocommunication Agency 2002.

[8] P. N. Fletcher and P. Darwood, "Beamforming for circular and semicircular array antennas for low-cost wireless LAN data communications systems," *IEE Proceedings of Microwaves, Antennas and Propagation*, vol. 145, pp. 153-158, 1998.

[9] J. R. De Luis and F. De Flaviis, "Frequency Agile Switched Beam Antenna Array System," *IEEE Transactions on Antennas and Propagation*, vol. 58, pp. 3196-3204, 2010.

[10] V. Zaharov, A. Gonzalez, J. Acosta, and M. Teixeira, "Implementing a Vector RLS Smart Antenna Beamformer Using Xilinx System Generator," in *2nd International Symposium on Wireless Pervasive Computing (ISWPC)* 2007, pp. 594-599.

[11] I. Khalifa and R. G. Vaughan, "Geometric Design and Comparison of Multifaceted Antenna Arrays for Hemispherical Coverage," *IEEE Transactions on Antennas and Propagation*, vol. 57, pp. 2608-2614, 2009.

[12] H. Liu, S. Gao, and T. H. Loh, "Frequency agile small smart antenna," in *Proceedings of the Fourth European Conference on Antennas and Propagation (EuCAP 2010)* 2010, pp. 1-4.

[13] P. Mousavi, M. Fakharzadeh, and S. Safavi-Naeini, "Design and implementation of a low cost adaptive antenna system for mobile satellite communication," in *IEEE International Symposium on Phased Array Systems and Technology (ARRAY)*, 2010, pp. 512-517.

[14] F. Rayal, "Why have smart antennas not yet gained traction with wireless network operators?," *IEEE Antennas and Propagation Magazine*, vol. 47, pp. 124-126, 2005.

[15] D. Piazza, P. Mookiah, M. D'Amico, and K. R. Dandekar, "Experimental Analysis of Pattern and Polarization Reconfigurable Circular Patch Antennas for MIMO Systems," *IEEE Transactions on Vehicular Technology*, vol. 59, pp. 2352-2362, 2010.

[16] P. Mookiah and K. R. Dandekar, "A Reconfigurable Antenna-Based Solution for Stationary Device Authentication in Wireless Networks," *International Journal of Antennas and Propagation (Hindawi)*, vol. 2012, p. 11, 2012.

[17] D. Piazza, J. Kountouriotis, M. D'Amico, and K. R. Dandekar, "A technique for antenna configuration selection for reconfigurable circular patch arrays," *IEEE Transactions on Wireless Communications*, vol. 8, pp. 1456-1467, 2009.

[18] J. T. Bernhard, "Reconfigurable antennas and apertures: State of the art and future outlook," in *Proceedings of SPIE Conference on Smart Electronics, MEMS, BioMEMS, and Nanotechnology*, 2003, pp. 1-9.

[19] C. G. Christodoulou, Y. Tawk, S. A. Lane, and S. R. Erwin, "Reconfigurable Antennas for Wireless and Space Applications," *Proceedings of the IEEE*, vol. 100, pp. 2250-2261, 2012.

[20] X.-X. Yang, B.-C. Shao, F. Yang, E. A. Z., and B. Gong, "A Polarization Reconfigurable Patch Antenna With Loop Slots on the Ground Plane," *IEEE Antennas and Wireless Propagation Letters*, vol. 11, pp. 69-72, 2012.

[21] J. Huang, K.-F. Tong, and B. C., "A new polarization reconfigurable microstrip antenna for diversity array," in *IEEE Radar Conference (RADAR '08)* 2008, pp. 1-4.

[22] C. Wenquan, Z. Bangning, L. Aijun, Y. Tongbin, G. Daosheng, and P. Kegang, "A Reconfigurable Microstrip Antenna With Radiation Pattern Selectivity and Polarization Diversity," *IEEE Antennas and Wireless Propagation Letters*, vol. 11, pp. 453-456, 2012.

[23] S. J. Orfanidis, *Electromagnetic Waves and Antennas*: Rutgers Education, 2008.

[24] C. B. Dietrich, Jr., K. Dietze, J. R. Nealy, and W. L. Stutzman, "Spatial, polarization, and pattern diversity for wireless handheld terminals," *IEEE Transactions on Antennas and Propagation*, vol. 49, pp. 1271-1281, 2001.

[25] W. C. Barott and P. G. Steffes, "Grating Lobe Reduction in Aperiodic Linear Arrays of Physically Large Antennas," *IEEE Antennas and Wireless Propagation Letters*, vol. 8, pp. 406-408, 2009.

[26] M. G. Bray, D. H. Werner, D. W. Boeringer, and D. W. Machuga, "Optimization of thinned aperiodic linear phased arrays using genetic algorithms to reduce grating lobes during scanning," *IEEE Transactions on Antennas and Propagation*, vol. 50, pp. 1732-1742, 2002.

[27] V. Kallnichev, "Analysis of beam-steering and directive characteristics of adaptive antenna arrays for mobile communications," *IEEE Antennas and Propagation Magazine*, vol. 43, pp. 145-152, 2001.

[28] T. Suda, T. Takano, and Y. Kazama, "Grating lobe suppression in an array antenna with element spacing greater than a half wavelength," in *IEEE Antennas and Propagation Society International Symposium (APSURSI)*, 2010, pp. 1-4.

[29] S. Wei-Xing and F. Da-Gang, "Angular superresolution for phased antenna array by phase weighting," *IEEE Transactions on Aerospace and Electronic Systems*, vol. 37, pp. 1450-1814, 2001.

[30] Y. Y. Bai, X. Shaoqiu, M. C. Tang, Z. F. Ding, and B. Z. Wang, "Wide-Angle Scanning Phased Array with Pattern Reconfigurable Elements," *IEEE Transactions on Antennas and Propagation*, vol. 9, pp. 4071 - 4076, 2011.

[31] P. J. Bevelacqua and C. A. Balanis, "Optimizing Antenna Array Geometry for Interference Suppression," *IEEE Transactions on Antennas and Propagation,* vol. 55, pp. 637-641, 2007.

[32] B. Lawrence and I. N. Psaromiligkos, "Single-Port MMSE Beamforming," *IEEE International Symposium on Personal Indoor and Mobile Radio Communications,* pp. 1557-1561, 2011.

[33] T. Ohira, "Adaptive array antenna beamforming architectures as viewed by a microwave circuit designer," in *Asia-Pacific Microwave Conference*, 2000, pp. 828-833.

[34] S. Farzaneh and A. R. Sebak, "Single-port direction of arrival estimation using adaptive null-forming," in *IEEE Antennas and Propagation Society International Symposium, (APSURSI '09)* 2009, pp. 1-4.

[35] C. A. Balanis, *Antenna Theory: Analysis And Design,* 3rd ed.: John Wiley & Sons Inc, 2005.

[36] "IEEE Standard Definitions of Terms for Antennas," *IEEE Std 145-1993,* p. i, 1993.

[37] S. Maddio, A. Cidronali, and G. Manes, "A New Design Method for Single-Feed Circular Polarization Microstrip Antenna With an Arbitrary Impedance Matching Condition," *IEEE Transactions on Antennas and Propagation,* vol. 59, pp. 379-389, 2011.

[38] T. A. Milligan, *Modern Antenna Design*: Wiley-IEEE Press 2005.

[39] S. Liang, "The elliptical microstrip antenna with circular polarization," *IEEE Transactions on Antennas and Propagation,* vol. 29, pp. 90-94, 1981.

[40] P. Sharma and K. Gupta, "Analysis and optimized design of single feed circularly polarized microstrip antennas," *IEEE Transactions on Antennas and Propagation,* vol. 31, pp. 949-955, 1983.

[41] M. Haneishi, T. Nambara, and S. Yoshida, "Study on ellipticity properties of single-feed-type circularly polarised microstrip antennas," *Electronics Letters,* vol. 18, pp. 191-193, 1982.

[42] Y. J. Sung, T. U. Jang, and Y. S. Kim, "A reconfigurable microstrip antenna for switchable polarization," *IEEE Microwave and Wireless Components Letters,* vol. 14, pp. 534-536, 2004.

[43] K. Boyon, P. Bo, S. Nikolaou, K. Young-Sik, J. Papapolymerou, and M. M. Tentzeris, "A Novel Single-Feed Circular Microstrip Antenna With Reconfigurable Polarization Capability," *IEEE Transactions on Antennas and Propagation,* vol. 56, pp. 630-638, 2008.

[44] C. Rui-Hung and J. S. Row, "Single-Fed Microstrip Patch Antenna With Switchable Polarization," *IEEE Transactions on Antennas and Propagation,* vol. 56, pp. 922-926, 2008.

[45] Y. J. Sung, "Reconfigurable Patch Antenna for Polarization Diversity," *IEEE Transactions on Antennas and Propagation,* vol. 56, pp. 3053-3054, 2008.

[46] R. L. Haupt, *Antenna Arrays: A Computational Approach*: Wiley-IEEE Press, 2010.

[47] S. A. Askeland, T. Cella, and J. Hjelmstad, "A Hemi-directional Antenna Array Concept for Automotive Radar," in *Progress In Electromagnetics Research Symposium*, Morocco, 2011, pp. 213-216.

[48] A. G. Toshev, "Multipanel Concept for Wide-Angle Scanning of Phased Array Antennas," *IEEE Transactions on Antennas and Propagation,* vol. 56, pp. 3330-3333, 2008.

[49] J. Volakis, *Antenna Engineering Handbook*, 4th ed.: McGraw-Hill Professional, 2009.

[50] L. Josefsson and P. Persson, *Conformal Array Antenna Theory And Design*: John Wiley & Sons, Inc., Hoboken, New Jersey, 2006.

[51] P. Ioannides and C. A. Balanis, "Uniform circular and rectangular arrays for adaptive beamforming applications," *IEEE Antennas and Wireless Propagation Letters,* vol. 4, pp. 351-354, 2005.

[52] R. L. Haupt, "Optimized Element Spacing for Low Sidelobe Concentric Ring Arrays," *IEEE Transactions on Antennas and Propagation,* vol. 56, pp. 266-268, 2008.

[53] S. S. Moghaddam, F. Akbari, and V. T. Vakili, "A novel array geometry to improve DOA estimation of narrowband sources at the angles close to the array endfire," in *19th Iranian Conference on Electrical Engineering (ICEE), 2011* 2011, pp. 1-6.

[54] B. K. Lau and Y. H. Leung, "A Dolph-Chebyshev approach to the synthesis of array patterns for uniform circular arrays," in *IEEE International Symposium on Circuits and Systems*, Geneva, 2000, pp. 124-127.

[55] M. Benedetti, R. Azaro, and A. Massa, "Memory Enhanced PSO-Based Optimization Approach for Smart Antennas Control in Complex Interference Scenarios," *IEEE Transactions on Antennas and Propagation,* vol. 56, pp. 1939-1947, 2008.

[56] B. Widrow and J. McCool, "A comparison of adaptive algorithms based on the methods of steepest descent and random search," *IEEE Transactions on Antennas and Propagation,* vol. 24, pp. 615-637, 1976.

[57] R. L. Haupt, "Adaptive antenna arrays using a genetic algorithm," in *Proceedings of the 2006 IEEE Mountain Workshop on Adaptive and Learning Systems*, Y. Motai and B. Sick, Eds., ed, 2006, pp. 249-254.

[58] O. A. Abu-Ella and B. A. El-Jabu, "Performance improvement of blind adaptive beamforming algorithms using pre-filtering technique," in *IEEE Aerospace Conference*, New York, 2007, pp. 1047-1050.

[59] M. Benedetti, R. Azaro, D. Franceschini, and A. Massa, "PSO-based real-time control of planar uniform circular arrays," *IEEE Antennas and Wireless Propagation Letters,* vol. 5, pp. 545-548, 2006.

[60] K. R. Mahmoud, M. El-Adawy, S. M. M. Ibrahem, R. Bansal, K. R. Mahmoud, and S. H. Zainud-Deen, "A comparison between circular and hexagonal array geometries for smart antenna systems using particle swarm optimization algorithm," *Progress in Electromagnetics Research-PIER,* vol. 72, pp. 75-90, 2007.

[61] N. H. Noordin, V. Zuniga, A. O. El-Rayis, N. Haridas, A. T. Erdogan, and T. Arslan, "Uniform circular arrays for phased array antenna," in *Loughborough Antennas and Propagation Conference (LAPC)* Loughborough, U.K., 2011, pp. 1-4.

[62] Y. C. Eldar, A. Nehorai, and P. S. La Rosa, "A Competitive Mean-Squared Error Approach to Beamforming," *Signal Processing, IEEE Transactions on,* vol. 55, pp. 5143-5154, 2007.

[63] J. A. Srar, C. Kah-Seng, and A. Mansour, "Adaptive Array Beamforming Using a Combined LMS-LMS Algorithm," *IEEE Transactions on Antennas and Propagation,* vol. 58, pp. 3545-3557, 2010.

[64] W. Liu, "Blind Adaptive Beamforming for Wideband Circular Arrays," in *2009 IEEE International Conference on Acoustics, Speech, and Signal Processing*, New York, 2009, pp. 2029-2032.

[65] M. Khodier and G. Saleh, "Beamforming and power control for interference reduction in wireless communications using particle swarm optimization," *AEU-International Journal of Electronics and Communications*, vol. 64, pp. 489-502, 2009.

[66] X. Song, J. K. Wang, and X. F. Niu, "Robust Adaptive Beamforming Algorithm Based on Neural Network," in *2008 IEEE International Conference on Automation and Logistics, Vols 1-6*, ed New York: Ieee, 2008, pp. 1844-1849.

[67] F. B. Gross, *Smart Antennas for Wireless Communications With MATLAB*: The McGraw-Hill Companies, Inc., 2005.

[68] M. Vitale, G. Vesentini, N. N. Ahmad, and L. Hanzo, "Genetic algorithm assisted adaptive beamforming," in *IEEE 56th Vehicular Technology Conference (VTC 2002-Fall)* 2002, pp. 601-605 vol.1.

[69] V. Zuniga, A. Erdogan, and T. Arslan, "Control of adaptive rectangular antenna arrays using Particle Swarm Optimization," in *Antennas and Propagation Conference (LAPC), 2010 Loughborough*, 2010, pp. 385-388.

[70] R. Yue, Y. C. Eldar, and A. B. Gershman, "Performance Tradeoffs Among Adaptive Beamforming Criteria," *IEEE Journal of Selected Topics in Signal Processing,* vol. 1, pp. 651-659, 2007.

[71] R. L. Haupt, "Phase-only adaptive nulling with a genetic algorithm," *IEEE Transactions on Antennas and Propagation,* vol. 45, pp. 1009-1015, 1997.

[72] M. M. Khodier, M. Al-Aqeel, "Linear And Circular Array Optimization: A Study Using Particle Swarm Intelligence," *Progress In Electromagnetics Research B,* vol. 15, pp. 347-373, 2009.

[73] K. R. Mahmoud, M. El-Adawy, S. M. M. Ibrahem, R. Bansal, K. R. Mahmoud, and S. H. Zainud-Deen, "Performance of circular Yagi-Uda arrays for beamforming applications using particle swarm optimization algorithm," *Journal of Electromagnetic Waves and Applications,* vol. 22, pp. 353-364, 2008.

[74] P. S. R. Diniz, *Adaptive Filtering Algorithms and Practical Implementation*, 3 ed.: Springer, 2008.

[75] K. Seung-Jean, A. Magnani, A. Mutapcic, S. P. Boyd, and L. Zhi-Quan, "Robust Beamforming via Worst-Case SINR Maximization," *IEEE Transactions on Signal Processing*, vol. 56, pp. 1539-1547, 2008.

[76] J. Yang and A. Swindlehurst, "Maximum SINR beamforming for correlated sources," in *International Conference on Acoustics, Speech, and Signal Processing ICASSP-95*, 1995, pp. 1916-1919 vol.3.

[77] D. S. Weile and E. Michielssen, "The control of adaptive antenna arrays with genetic algorithms using dominance and diploidy," *IEEE Transactions on Antennas and Propagation,* vol. 49, pp. 1424-1433, 2001.

[78] V. Zuniga, A. T. Erdogan, and T. Arslan, "Adaptive radiation pattern optimization for antenna arrays by phase perturbations using particle swarm optimization," in *NASA/ESA Conference on Adaptive Hardware and Systems (AHS)*, 2010, pp. 209-214.

[79] J. Robinson and Y. Rahmat-Samii, "Particle swarm optimization in electromagnetics," *IEEE Transactions on Antennas and Propagation*, vol. 52, pp. 397-407, 2004.

[80] M. M. Khodier and C. G. Christodoulou, "Linear Array Geometry Synthesis With Minimum Sidelobe Level and Null Control Using Particle Swarm Optimization," *IEEE Transactions on Antennas and Propagation*, vol. 53, pp. 2674-2679, 2005.

[81] Eberhart and S. Yuhui, "Particle swarm optimization: developments, applications and resources," in *Evolutionary Computation, 2001. Proceedings of the 2001 Congress on*, 2001, pp. 81-86 vol. 1.

[82] K. R. Mahmoud, M. I. Eladawy, R. Bansal, S. H. Zainud-Deen, and S. M. M. Ibrahem, "Analysis of uniform circular arrays for adaptive beamforming applications using particle swarm optimization algorithm," *International Journal of RF and Microwave Computer-Aided Engineering*, vol. 18, pp. 42-52, Jan 2008.

[83] M. Clerc. Available: http://clerc.maurice.free.fr/pso/

[84] Eberhart and S. Yuhui, "Particle swarm optimization: developments, applications and resources," in *Proceedings of the Congress on Evolutionary Computation*, 2001, pp. 81-86 vol. 1.

[85] S. Farzaneh and A. R. Sebak, "A novel amplitude-phase weighting for analog microwave beamforming," *IEEE Transactions on Antennas and Propagation*, vol. 54, pp. 1997-2008, 2006.

[86] L. Gargouri, R. Ghayoula, N. Fadlallah, A. Gharsallah, and M. Rammal, "Steering an adaptive antenna array by LMS algorithm," in *Electronics, Circuits, and Systems, 2009. ICECS 2009. 16th IEEE International Conference on*, 2009, pp. 459-462.

[87] R. M. Shubair, "Robust adaptive beamforming using LMS algorithm with SMI initialization," in *IEEE Antennas and Propagation Society International Symposium*, 2005, pp. 2-5 vol. 4A.

[88] J. A. Srar and C. Kah-Seng, "RLMS algorithm for fixed or adaptive beamforming," in *Communications (MICC), 2009 IEEE 9th Malaysia International Conference on*, 2009, pp. 163-167.

[89] V. V. Zaharov and M. Teixeira, "Modified implementations of RLS digital beamformer," in *IEEE Antennas and Propagation Society International Symposium* 2005, pp. 275-278 vol. 3A.

[90] J. Zhang, W. Wu, and D.-G. Fang, "Single RF Channel Digital Beamforming Multibeam Antenna Array Based on Time Sequence Phase Weighting," *IEEE Antennas and Wireless Propagation Letters*, vol. 10, pp. 514-516, 2011.

[91] J. D. Fredrick, W. Yuanxun, and T. Itoh, "A smart antenna receiver array using a single RF channel and digital beamforming," *IEEE Transactions on Microwave Theory and Techniques*, vol. 50, pp. 3052-3058, 2002.

[92] A. Cantoni, "Application of orthogonal perturbation sequences to adaptive beamforming," *IEEE Transactions on Antennas and Propagation*, vol. 28, pp. 191-202, 1980.

[93] L. Godara and A. Cantoni, "Analysis of the performance of adaptive beam forming using perturbation sequences," *IEEE Transactions on Antennas and Propagation*, vol. 31, pp. 268-279, 1983.

[94] S. Farzaneh and A. R. Sebak, "Microwave Sampling Beamformer - Prototype Verification and Switch Design," *IEEE Transactions on Microwave Theory and Techniques*, vol. 57, pp. 36-44, 2009.

[95] J. Zhang, W. Wu, and D.-G. Fang, "Calibration method for the single RF channel digital beamforming antenna array," in *Cross Strait Quad-Regional Radio Science and Wireless Technology Conference (CSQRWC)*, 2011, pp. 442-445.

[96] H. Wang, D. G. Fang, and M. Li, "A Single-Channel Microstrip Electronic Tracking Antenna Array With Time Sequence Phase Weighting on Sub-Array," *IEEE Transactions on Microwave Theory and Techniques*, vol. 58, pp. 253-258, 2010.

[97] Y. Zhu, B. Li, and X. Xu, "Spectral Reconstruction and Accuracy Appraisal Based on Pseudo Inverse Method," in *2012 Symposium on Photonics and Optoelectronics (SOPO)*, 2012, pp. 1-3.

[98] V. V. Selivanov, M. D. Lepage, and R. Lecomte, "Real-time PET image reconstruction based on regularized pseudo-inverse of the system matrix," in *2001 IEEE Nuclear Science Symposium Conference Record*, 2001, pp. 1737-1741 vol.3.

[99] Z. Chunyang and W. Youzheng, "Signal reconstruction for Compressive Sensing via iterative pseudo-inverse multiplication," in *2012 International Conference on Systems and Informatics (ICSAI)*, 2012, pp. 1751-1754.